ECG-DERIVED RESPIRATION IN ATRIAL FIBRILLATION

Danilo Sergio Pupo and Luisa Rusconi

2017

LUND
UNIVERSITY

Master´s Thesis in
Biomedical Engineering

Faculty of Engineering LTH Department of
Biomedical Engineering

Supervisor: Frida Sandberg

ABSTRACT

In past years, the demand for an indirect extraction of respiration and the interest in a joint study of respiratory and cardiac systems represented the driving forces for the development of Electrocardiogram Derived Respiration (EDR) algorithms. The main advantage of them consists in deriving a sufficiently reliable surrogate respiratory signal by only exploiting the normal electrocardiogram (ECG) equipment, without requiring the common devices used to record respiration, which are cumbersome and expensive, besides to possibly interfere with natural breathing. However, the validity of EDR methods has been mainly demonstrated on healthy subjects and in certain clinical applications. At the present time, the possibility to extract non-invasively the respiratory signal during arrhythmia, by applying an EDR method, has never been explored on a sufficiently large dataset and with a systematic study. Atrial Fibrillation (AF) represents the most common arrhythmia, characterized by a fast and irregular beating with an increasing incidence that is especially prominent in the developed world.

Therefore, this master thesis aims to verify the feasibility of extracting the respiratory rate from ECG during Atrial Fibrillation (AF). Four EDR methods are implemented and evaluated, by selecting only among the techniques based on respiration-induced variations in beat-to-beat morphology, since the abnormal heart rhythm in AF does not lend itself to be used for deriving respiration. The different techniques are tested on a dataset of 49 patients, containing a two non-orthogonal leads ECG recording and a simultaneous belt respiratory signal for each of them. The recordings are of about ten minutes long and were acquired in rest phase.

A code workflow has been designed to handle the characteristics of the signals and reliably estimate the respiratory rate from the surrogate respiratory signal and from the reference signal. Since the fibrillation activity may mask the

respiratory information contained in the beat morphology, an important stage of the workflow is represented by the subtraction of the fibrillation signal from the QRS interval. The actual benefit of this step is tested by comparing the methods performances by selectively allowing or not its performing. The estimation accuracy of each method is assessed by comparing the respiratory rate estimates from EDR signal and reference signal in terms of mean absolute and relative intrasubject error, percentage of the record duration where an estimate is given from both signals and RMS error computed on the entire dataset.

The results do not point out any improvement in the performances of the methods after removing the f-waves from the QRS complex. This do not ensure that different results may be observed by applying another technique, since the method applied in this thesis suffers of sensitivity to noise that should be further investigated. From the comparison of the results of the methods, it turned out that the methods that extract respiratory information independently from the two leads outperformed the other ones, which combine this information from both leads and derive only one rotation angle series. The method based on QRS slopes and R waves angles estimated the respiratory frequency of the subjects in the dataset more accurately than did the other tested methods, achieving a mean intrasubject error $\mu=0.0227\pm0.0217$ ($8.45\% \pm 8.83\ \%$). In general, all the tested methods achieved estimation errors higher with respect to previous studies on healthy subjects, but still comparable as order of magnitude. This indicates that further studies on the extraction of electrocardiography derived respiration in patients with atrial fibrillation are justified.

ACKNOWLEDGMENTS

First, we would like to express our gratitude to our supervisor Frida Sandberg for her useful comments, remarks and wise suggestions during the challenging time of this master thesis. Furthermore, we would like to thank also our supervisor from Italy Valentina Corino, for her remote assistance on the project and for providing the database for this work.

A heartfelt thanks to Professor Leif Sörnmo and Professor Luca Mainardi for introducing us to the topic and for letting us to carry a collaborative work out between Lund University and Politecnico of Milan.

We wold like to express our sincere gratitude to Spyros Kontaxis from the University of Zaragoza for the helpful collaboration and valuable advices.

A special thank you to friends who have made our time in Lund very enjoyable during the last two years. Finally, we would like to thank all others who have supported us, not only through this master thesis, but during the whole education.

CONTENTS

INTRODUCTION

1.1 MOTIVATION

Technology advancement in signal processing aims to enhance the capability to extract medical information from the recording of body signals. The research, in particular, strives to improve robustness and accuracy of the medical devices as well as to reduce costs and bothers for the patients. The thesis moves in this direction, center in on the possibility to extract respiratory information from electrocardiogram (ECG) in case of atrial fibrillation (AF). Respiration is usually recorded by techniques that make use of devices that are bulky, expensive and may interfere with natural breathing. Therefore, the main advantage would be to derive synchronous signals from the heart and the lung activities without the use of any additional device, but only exploiting the ECG equipment commonly used to diagnose and monitor many cardiac dysfunctions.

1.1.1 Clinical issues

This simultaneous observation is generally required in clinical applications such as ambulatory monitoring, stress testing and sleep studies [1], where the use of cumbersome devices to detect respiration is unmanageable. In everyday life, the influence of voluntary activities like eating or speaking is more pronounced on respiration compared to that on the heart, so affecting the determination of respiratory oscillations with the traditional techniques. In sleep studies, instead, involuntary movements, or other activities, like snoring, could be sources of artefacts and unreliable measures of respiration. Moreover, the bothers to the patient deriving from the addition of more sensors and a new device are often the cause of interference with the natural activities of the organs under investigation. Nevertheless, the contemporaneous monitoring of respiration, when the first concern lies with the heart, is often needful and it is even exploited to understand the clinical significance of certain cardiac arrhythmias

with reference to respiration [2]. Another reason to demand for reliable measures of respiration without the use of bulky devices is the synchronisation and the compensation of MRI scans in chest and thorax sequences [3]. Yet another application deals with post-operative care: the recording of both cardiac and respiratory functions in post-operative patients is important to monitor how analgesics depress respiration [4].

The trace of respiration is important for apnoea's studies, like in [5] and [6], where a good tracking of the breathing cycles is required. Furthermore, looking for the respiratory rate has a big relevance, because it remains the first and often the most sensitive marker of acute respiratory dysfunction [7]. During out-of-hospital emergency care it is also a sensitive indicator, among others, of critical illness defined as severe sepsis, delivery of mechanical ventilation, or death during hospitalization [8]. The respiratory rate is also very relevant in sports training, since it is used to determine the point when the exercise shifts from aerobic to anaerobic, together with other parameters [9].

Therefore, the relevant clinical reasons and research studies above mentioned represent the main motivation on which the thesis is based and would like to make a contribution.

1.1.2 Current respiratory monitoring devices

Nowadays the existing methods for the acquisition and the analysis of the respiratory patterns can be divided in two categories: direct and indirect measures. Respiration can be directly monitored by measuring the flow, pressure, temperature or chemical composition of the air transported into and out of the lungs for example with spirometers, nasal thermocouples or with carbon dioxide sensors. It is indirectly measured through thoracic volume changes with transthoracic inductance or impedance plethysmographs, strain

gauge measurements of thoracic circumference, pneumatic respiration transducers and whole-body plethysmographs [2].

However, these techniques require the use of bulky, expensive or uncomfortable devices. Moreover, some equipment can interfere with natural breathing or being unsuitable and unmanageable in certain critical applications. For these reasons, different methods have been developed to obtain indirectly respiratory information taking advantage of other devices. The ECG-Derived Respiratory information (EDR) is one of those and it is extracted by exploiting ECG-artefacts given by respiratory activity. This signal varies in amplitude corresponding to the different phases of respiration, thus it enables the estimation of the respiratory rate and the temporal pattern of respiration [10]. Different methods have been elaborated based on the rotation of the heart's electrical axis and changes in beat morphology caused by chest movement and variations in thorax impedance during the respiratory cycle [2]. Others mostly deal with Heart Rate (HR) series and still others derive the respiratory signal by using both beat morphology and HR information [1]. However, the latter two groups are not suitable for the estimation of the respiratory frequency when the heart rate is affected by a dysfunction of the sinus atrial (SA) node. The most important methods based on morphology variations are extensively described in Chapter 3.

1.1.3 EDR in Atrial Fibrillation

Since the use of methods for indirect extraction of respiratory information from ECG is still particularly attractive to pursue [1], the research focuses on the development of accurate and reliable EDR-algorithm in every clinical situation. Atrial fibrillation is the most common arrhythmia of clinical significance and it is associated with increased morbidity, especially stroke and heart failure, as well as increased mortality [11]. In 2014 the statistical work of Chugh et al. [11] provided evidence of progressive increases in overall burden, incidence,

prevalence of atrial fibrillation and AF-associated mortality between 1990–2010. They estimated globally 33,5 million of individuals with AF in 2010. Most recent studies, carried out in European perspective, have confirmed that the prevalence of AF in the general adult population is more than double that reported just one decade earlier, ranging from 1.9% in Italy, Iceland, and England to 2.3% in Germany and 2.9% in Sweden [12]. The major incidence, consequently, determines growing health care costs with an increasing number of hospitalizations, emergency room visits and burden of outpatient visits for AF.

To the best of our knowledge, at the present time, only a few studies (as [13] and [14]) have dealt with EDR-methods in AF. They are mainly clinical studies based on a small database and not supported by a complete, meticulous, and detailed analysis of the existing methods.

For these reasons, the thesis explores the applicability of EDR-methods in AF, adducing an engineering point of view to possibly achieve advancements in the reliable extraction of synchronous signals from the heart and the lung activities without the use of any additional device. The results could produce many advantages in medical research, like studies on cardiac arrhythmia, as well as in economical aspects and in medical care.

Moreover, a robust EDR-algorithm does not require supplementary transducers or hardware modification, thus the normal equipment for ECG recording can be exploited. Its adoption could rapidly spread and further encourage the simultaneous monitoring of respiration in cardiac care without devoting more resources, since the electrocardiogram is the standard tool for having a macro description of the cardiac activity since long all around the world.

1.2 AIM

The thesis aims to verify the feasibility of extracting respiratory information from ECG in case of AF. Different methods are tested on a database with real data in order to understand which is the most reliable and robust. The purpose is to derive an algorithm which is trustworthy to be applied on diagnosed cases of atrial fibrillation, thus dealing with the characteristics of real ECG with different signal qualities.

1.3 OBJECTIVES

Given a dataset with simultaneous recordings of two-leads ECG and respiratory signals of 57 patients in atrial fibrillation, the first objective is to perform the most suitable pre-processing in order to improve the quality of the signals. Two major issues are addressed in it: the baseline wander removal and the AF artefacts cancellation through the estimate of the TQ-based fibrillation signal.

Starting from the literature of the EDR-algorithms used so far, the study of the state of the art mainly focused on techniques that exploit beat-to-beat morphologic variations, given the characteristics of an ECG in AF. Among these, the most recent works have been analysed more accurately and the most suitable ones for the problem of this thesis have been selected for implementation, adaptation to the database and testing. The methods of Bailon et al. [1], Caggiano et al. [15], Mason et al. [16] and Lázaro et al. [17] turned out to fulfil the requirements, since they efficiently extract respiration by considering different features in ECG which should be unrelated with AF. Their performance comparison is carried out with and without preliminary cancellation of AF artefacts in order to figure out if a real advantage subsists in performing a specific pre-processing step for this case.

1.4 THESIS OUTLINE

After the introduction of the first chapter, Chapter 2 leads up to the anatomy of the heart and its physiology with a particular attention to the atrial fibrillation condition. Moreover, it stresses the relationship between the respiratory and the cardiac systems clarifying the respiratory-induced morphology modulation of the heart beats, which is a key point in this thesis.

Chapter 3 presents the examined database and describes the types of signals included in it: the electrocardiogram and the belt respiratory signal.

Chapter 4 is an overview of the most important EDR algorithms with focus on the ones exploiting beat-to-beat morphological variations in ECG. This section is a general background, helpful to the reader to perceive the area where the thesis is positioned.

Chapter 5 describes in details the workflow, that has been designed to attain the goal of the thesis. The used algorithms are gathered and explained in relation to their functions:

- the pre-processing of the signals deals with the primary requirement of increasing the quality of the raw signals;
- the beat analysis handles the presence of abnormal and noisy beats in the ECG;
- the EDR algorithms section represents the core of the thesis, describing the implemented methods to extract the respiratory signal from the ECG;
- the post-processing of the EDR signal considers the procedures to exclude misleading samples and obtain an evenly sampled signal from a beat-to-beat series;
- the final step elucidates how the respiratory rate is estimated along the time for both the EDR signal and the reference respiratory signal.

In case of ECG signals during AF, an important stage before applying the EDR algorithm could be the handling of the AF artefacts in the beat morphology. Their removal is an important issue in this thesis. Thus, the workflow is carried out with and without this step, in order to understand if their presence in the ECG influences the EDR signal estimate and a prior subtraction is required.

Chapter 6 presents the techniques used to assess the accuracy of estimation, taking into account the correspondence between the estimated respiration rates from the EDR and the respiration rate from the ground truth.

Chapter 7 exhibits all the results of different methods and parameters settings. A discussion on this data is takes place in Chapter 8 and it is followed by a general conclusion, where the carried work is summarised.

Chapter 2. MEDICAL BACKGROUND

In the following chapter a general description of the anatomy and physiology of the heart is firstly reported. Then the reader is introduced to the mechanisms of the cardiac conduction system and the respiratory-induced modulation of the cardiac activity. At last, the focus is on the pathology of AF and on how its characteristics impact on the estimation of the EDR signal.

2.1 CARDIAC ANATOMY AND PHYSIOLOGY

The heart is a muscular organ situated in the "middle mediastinum" at the center of the thoracic cavity behind the sternum, where it is folded by a double membrane sac, called pericardium, which is attached to the mediastinum and keeps the heart in position.

The heart consists of two parallel pumps: a "right heart" that pumps blood through the lungs and a "left heart" that pumps blood through the peripheral organs. The two compartments have some anatomical differences mainly connected to their different operating districts and they are divided by a muscular wall, called the septum. Nevertheless, the pumping principle is the same and consists of a pulsatile two-chamber pump: one upper and receiving chamber, the atrium, and one lower and discharging chamber, the ventricle. Each atrium is separated from its ventricle by a passive valve, which is structurally designed to allow the flow only in one direction, from the atrium to the ventricle. One additional semilunar valve sits at the exit of each ventricle, allowing the emptying into the artery leaving the heart. The cardiac valves passively close and open in response to the pressure gradient across them according to the direction of the flow and help to maintain the pressure required to pump the blood.

The main function of the heart is to pump de-oxygenated blood to the lungs to be saturated with oxygen and then to the body to supply the cells with the oxygen. Thanks to the action of the autonomic nervous system (ANS), the heart is able to regulate the pumping rate and the pressure values in the cardiovascular system adapting to the body requests and compensating for external changes.

The blood flows through the chambers of the heart following a precise pathway, as illustrated in Figure 1.

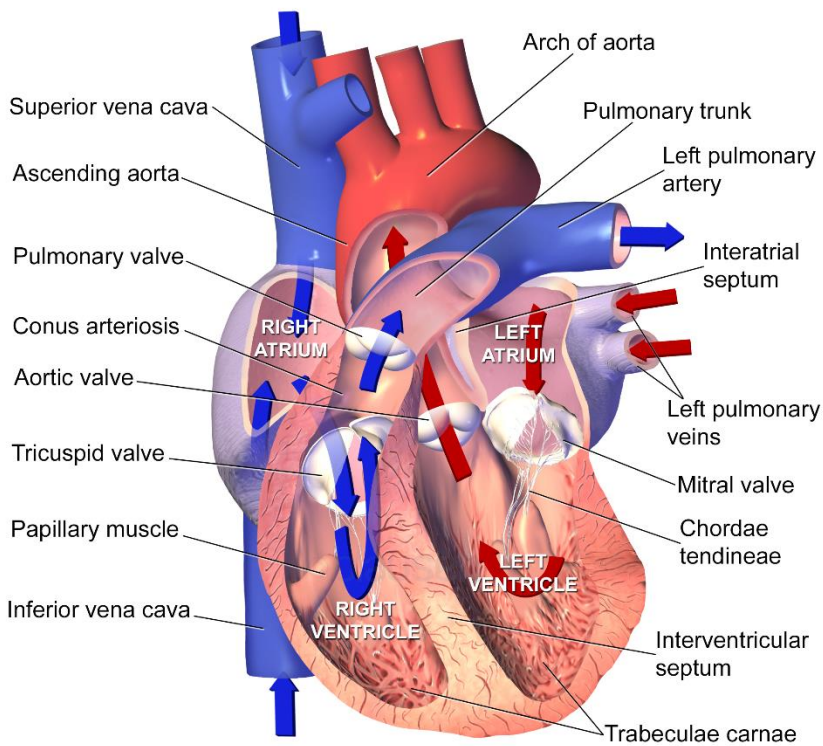

Figure 1 – Graphical representation of the blood flow into the chambers of the heart. The blue arrows represent the venous blood coming from the sistemic circulation, while the red ones indicate the arterial blood coming from the lungs.

The sequence of mechanical events that defines a cardiac cycle can be assumed to start in the "right heart" where deoxygenated blood of the systemic circulation is collected from two large veins, the superior and inferior venae

cavae. The right atrium receives and pumps the blood through the tricuspid valve into the right ventricle. Once the ventricle has been filled and the atrioventricular valve is closed to prevent any flow backwards to the atrium, the blood is pumped to the pulmonary artery passing through the pulmonary valve. Then the blood reaches the lungs where the gas exchange happens at the level of the pulmonary capillaries and alveoli through the passive process of diffusion and under conditions of partial pressure of oxygen. After being oxygenated, the pulmonary venous blood comes back to the heart entering the left atrium from the pulmonary veins. It is then pumped into the left ventricle through the mitral valve and into the aorta through the aortic valve. After that the systemic circulation begins and in the systemic capillaries, exchange with the tissue fluid and cells of the body occurs; oxygen and nutrients are supplied to the cells for their metabolism and exchanged for carbon dioxide and waste products [18].

The heart is composed of three major types of cardiac muscle: atrial muscle, ventricular muscle, and specialized excitatory and conductive muscle fibers. The atrial and ventricular muscle cells have typical myofibrils that contain actin and myosin filaments, which slide along one another during the contraction and produce the force needed to pump the blood out of the heart. The presence of these cytoskeletal contractile proteins arranged in a lattice is what gives to myocardium the striated appearance under the microscope, also typical of the skeletal muscle. Contraction of each cell normally starts when electrical excitatory impulses, the action potentials, generate at a specific potential along its surface membrane, that is due to the different ions concentrations across it. As with other cell types, the bilayer membrane contains a series of ion channels and pumps, which allow the passage of ions from inside to outside the cells and vice versa. In cardiac muscle, the action potential (AP) is caused by opening of two types of channels: the fast sodium channels and another entirely different population of slow calcium channels, with a different opening and closing

times. The muscle fibers of the heart are made up of many muscle cells, whose membrane fuse with another in correspondence of dark crossing areas called intercalated discs (see Figure 2) in such a way that they form permeable "communicating" junctions, the gap junctions, that allow almost totally free diffusion of ions. The interconnecting nature of cardiac muscle fibers jointly with their latticework arrangement makes the cardiac muscle to work as a "syncytium": the individual cardiac cells are so interconnected with one another that when one of these cells becomes excited, the action potential spreads to all of them throughout the latticework interconnections [19].

Conversely, the specialized excitatory and conductive muscle fibers have only feeble contraction properties since they have few contractile fibrils. They rather exhibit automatic rhythmical properties and their main scope is the conduction of AP through the heart along the cardiac conduction system.

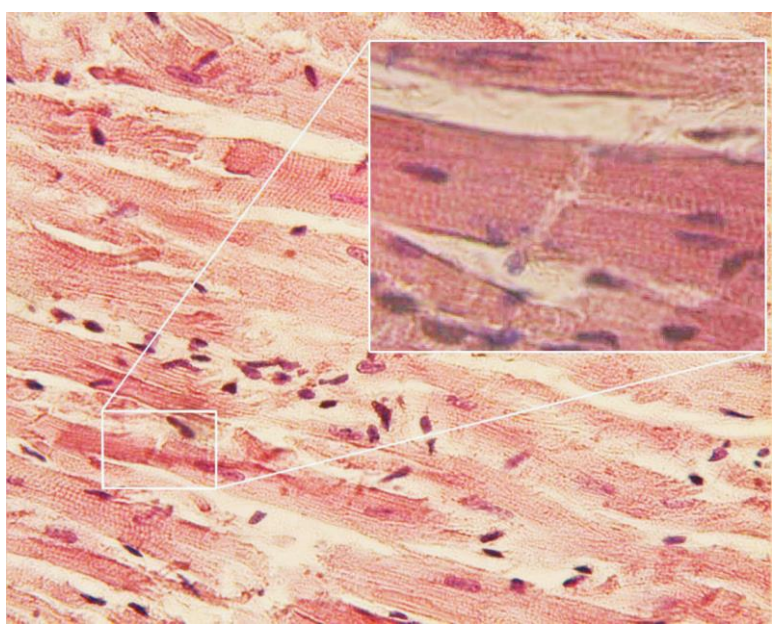

Figure 2 – Histological image of the heart's muscle fibers. Adapted from OpenStax College. In: Micrograph. Regents of University of Michigan Medical School, 2012.

2.2 THE CARDIAC CONDUCTION SYSTEM

In order to carry out the pumping function efficiently, an organized and rhythmic contraction of the heart is also required. It is accomplished through a precise coordination of myocardial contractions and a regular action potentials generation.

In the healthy heart, the initialization of a cardiac cycle occurs in a mass of cells with the ability to spontaneously fire an electrical impulse that is situated in the upper part of the right atrium. These cells are collectively referred as "sinoatrial node" (SA node) and work as a natural pacemaker for the heart [20], since the natural and repetitive depolarization of their membrane potential is responsible for the normal cardiac rhythm. The key of the rhythmic activity of the pacemaker cells is the slow depolarization, which is completely autonomous and does not need any outside innervation from the autonomic nervous system to trigger an AP. In fact, it is due to the relative ion concentration changes in resting conditions that normally do not occur in other cells. However, if the mechanisms of the slow depolarization are independent from any innervation, the native discharge rate originating from SA node is conversely constantly modified by the activity of sympathetic and parasympathetic nerve fibers via the ANS. More specifically, the sympathetic system is excitatory, so it increases the spontaneous firing rate of the SA node and consequently the frequency of the ventricular contraction, whereas the parasympathetic system has a relaxing effect and works in the opposite direction. This neural modulation is of great relevance, since without it the heart would not be able to adapt its pumping rate to the body demands.

The electrical signals arising in the SA node travel through the cardiac conduction system, whose anatomy is illustrated in Figure 3.

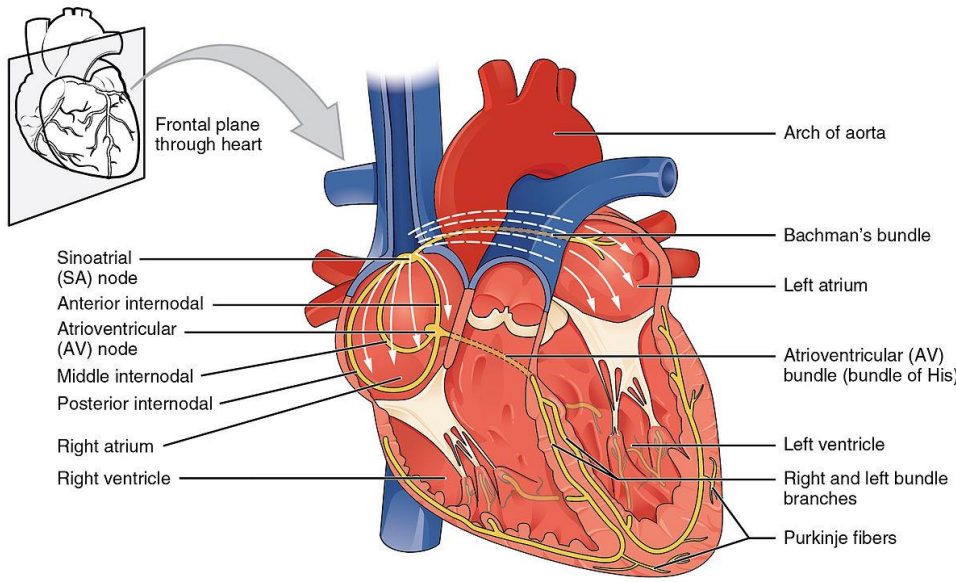

Figure 3 – Graphical representation of the atrial cardiac conduction system in the heart (white arrows). In particular, the yellow paths represent the electric conduction fibers for the propagation of the stimuli through the whole heart.

The function of the cardiac conduction system is to transmit the electrical impulses generated usually by the SA node to cause contraction of the muscle cells in the various parts of the heart with the right timing. After SA nodal excitation, in the normal heart the depolarization wave front spreads causing first the electrical activation of both the atria. Then, the impulse is collected and delayed at the atrioventricular node (AV node) before it enters the ventricular walls. Previously, the conduction between the two nodes was thought to occur only through direct stimulation and conduction between normal atrial myocytes. This theory, however, is not able to explain why the impulses arrive to the AV node quicker than expected by considering the simple myocyte conduction. For this reason, it is now generally accepted that there are microscopically identifiable structures in the atrial walls working as preferential conduction pathways between the SA node and the AV node. In more detail, three "internodal pathways" have been reported: the anterior, the middle and the

posterior tract. In the area where the internodal pathways connect to the AV node, in the "floor" of the right atrium, the atrial stimuli are delayed approximately 0.12 s. The reason of this delay is ascribable to the heart as composed by two "syncytia": the atrial syncytium that constitutes the walls of the two atria and the ventricular syncytium that constitutes the ventricular walls [19]. The atria are separated from the ventricles by fibrous tissue that surrounds the atrioventricular valvular openings and causes the impulse to slow down, as it leaves the internodal pathways and enter the AV node. The delay is of functional importance, since it allows the synchronous contraction of the atria to further fill the ventricles with blood, before the ventricular contraction occurs. It also protects the ventricles from excessively fast rate response to atrial arrhythmias.

The AV node is a group of specialized cardiac muscle fibers where, in normal condition, the conduction occurs through two different pathways: the first pathway, located anteriorly and in close proximity to the "His bundle", and the second pathway, situated posteriorly and inferiorly to the compact node. The first pathway is also called "fast pathway", since it has a faster conduction velocity with a longer refractory period. Conversely, the second pathway is commonly referred as "slow pathway" and it is characterised by a slower conduction velocity with a shorter refractory period.

After AV nodal excitation, the conduction of the impulses proceeds through the "His bundle", the only location that electrically connects the atria and the AV node/ventricles. From the bundle of His, the cardiac depolarization signal is transferred to the ventricles through the bundle branches and then further into an extensive network of specialized conduction fibers, called Purkinje fibers. The signal travels as great as 4 m/sec at this level from only 0.05 m/s at the AV node, which allows reasonably rapid conduction of the excitatory signal to the different parts of the heart. The distribution of the impulse to the larger

ventricular myocardium must be performed very quickly, to initiate a unified contraction of the ventricles.

The electrical impulses travel along a specified direction through the heart at a given instant during the cardiac cycle, so defining a heart current flow which is responsible for the action potentials generation in different compartments with the right timing. The electric generator of the heart can be consequently described by a dipole and it is natural to visually portray the electric generator of the heart in vector form, i.e. the cardiac electrical vector. At any instant, the direction and the module are given respectively by the preferential direction and by the summation of the electrical potentials generated at that instant. This vector account for the electrical activity of the heart and it represents the source of the signal commonly registered through electrodes placed on the skin, as extensively explained in Chapter 3. During most of the cycle of ventricular depolarization, the direction of the electrical potential (negative to positive) is from the base of the ventricles toward the apex [19]. This preponderant direction of the potential during ventricular activation is called the heart electrical axis.

2.3 RESPIRATORY-INDUCED MODULATION OF THE CARDIAC ACTIVITY

It is well known that, in physiological conditions, a dynamic and bidirectional interaction exists between the respiratory and the cardiac system [21]. The relationship is quite evident during exercise when both systems assist to rapidly supply oxygen to the body's cells and organs, but there is also an ongoing interplay at rest. If the main function of the cardiac activity is to pump blood to all the cells of the body where the gas exchange take place, the goals of the respiratory activity are to provide the oxygen for the cell metabolism and release the waste products of it, meeting the respiratory demands of the cells. To accomplish those tasks continuously and adapt to the body requests, the respiratory act is normally under control of the ANS via the medulla oblongata

of the brain. During respiration, the mechanics of pulmonary ventilation make possible the inflow and outflow of air between the atmosphere and lungs, which change their volume because of their elastic structures.

The lungs can be expanded and contracted in two ways: (1) by downward and upward movement of the diaphragm to lengthen or shorten the chest cavity, and (2) by elevation and depression of the ribs to increase and decrease the anteroposterior diameter of the chest cavity [19]. At inspiration, the expansion of the chest cavity facilitates a decrease in internal air pressure, which forces air from outside the thorax into the lungs. Conversely during expiration, the reduction in size of the thoracic cavity increases the pressure, forcing air out of the lungs. In normal conditions, the expiration process is simply driven by the elastic recoil of the lungs. Each breathing cycle is thus defined as composed of the two phases of inspiration and expiration. Respiratory rate is the number of breaths within a set amount of time, usually one minute. Normal respiratory rate, called eupnoea, ranges from 12 to 20 breaths per minute (0.2 Hz to 0.33Hz) in resting healthy adults.

The respiration is known to influence the physiology of the heart in various ways, with effects which are essentially ascribable into two main classes: modulation of the heart rate (HR) and modifications of the heart electrical axis. Modulation of the heart rate essentially refers to oscillations in the interval between consecutive heart beats as well as the oscillations between consecutive instantaneous heart rates, i.e. heart rate variability (HRV). When heart rate variability is related with respiration, the phenomenon is called respiratory sinus arrhythmia (RSA), by which the interval between consecutive beats is shortened during inspiration and prolonged during expiration [22]. The magnitude of the oscillation is variable and changes from individual to individual. It has been demonstrated that RSA is a result of the functioning of SA node as cardiac pacemaker, whose firing rate is determined by the balance between the cardiac

sympathetic and vagal activities to the sinus node. The activity of the cardiac vagal nerve is assumed to be modulated by respiration and hence the sinus node activity is secondarily modulated by the respiratory rhythm. Regarding the genesis of RSA, both the respiratory and circulatory centers in the brainstem appear to be responsible [23].

Modifications of the heart electrical axis means the phenomenon of rotation and modulation of the cardiac electrical vector caused by contraction and expansion of the thoracic cavity during a respiratory cycle. The variations of the electrical vector connected with respiration arise from filling and emptying of the lungs and from the respiration-induced displacements of the heart [22]. The air flowing through the lungs leads to changes in the chest impedance distribution so affecting the measurements, whereas the cardiac shift is mainly due to the diaphragm movements since the pericardium is firmly attached to the central tendon of the diaphragm. During inspiration, the apex of the heart is stretched towards the abdomen because of the filling of the lungs, helped by the shifting down of the diaphragm. During expiration, the elevation of the diaphragm, for emptying of the lungs, compresses the apex of the heart towards the breast. Therefore, respiration induces a modulation of the heart electrical axis since it changes the angle that the electric cardiac vector makes with a reference line [24].

On the other hand, it has been observed a temporal variation in respiratory rate (RRV) during spontaneous breathing due to the bidirectional relationship between respiration and heart rate [21]. The RRV is caused by feedback mechanisms in much the same way that beat-to-beat heart rate fluctuations reflect different feedback mechanisms in cardiovascular control [25]. It has been demonstrated, that cardiac timing can be a significant determinant of RRV, altering breath-to-breath respiratory frequency.

2.4 ATRIAL FIBRILLATION

Atrial fibrillation is the most common arrhythmia, a serious and abnormal deviation of the normal heart rhythm generally associated with a rapid and irregular beating. It can occur at any age, but the incidence is rare in younger population and it becomes extremely common in elderly, with higher rates in subjects over 65 years old. Moreover, regional studies have reported a general increasing prevalence of AF compared to the last decade, especially prominent in the developed world [12]. The rise in prevalence is predominantly attributed to ageing of the population and to increasing incidence of cardiovascular diseases closely linked to AF, such as hypertension, coronary artery disease, heart failure, valvular heart disease, obesity and sleep-apnoea syndrome.

In contrast to normal sinus rhythm, when a single depolarization wave front propagates trough the atria from the SA node towards the ventricles causing contraction, atrial fibrillation is characterized by a disorganised depolarization of the atria with multiple wave fronts traveling simultaneously. The origin of this chaotic behaviour is ascribable to the presence of electrical discharges that overwhelm the regular impulses produced by the SA node. The sources of these disturbances are either automatic foci, often localized in the roots of one of the pulmonary veins, or continuing re-entry of an electrical impulse in the atria.
Normally, regular electrical impulses from the SA node are transmitted to AV node where they are delayed before entering the ventricular walls, but during AF the irregular stimulation causes the atrial activation to be shorter than the refractory period of the nodal cells. Consequently, the AV node works as a filter, blocking some electrical stimuli and limiting the number of ventricular beats. Rapid and irregular ventricular beating is anyway observed.
Moreover, the uncontrolled stimulation of the myocardium leads the atria to lose coordination with the ventricles, so the mechanical action turns out to be inefficient. Therefore, the blood flows passively through the atria into the

ventricles and the efficiency of ventricular pumping is considerably decreased, since the ventricles cannot be completely filled before each contraction. This condition is known to increase the risk for complications of AF, mainly stroke, which is likely to occur when a blood clot, arising from the blood stagnation of the inactive atria, is pumped out of the heart.

Atrial fibrillation may be also classified into acute and chronic forms. Three different types of clinical conditions are generally recognised: paroxysmal, persistent and permanent. In paroxysmal atrial fibrillation, the faulty electrical signals and irregular heart rate begin suddenly and then stop on their own within about a week. Persistent atrial fibrillation is defined by recurrent episodes of abnormal heart rhythm that last for more than a week; the episode may stop on its own or requiring a treatment. In case the treatment fails and the normal heart rhythm cannot be restored, the arrhythmia is referred to as permanent.

The intention of this work is to investigate the presence of respiratory modulation in the electrical activity of a diseased heart, hence the main challenge is to bypass the influence of the cardiac disorder. In our case, it is highly unlikely that RSA could be observed during arrhythmia, since the action of the ANS on the heart rate variability is masked by the numerous and irregular atrial contractions. Therefore, the indirect extraction of respiratory activity can be pursued only counting on measures of the variation of the heart electrical axis, as it will be better explained later in Chapter 3.

Chapter 3. THE ECG AND THE RESPIRATORY SIGNAL

3.1 THE ELECTROCARDIOGRAM (ECG)

The electrocardiogram (ECG) is the standard, risk-free and inexpensive tool, which tapes the electrical activity from the heart in order to detect a wide variety of cardiac abnormalities. It is based on a number of electrodes on the body surface, which record the electrical field around the main electrical impulse propagation (current) in the heart. For this reason, the ECG reflects information from a relatively large body volume, thus making spatial resolution poor [26].

The ECG signal, often called just ECG, is the tracing of potential difference measured between two electrodes (lead), which means that a minimum of two electrodes must be placed on the subject. The location of electrodes influences the recorded signal and produces a view of the heart from different angles (Figure 4). Therefore, each lead includes a specific information and a type of noise, which are different from the others. For this reason, it is useful to have multiple leads, that offers a complete view of the heart. Traditionally, the ECG is measured with three different lead systems[1] : the three bipolar leads (I, II and III), the six precordial leads (V1 –V6) and the three augmented unipolar leads (aV1 – aV3). These leads are collectively referred to as the standard 12-leads ECG configuration [20]. The three bipolar leads are originally described by Einthoven [27] and known as Einthoven's Triangle; they are originated with fixed electrodes to the right arm, left arm and left leg. Together with the augmented limb leads they form the electrical frontal plane of the heart. The six precordial leads are measured by placing six electrodes directly on the chest for recording the potentials of the hearts electrical axis in the horizontal plane.

[1] For more detail on ECG electrical leads refer to the book *Bioelectrical signal processing in cardiac and neurological applications* [20].

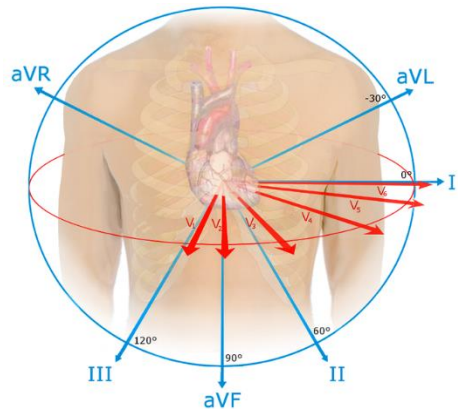

Figure 4 – Spatial orientation of different leads. The arrows indicate the direction of each lead; in particular, the blue ones define the frontal plate of the heart, while the red ones establish the horizontal plane. [https://commons.wikimedia.org/wiki/File:EKG_leads.png]

Another typical placement of electrodes on the body surface is the orthogonal lead configuration, where a pair of electrodes are positioned along mutually perpendicular lines. These orthogonal leads are also synthesized through a transformation of the standard 12-lead ECG (Dower Transformation) and used to have three leads with perpendicular axes. They are fundamental for producing the vectocardiogram (VCG), which is traced out by plotting the end point of the cardiac electrical vector in a three-dimensional space over the cardiac cycle. It provides a time-varying description of how the magnitude and direction of the dominant depolarization waveform change over time [20].

When a depolarization wave front is moving towards the electrode a positive-value amplitude is observed in that lead (channel) and a negative when moving away. Similarly, a repolarization wave front gives a negative-value amplitude when moving towards the electrode and so on. So according to the heart conduction system explained in the Chapter 2, the ECG has a typical structure for the first bipolar lead shown in the Figure 5.

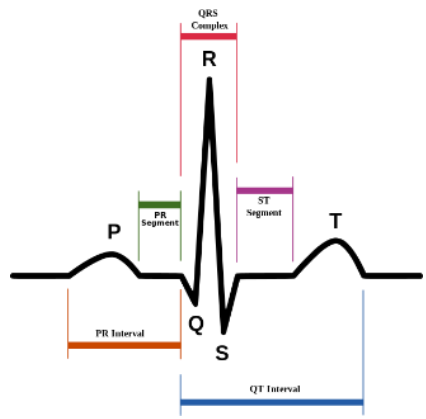

Figure 5 – A schematic representation of part of an ECG waveform, corresponding to a cardiac cycle. The y-axis corresponds to potential and the x-axis to time. [https://commons.wikimedia.org/wiki/File:SinusRhythmLabels.svg]

The P wave is caused by the propagation of the depolarization wave front during atrial depolarization. The QRS complex is a result of ventricular depolarization and the last deflection is the T wave which corresponds to ventricular repolarization. Atrial repolarization occurs at approximately the same time as the QRS complex and is therefore invisible [26].

This typical structure of the ECG is altered by cardiac dysfunction, so different shapes, amplitudes and rate could be observed. In case of atrial fibrillation, the ECG is characterized by an irregular ventricular rhythm and a fluctuating baseline in the form of f-waves, which occur in place of P waves [26]. The P wave indicates the depolarisation of the atria, while their contraction begins about 25 ms after the onset of the P wave [28]. Since the non-coordinated depolarization wave front propagates within the atria to the SA node during the atrial fibrillation, as described in Chapter 2, the P wave is not registered. Thus, multiple wave fronts may exist simultaneously and propagate around blocked regions, which make an irregular transmission of the impulses to the ventricles [29]. These re-entry loops are shown in the ECG signal as f-waves, so, in case of AF, these small fluctuations cover the isoelectric line. The Figure 6 shows two ECGs: the one on the top in AF, while the other one in normal condition.

The arrows highlight the differences between them: the red one shows the f-waves and the purple one indicates the P wave, which is missed in an ECG in AF.

Figure 6 – Scheme of atrial fibrillation (top) and sinus rhythm (bottom). The purple arrow indicates a P wave, which is lost in atrial fibrillation. [https://commons.wikimedia.org/wiki/File:Afib_ecg.jpg]

3.2 THE BELT RESPIRATORY SIGNAL

The belt respiratory signal gives a measure of changes in chest and/or abdominal volume and it is also known as plethysmogram [30].

There are two primary methods of non-invasive chest and abdominal plethysmography, which are based on different kinds of sensor fixed to a long hook and loop strap that is placed around the chest or abdomen. Optionally, in some application a second respiration sensor is placed around the chest for helping abdominal breathing recording. So according to the integrated sensors, there are measurement of changes in elastic belt tension and measurement of changes in electrical inductance.

3.2.1 Elastomeric plethysmography

An elastic belt will exhibit a change in tension as the chest or abdomen expands or contracts. This change in tension can be easily measured and converted to a voltage by a variety of methods. The most common is through piezo-electric sensor, i.e., a crystal that directly generates a voltage when compressed or stretched [30]. This resistive belt has the disadvantage that all types of

movements, as turning of the torso, will cause spike wave distortion in the piezo; for this reason, it is more sensitive to movement artefacts compared with the others. The resistive belts have signals with lower amplitude and more noise, but they are cheaper and easier in use [31].

3.2.2 Respiratory inductance plethysmography (RIP)

An elastic belt into which a coiled wire is sewn (to allow for expansion and contraction) is worn around the chest or abdomen. An alternating current (AC) is passed through the belt, i.e. a loop of wire, generating a magnetic field normal to the orientation of the loop (Faraday's Law). The frequency of the alternating current is set to be more than twice the typical respiratory rate in order to achieve adequate sampling of the respiratory effort waveform. The act of breathing changes the cross-sectional area of the patient's body creating an opposing current within the loop directly proportional to the change in the area (Lenz's Law). This opposing current can be measured through changing in the frequency of the applied current and it represents an accurate representation of the change in cross-sectional area [30]. The signal from inductive belt always have a large amplitude and are rather stable in relation to movement artefacts, because it does not rely on belt tension [31].

The Figure 7 shows the RIP signals extracted from two belts on the chest and abdomen, they are used to obtain indirectly other respiratory information as the respiratory rate and tidal volume, i.e. the volume inspired and expired with each breath [32].

The Figure 8 represents a belt respiration signal from the database; the cycles of respiration (inhalation and exhalation) are clearly visible. The signal reflects the sinusoidal profile of the respiration.

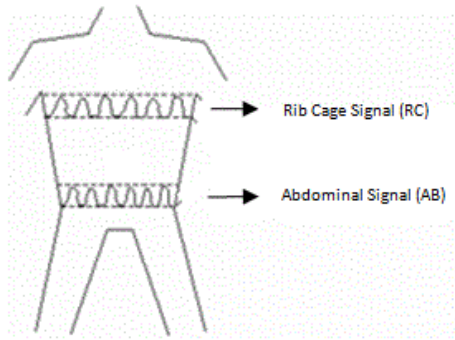

Figure 7 – Drawing of dual band respiratory inductance plethysmograph with bands on torso. [https://commons.wikimedia.org/wiki/File:Rip_Bands.gif]

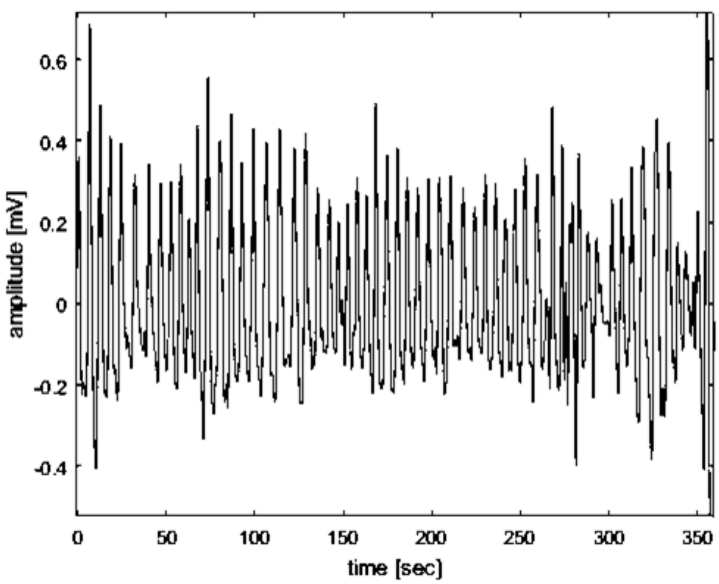

Figure 8 – Reference respiration of a patient from the used database.

3.3 DATASET

The study is based on a dataset containing registers from 57 patients with persistent AF (67 ± 7years, 16 females) acquired at the Cardiology department of San Paolo Hospital in Milan, Italy. Patients underwent electrical cardioversion, according to the international guidelines (i.e. an AF episode

lasting longer than 7 days and requiring termination by electrical cardioversion). The mean duration of arrhythmia was 6±1 months.

Before electrical cardioversion, every patient underwent physical examination, transthoracic and trans-esophageal echo-cardiographic evaluation. Two non-orthogonal leads (fs = 1000Hz) and the belt respiratory signal (fs = 50 Hz) were obtained with a Task Force® Monitor (CNSystem; GRAZ, Austria) recording system. The morning before electrical cardioversion, recordings were acquired at rest in all patients, and during a passive orthostatic stimulus (75 degree of tilting) in 25 patients of the study group.

Head-up tilt test was performed at 75°, with 10 second time necessary to move from 0 to 75° or to go back. Both phases lasted about 15 min. Raw data were exported as ASCII text files for off-line analysis. The study was approved by the Ethics Committee, and all patients gave their written informed consent to participate.

After a first inspection of the database, a total of eight patients was excluded from the study for the following reasons:

- 3 of them because of insufficient quality of the respiratory signal since the spectra of the respiratory signal did not exhibit a dominant peak in at least 50% of the total duration of the recording;
- 2 of them because of the presence of an evident periodic modulation of the respiratory signal, which may refer to the Cheyne-Stokes pattern;
- 2 of them because of the percentage of ectopic beats higher than 20% over the total number of beats;
- 1 of them because the heart rate was not high enough to assure aliasing-free estimation of the respiratory frequency.

In conclusion, a dataset of 49 patients has been selected for this study.

Chapter 4. STATE OF ART: EDR ALGORITHMS

The electrocardiogram signal includes considerable respiratory information due to a mutual bond between the cardiac and the pulmonary system as explained in Section 2.3. This relationship can be observed in changes of QRS morphology and heart rate, which are not considered for the intended-use of the ECG signal. In particular, there are three dominant effects of respiration on ECG: the respiratory sinus arrhythmia, the QRS morphology modulation and the baseline wander.

The action of breathing results in the same kind of frequency modulation in the ECG spectrum. It has been shown that respiration and HR are strongly correlated at around 0.3 Hz [22]. This type of HRV is called respiratory sinus arrhythmia (RSA) and it refers to the cyclic variation in heart rate, which accelerates during inspiration and decelerates in expiration [33]. The Figure 9 makes a comparison of the ECG and the arterial blood pressure (ABP) with the respiratory signals, which are the tidal volume (TV) and the airway of O2 tension [34]. It is noticeable the relation between the heart rate variability and the respiration.

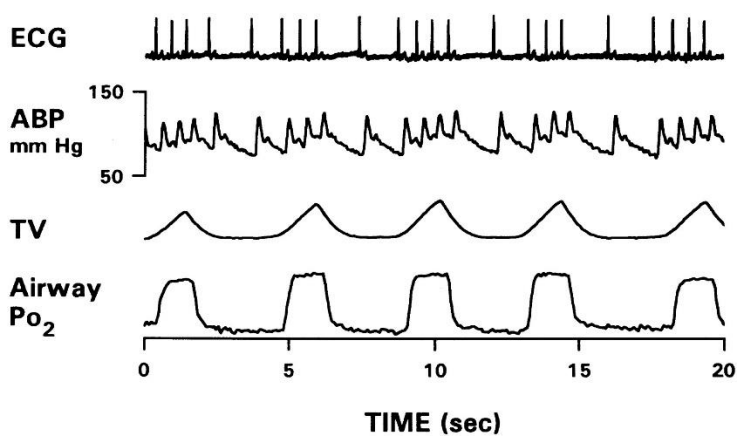

Figure 9 – The picture compares different type of signals: electrocardiogram, arterial blood pressure, tidal volume and airway O2 tension [34].

Yet another influence of the respiration on the ECG signal is the QRS morphology alteration due to changes in the main cardiac vector, since it is noticed a modulation of the RS amplitude and the slopes of the QRS complex over time. These modifications for each beat are discovered to be linked with the act of breathing [24]. It has been experimentally shown that respiratory induced modulation of the electrical axis is caused mainly by the motion of the electrodes relative to the heart, while the thoracic impedance changes contribute to the electrical rotation as a second order effect [22]. Appropriate positioning of the ECG electrodes can maximise the respiration-induced modulation; it is suggested that Lead II for example, shows greater modulation than lead I [35]. Figure 10 represents a one-lead ECG and the corresponding reference respiration signal from Moody et at. [2] work. The R-S amplitude of the ECG changes with respiration along time and it is roughly proportional to respiratory tidal volume [2].

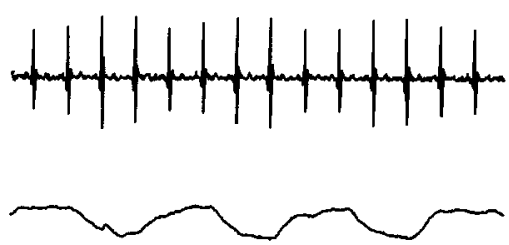

Figure 10 – The first signal is an ECG signal with a clear QRS amplitude variation that resemble the respiration (second signal) [2].

The last effect of respiration on ECG is a sinusoidal low frequency wander, which can also be caused by respiration [20] due to the motion of chest electrodes with respect to the heart. The amplitude of the ECG signal also varies by about 15 percent with respiration [36]. This can be clearly noticed in a signal of the studied dataset, as shown in the Figure 11, where ECG contains low frequency variation that visually seem to resemble the respiration.

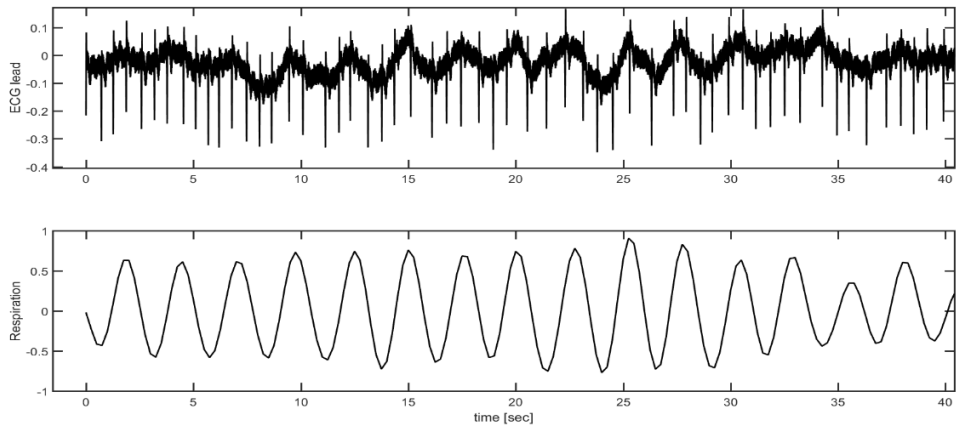

Figure 11 – ECG and respiration of a patient over 40 sec.

Different ECG – Derived Respiration (EDR) methods have been developed during years in order to extract respiratory information from ECG exploiting these alterations induced by respiration. They can be divided in three principal categories based on: morphological beat variations, heart rate changes and techniques which take advantage from both of them. Some methods are a very accurate during sleep studies, whereas others are proved to be robust during stress testing, so the choice of a particular EDR algorithm depends on the application.

As mentioned the respiration modulates the heart rate, increasing during inspiration and decreases during expiration, and thus the EDR can be extracted by methods based on RSA. In particular, these techniques take into account the HF components in the HRV signal (above 0.15Hz) where the respiratory information are included. The first, who investigated this field, were **Pallas-Areny et al.** [35]; they showed that the respiration results in the same kind of frequency modulation in the ECG spectrum as does RSA. Thus, the EDR could be obtained from RR interval series using singular value decomposition to track the most important instantaneous frequencies of the interval series [37]**.** The respiratory information can also be extracted through other methods based on

HR series using S-transform [38] or adaptive filters, applied to a series of RR intervals and the corresponding series of R wave amplitudes [39]. These techniques based on HR cannot be used in case of atrial fibrillation, where the RR intervals are irregular and so they do not contain any respiratory information as explained in the section 2.4. For this reason, these methods are not considered and described in more detail and the same is applied for those which combine the HR information with beat morphologic variations. Just to quote an example, **Leanderson et al.** [40] presented a method to extract respiratory frequency from the dominant frequency of the cross-power spectrum of the signals related to rotation angles and heart rate.

For the scope of the thesis, only the methods that exploit morphological beat variations can be considered, since RSA cannot be observed in case of atrial fibrillation. The table below shows a list of the main methods based on beat-to-beat morphological variations.

QRS area:	1985	Moody et al. [2]
	1994	Zhao et al. [41]
	1996	Caggiano et al. [15]
	1998	Travaglini et al. [24]
	2003	De Chazal et al. [42] Mazzanti et al. [43]
	2008	Park et al. [44]
	2015	Atri et al. [5]
R amplitude:	1992	Khaled et al. [45]
	1997	Felblinger et al. [3]
	1998	Dobrev et al. [6]
	2001	Mason et al. [16]

	2003	De Chazal et al. [42]
	2007	O'Brien et al. [46]
Angles from VCG-loop alignment:	1985	Pinciroli et al. [47]
	2003	Leanderson et al. [40]
	2006	Bailon et al. [1]
QRS characteristics:	2014	Làzaro et al. [17]
Discrete Wavelet Transform and Band-pass Filtering:	2002	Yi et al. [48]
	2009	Boyle et al. [49]
PCA:	2003	Bianchi et al. [50]
	2010	Langley et al. [10]

Specifically, the beat-to-beat variations in QRS-morphology are caused by rotation of the electrical axis of the heart due to chest movements and changes in the thorax impedance distribution. The first, who studied this effect of respiration –induced heart displacement on ECG, was **Einthoven et al.** [27] and later **Flaherty et al.** [51]. Then the first EDR method based on morphologic variation was proposed by **Wang et al.** [52] in 1974. Their work shows that it is possible to estimate respiration from the rotation of the intrinsic components of the vectocardiogram (VCG) relative to the torso.

Later in 1985 **Pinciroli et al.** [47] proposed an algorithm which exploits variation in the direction of the electrical axis. This was calculated as the least-squares (LS) straight line which fits the projections of the VCG on the plane

defined by two leads. The variations of the angle between the electrical axis and a reference direction was defined as an EDR signal. In the same year, **Moody et al.** [2] present a simple technique to extract respiratory patterns through multi-leads QRS area measured over a fixed window. The technique can be applied with one or two leads, preferably with orthogonal leads to avoid a systematic but harmless error in axis direction estimation. This method based on beat-by-beat measurements of the mean cardiac electrical axis direction relative to lead axis direction has been shown to be robust and accurate, unless some disturbances, which are reflected only in tidal volume changes as obstructive apnoea. **Zhao et al.** [41] use a similar method applied during heart rate variability (HRV) studies. In addition, they figured out a more analytical way to determine how well the derived waveforms correspond to the recorded respiration signal through the comparison of their power spectra. The following year **Caggiano et al.** [15] studied the effect of variable window for the calculation of QRS area with two methods: independent and dependent leads. The QRS complex is not assumed to be symmetrical; so the Q, R, and S-waves are detected for each QRS complex and for each lead (Independent leads method) or just for one lead (Dependent leads method). Based on the cross-correlation and coherence results, the variable QRS window, dependent leads method was consistently more accurate than the other tested methods. In 1998 **Travaglini et al.** [24] continued the study for extracting the EDR from the angle changes in the cardiac vector proposed by Pinciroli et al. [28]. After the definition of an eight-dimension space by eigenvalue analysis of a learning set, each 8D QRS area vector was projected onto the main direction, which was considered as particularly sensitive to respiratory information, and this projected QRS area was used to define the EDR signal. In 2003 **de Chazal et al.** [42] produced an EDR signal from the area enclosed by the baseline corrected ECG signal in a window of 100ms after the R wave. In the same year **Mazzanti et al**. [43] applied the method of Travaglini et al. [24] to extract the

respiratory frequency and to detect the presence of apnoea. In 2008 **Park et al.** [44] considered the area enclosed by the QRS complex in a 60ms fixed window centred in the R-waves. They also proposed a method for the optimal lead selection with Hilbert transform. The latest work based on QRS area, in the best of our knowledge, is the study of **Atri et al**. [5] in 2015. The ECG-derived respiration signals, in this case, were acquired by summing the amplitudes in an R-peak-centered window of 100 ms (from 50 ms before R peak to 50 ms after R peak). Moreover, they proposed a new feature obtained by higher order spectrum analysis of HRV and EDR regarding their non-linearity and non-Gaussianity in order to automatically detect obstructive sleep apnoea.

In 2003 **Leanderson et al.** [40] proposed a method based on least squares estimation of the rotational angles of the heart electrical axis between successive VCG loops and a reference loop. It exploits the fact that the normal range of respiration-induced axis shift is between 2 and 12 degrees, peak-to-peak [2]. In other words, the three EDR signals obtained are the angles of the rotation matrix defined by the minimisation of a distance criterion after the spatiotemporal alignment of VCG loops with the reference. Moreover, this study found out that the orthogonal leads constitute a better basis for estimating the respiratory frequency than do a subset of the leads. **Bailon et al.** [1] extended this method introducing an exponentially updated reference loop and testing it on a stress test database.

Among others in 1992 **Khaled et al.** [45] found out that a respiratory surrogate can be obtained by simply plotting the peak of the R waves with respect to baseline after filtering the ECG with an eighth-order 2.5–25Hz band-pass filter. **Felblinger et al.** [3] affined this method for a single channel of ECG during respiration monitoring in magnetic resonance sequences. In a similar manner **Dobrev et al.** [6] used a single lead QRS complex peak-to-peak amplitude method to extract the EDR in order to detect apnoea in infants. In particular,

after high-pass filtering with 5 Hz cut-off and then a 40 Hz low-pass filtering on the ECG, the EDR sample is the sum of the absolute values of the R- and the S-waves amplitudes (smoothed with a second order Butterworth 2 Hz cut-off low-pass filter). These methods based on R-wave amplitude either with respect to the baseline or to the S-wave amplitude from a single channel of ECG are also applied in the work of **Mason et al.** [16] in 2001. In particular, the S-wave was defined as the minimum value in a window of 0.1 seconds after the R-wave. However, the main aim of Mason et al. [16] is the definition of a method for quantitatively assessing respiration derivation algorithms. Finally, **O'Brien et al.** [46] used the R-wave to baseline method and then the amplitudes were evenly interpolated in time corresponding to the average heart rate of the given series. They ascertained that single ECG lead methods for estimating the respiratory signal are well correlated with inductance plethysmographs and that single lead respiratory estimates can classify epochs of sleep disordered respiration with approximately 82% accuracy.

A new method for estimating the EDR signal was proposed by **Lázaro et al.** [17] in 2014. This is based on QRS slopes and R-wave angle, which reflect respiration–induced beat morphology variations. This work combined the information from several EDR signal in order to increase the robustness of estimation. The proposed techniques outperformed other methods in two different clinical tests (tilt and stress test).

Yet another group of EDR methods based on beats morphology variation includes the work of **Yi et al.** [48] and **Boyle et al.** [49]. The former derived the EDR by reconstructing the detail signal of 9th decomposition from discrete wavelet transform of the ECG. The latter compared different wavelet decomposition methods, band pass filtering methods, and HRV based methods tested on a database, which covers activities of daily living and overnight

studies. It concluded that the best results are obtained combining a HRV method with a filter between 0.2 and 0.8Hz.

The work of **Bianchi et al.** [50] found out a method to extract respiratory information through the first principal component of the centre of gravity and the three directions of the three-inertial axes, where their estimate axis was obtained through spatiotemporal alignment of successive QRS-VCG loops with respect to a reference loop. Another algorithm for analysing changes in ECG morphology based on principal component analysis (PCA) was presented in 2010 by **Langley et al.** [10]. PCA is applied to the aligned collection of beat features from single-lead ECG recordings (P wave, QRS complex, T wave or the full ECG cycle). The PCs are a linear transformation of the beats with transformation coefficients given by the eigenvectors, that provide the surrogate respiratory signal in the analysis.

Chapter 5. SIGNAL PROCESSING METHODS

5.1 INTRODUCTION

This chapter follows and explains the general structure of the workflow, which is shown in the block diagram Figure 12, designed to answer the main question of this thesis. Given a database with two leads ECG and a belt respiratory signal for each patient, a pre-processing step and then a beat analysis are performed to reduce as much as possible misleading estimates caused by conditions of poor signal quality. Then, a method for f-waves cancellation in QRST interval could possibly be included at this stage. Its contribution for improving the accuracy in the estimation of the respiratory frequency of the overall process can be evaluated, by carrying out a comparison with the same workflow without any cancellation of the fibrillation activity.

Different EDR methods are applied and they are elucidated later in this chapter. Thereafter the output of this block, the EDR signal, is processed similarly to the respiratory signal to compare them in a reliable way. For a further comparative relation, the dominant respiratory rate over time is estimated from both signals; then, by comparing with the gold standard, a statistical analysis is applied to determine which EDR methods turn out to be reliable for the extraction of the actual respiratory rate from the ECG in our case.

The different used algorithms and processing methods have been implemented in MATLAB, a high-level language and interactive environment for numerical computation, visualisation, and programming [53].

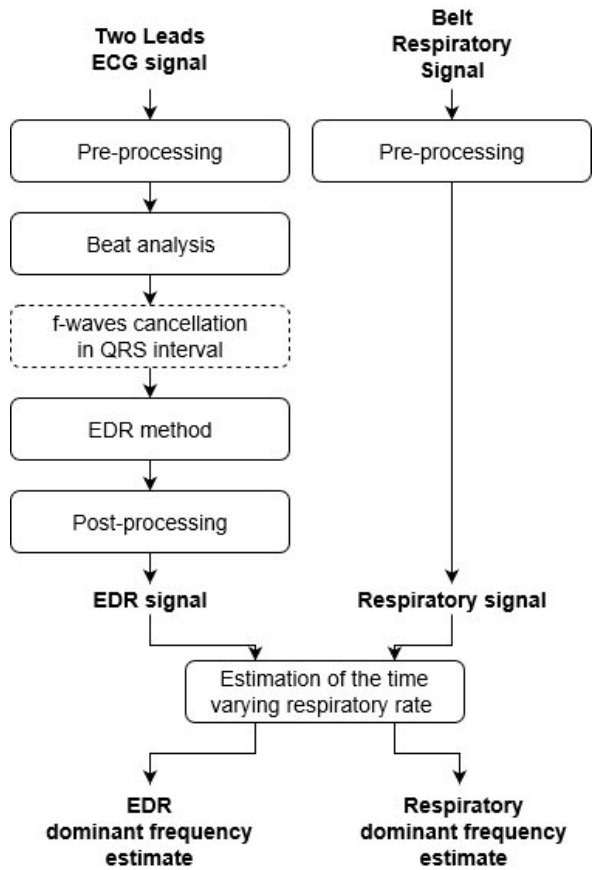

Figure 12 – Block diagram of the code workflow.

5.2 ECG PRE-PROCESSING

The pre-processing step is an essential stage in every signal-processing algorithm whose scope is to extract the desired information from a signal. It is performed with the purpose of improving the quality of the original raw signal, by removing and/or attenuating those components that are considered as noise, depending on the main scope of the study.

When dealing with an ECG signal, the most common noise components are represented by baseline wander, power-line interference and artefacts coming from electrodes displacement and muscular activity. The latter types of noise are generally the most challenging in many ECG applications, since their

spectral content overlaps the frequency band of the ECG and exceeds at higher frequencies. Examples of baseline wander, powerline interference and high frequency noise are shown in Figure 13 a, b and c respectively.

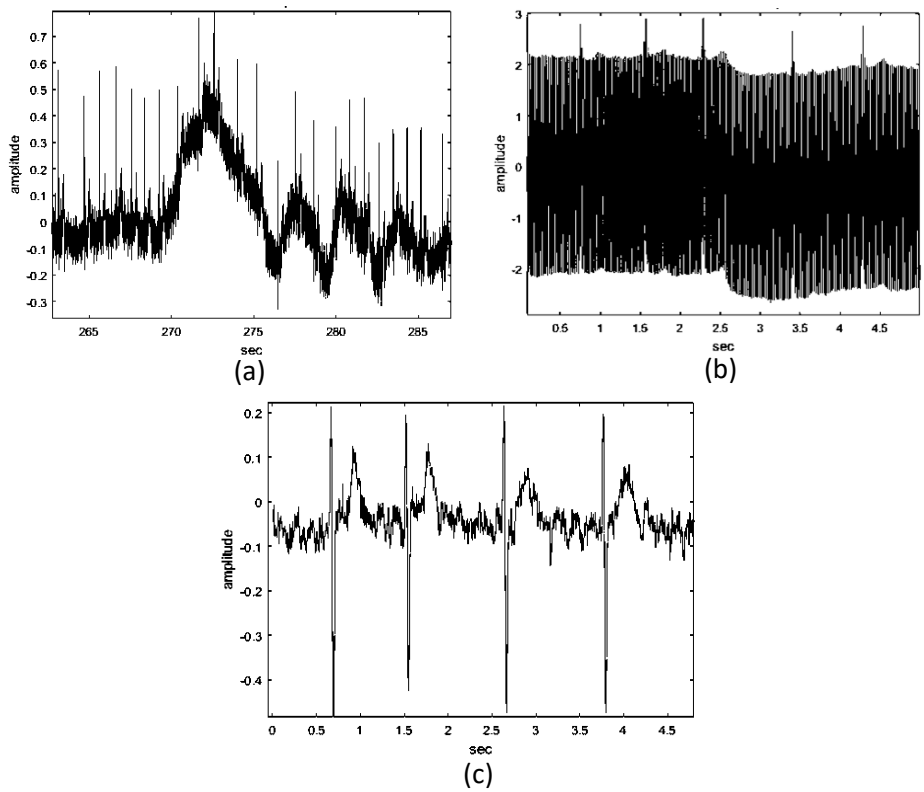

Figure 13 – Examples of signal noises that are treated in the pre-processing step: a) baseline wander, b) powerline interference and c) high frequency noise.

Through the years, a wide range of different filtering techniques have been proposed to deal with ECG noise. However, in most cases their applicability strongly depends on the application and should be tested against the distortion of the desired information. After previous verification, the pre-processing methods that turned out to suit properly to the case of this thesis are performed and they are described in the following sections.

5.2.1 Baseline wander

Baseline wander is an extraneous, low-frequency activity in the ECG whose removal is required in order to minimize changes in beat morphology, which do not have cardiac origin. In fact, it may commonly result from a variety of noise sources including perspiration, respiration, body movements, and poor electrode contact [20]. In case of an ECG with atrial fibrillation, yet another source of minor fluctuations in the baseline is represented by f-waves. The most common technique for dealing with the baseline wander removal is the cubic spline method[2], which is also applied as pre-processing step for EDR algorithm in other works as in [1]. However, the presence of f-waves makes infeasible its application in the case study, because of the poor accuracy in the determination of representative samples ("knots") within the isoelectric line.

Therefore, instead of performing polynomial fitting, a linear, time-invariant, high-pass filtering with cut-off frequency at 0.5 Hz is applied to the signals in the database. The cut-off frequency has been selected according to the frequency content of the baseline wander, which is usually in the range below 0.5 Hz, and according to the lowest frequency component of the ECG spectrum so that the signal remains undistorted [20].

A forward-backward IIR filtering is employed to meet the magnitude requirements more easily by using a much lower filter order, which turns out to be doubled by filtering in both directions, in addition to the zero-phase transfer function. However, when dealing with high ECG sampling rate, like in our case 1000 Hz, the only use of the forward-backward filtering to remove baseline wander should be avoided, due to the risk of instability of the filter. For this reason, a "sampling rate alteration" stage, described in [20], is added to perform the filtering of the baseline wander on a signal sampled at a much lower rate

[2] For more information regarding the cubic spline technique for attenuation of the baseline in a ECG lead, the authors refer to the book [20].

than the original ECG. An example of the outcome of such filtering procedure is shown in Figure 14. Therefore, the baseline wander removal consists of three steps, as shown in Figure 15:

- decimation of the original signal to a lower sampling rate, in this case 100 Hz, better suited to filtering in order to remove high-frequency content of the signal,
- forward-backward low-pass filtering (5th-order Butterworth filter) to estimate the baseline wander,
- interpolation of the processed signal back to its original sampling rate.

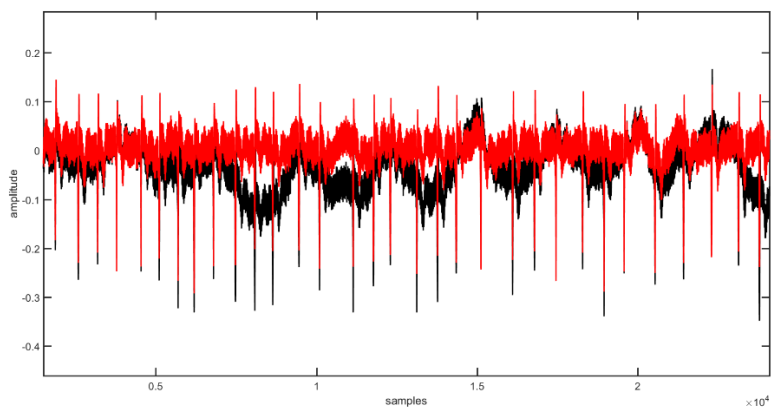

Figure 14 – Example of an ECG before and after baseline removal

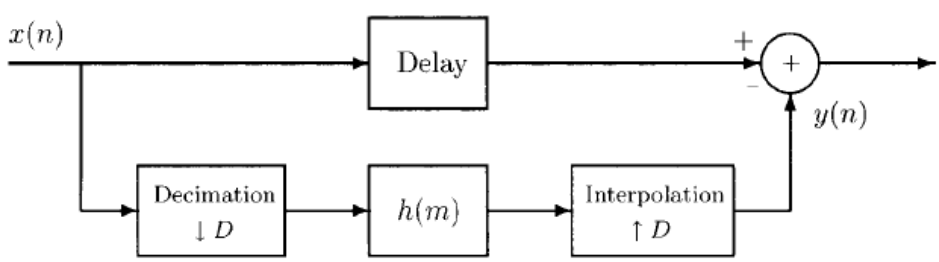

Figure 15 – Block diagram of the used baseline removal method. Adapted from [20]

5.2.2 High frequency noise and power-line interference

The high frequency noise, which may be caused by different sources such as electrode motion and muscle activity, are attenuated in this work through a fourth order Butterworth low-pass filter. The cut-off frequency is set at 40 Hz in order to keep only the information contained in the frequency band of the QRS complex, which spans from few hertz to 40Hz [20], and discard all the other components which may mask the desired respiratory information.

After filtering in the forward direction, the filtered sequence is then reversed and run back through the filter using the filtfilt function in MATLAB. The forward-backward filtering makes possible the use of IIR filter, since the overall result is filtering with a zero-phase transfer function that remedies the non-linear phase response of the IIR filter [20].

Although the low-pass filtering at 40Hz, the ECG signal may still contain an attenuated powerline interference, characterized by 50 or 60 Hz sinusoidal noise that must be removed. Several techniques were presented to remove this kind of noise, ranging from straightforward linear, band-stop filtering to more advanced techniques which handle variations in powerline frequency and suppress the influence of transients manifested by the occurrence of QRS complexes [20]. In this thesis, a forward-backward IIR filtering is applied by using a fourth-order Butterworth stop-band filter at 50 Hz. It has been visually verified that the stop-band filter is not introducing ringing artifacts at both sides of the QRS complex. The Figure 16 and Figure 17 show an example of ECG signal in the database and the correspondent FFT before and after the removal of the powerline interference.

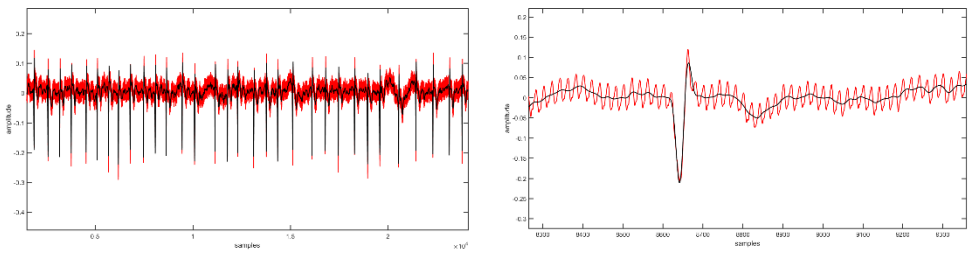

Figure 16 - The first plot shows the entire ECG before the filtering (red) and after it (black). A short segment is zoomed in the second plot for better visualisation.

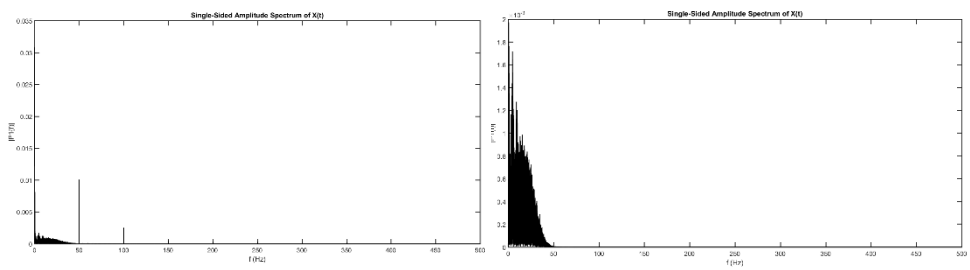

Figure 17 - The spectrum of the ECG shown in the Figure 16 is represented before and after filtering.

5.3 BEAT ANALYSIS

For each subject the information about time locations of heartbeats, referred as fiducial point in this thesis, and beats classification have been extracted through the LundECG Signal Processing Toolbox for MATLAB, developed by the Biomedical Signal Processing research group at Lund University.

After that, an analysis of the beats in the ECG signal is required in order to remove or substitute those QRS complexes with a strange morphology and select those with a predominant morphology before applying any EDR method. In this context, two different categories of beats are considered noteworthy: beats with abnormal morphology and noisy beats. Some examples of these beats in the analysed database are shown in Figure 18, Figure 19, Figure 21 and Figure 22.

The first category includes those QRS complex whose morphology is either clearly affected by an unusual conduction of the electrical impulse through the heart, i.e. ectopic beats, or altered by artifacts of exogenous origin, such as sudden body movements or electrode motion. They are signal alterations that could not be completely removed in the pre-processing step without introducing any distortion of the desired information and so they are treated in this phase.

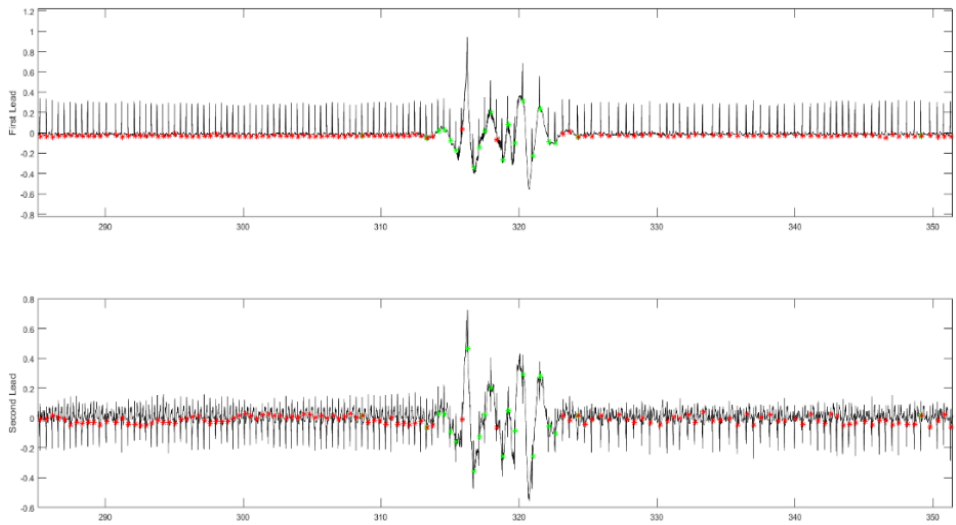

Figure 18 - Example of an artifact in the ECG due to sudden body movement

The second category refers to beats whose signal-to-noise ratio (SNR) remains poor even after pre-processing and therefore it is reasonable to exclude them from consideration in the EDR algorithm.

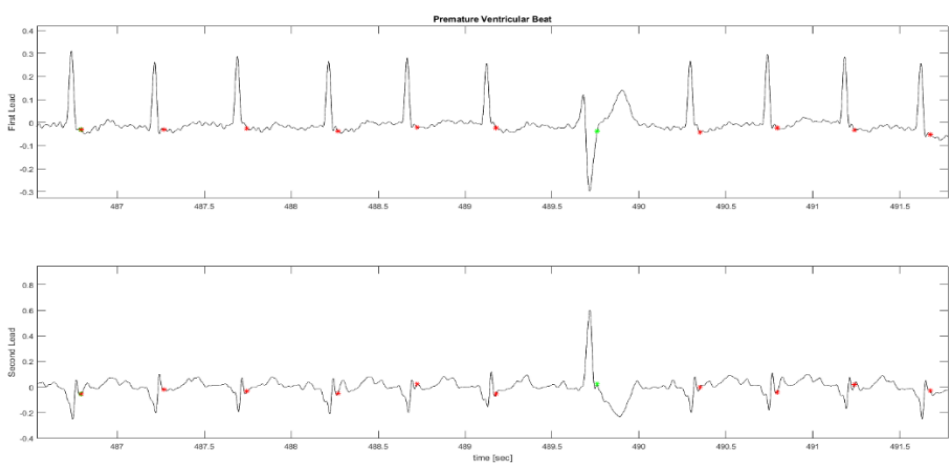

Figure 19 - Example of a premature ventricular contraction clearly visible in both leads.

The two categories of beats are managed in different way. The beats with abnormal morphology generally are common to both leads, so they are always discarded. As regarding noisy QRS complex, instead, they are substituted when occurring in just one lead and discarded when detected in both leads, since the SNR measurement is lead independent.

The object here is to perform a beat analysis proper enough for the scope of the thesis, in order to prevent the performances from being affected by the presence of spurious QRS complex in the ECG signal.

5.3.1 Detection of beats with abnormal morphology

The algorithm used in this thesis for the detection of abnormal beats is inspired to the work of Martinez et al. [54] and it is based on a morphological characterization of each ventricular beat in atrial fibrillation ECG recordings. More specifically, it makes use of morphological descriptors and thresholds to obtain a decision rule and determine if a beat is normal or not. Differently from the cited work, some of the original descriptors are rejected and a new one is added to perform the detection on a database with two unspecified leads. It means that the typical morphology of the normal QRS complex for the single lead is unknown a-priori; therefore, it has been required to make the algorithm more flexible for different QRS shapes referring to normal contractions.

As a preliminary step, the time occurrences of R-peaks t_k are estimated by considering an interval from 100 ms before to 20 ms after the fiducial point r_i. The direction of the R-peak (if upward or downward) is determined from the average beat of each lead: if the prominence of the highest positive peak in the QRS complex is over 150 μV, the R-peak is considered upwards and downward otherwise.

Thereafter, two points around the R-peak, γ_{QRS-} and γ_{QRS+} are established. They are defined as the closest points to the R-peak in which the amplitude is 30% of this peak amplitude, $y(\gamma_{QRS-}) = y(\gamma_{QRS+}) = 0.3y(t_k)$.

Finally, four descriptors to characterize the QRS morphology of the beat are defined, see Figure 20, as:

- Area of the QRS complex (At_k), i.e., the sum of the pre-processed ECG samples between the identified boundary points:

  $At_k = \sum_{i=\gamma t_k\, QRS+}^{\gamma t_k\, QRS-} y(i)$.

- Number of samples between γt_{kQRS+} and γt_{kQRS-} (Dt_k), i.e.:

  $Dt_k = \gamma t_{kQRS+} - \gamma t_{kQRS-}$.

- Amplitude of the R-peak, i.e.: $y(t_k)$.
- ECG amplitude at the fiducial point, i.e.: $y(r_i)$.

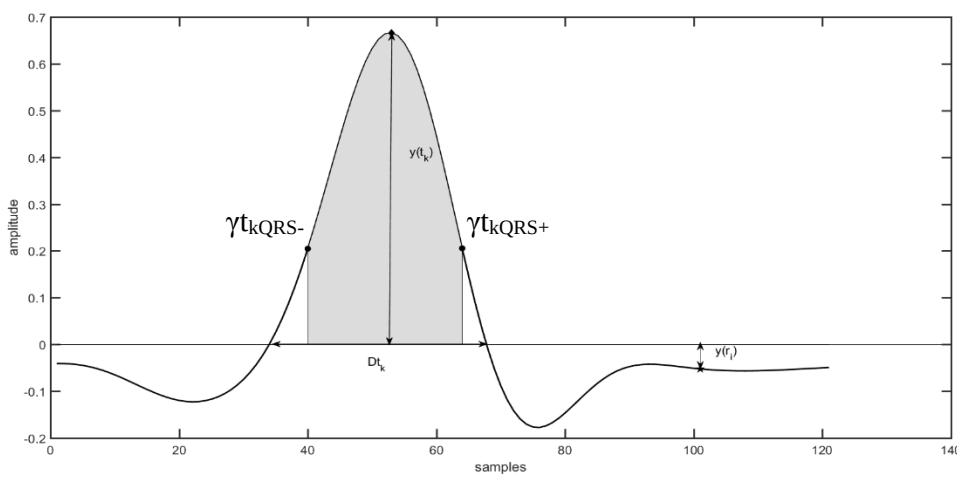

Figure 20 - QRS complex with the descriptors used.

To classify a ventricular beat as normal or not, its descriptors are compared with those corresponding to the average of its preceding 25 beats detected as normal. A decision scheme based on a sequence of four rules is built, such that a beat is classified as normal when none of the rules is satisfied in none of the two leads. In contrast, it is considered as abnormal when any of the rules is fulfilled in each of the two leads. These rules have been experimentally obtained and can be mathematically expressed as follows:

- Rule 1: $|\mathrm{A}t_k - \overline{At}| > C * \sigma_{At}$
- Rule 2: $|\mathrm{D}t_k - \overline{D}| > C * \sigma_D$
- Rule 3: $\left|\mathrm{y}(t_k) - \overline{y(t)}\right| > C * \sigma_{y(t)}$
- Rule 4: $\left|\mathrm{y}(r_k) - \overline{y(r)}\right| > C * \sigma_{y(r)}$

$\overline{At}$, $\overline{D}$, $\overline{y(t)}$ and $\overline{y(r)}$ are the descriptors averaged for the 25 normal beats preceding those under classification, i.e. the *k*th beat; σ_{At}, σ_D, $\sigma_{y(t)}$ and $\sigma_{y(r)}$ are the standard deviations of the descriptors for the same beats and $C = 7$. When a beat turns out to have a strange morphology in just one of the two leads, a second check is performed in the lead when none of the rules has been satisfied, by applying the same decision scheme but lowering the value of C to 5 for all the rules. If the beat results then to be abnormal in both leads, then it is rejected or classified as normal otherwise.

Obviously, this approach requires, as a starting point, the selection of 25 normal beats, which are considered enough to derive the physiological variance in terms of QRS shape among normal beats. Instead of using manual selection, the initialization is based here on the average of the cross-correlation values of each beat with all the other beats in an initial 30-beats segment of the ECG. The first 25 beats, whose cross-correlations values are larger than a certain threshold, set to the median minus three standard deviation of the mean correlation values, are initialized as normal beats.

5.3.2 Detection of noisy beats

The excessive noise present in a single lead, which could not be removed in the pre-processing step, may mask the respiratory-induced variation in the ECG, especially in terms of the rotation information [1] and the morphology modulation. It leads to the risk of increasing the presence of outlier estimates in the EDR signal. Hence, a noisy beat detection is performed in each lead and if possible the detected ones are substituted by using an exponentially update beat as it is carried out in the work of Bailon et al. [1].

This passage follows two main steps: the characterization of the noisy beats with high Signal-Noise Ratio (SNR) and the replacement of them with an exponential average beat.

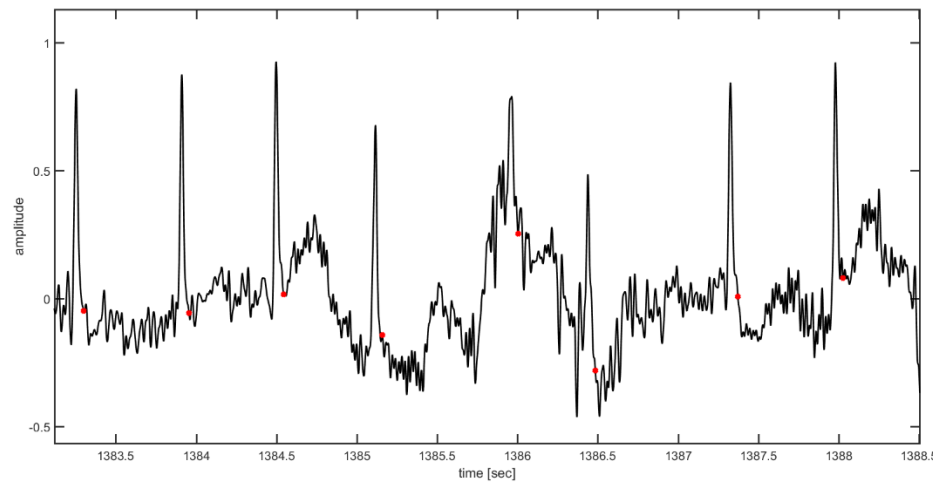

Figure 21 - Example of a beat with poor SNR at low frequencies.

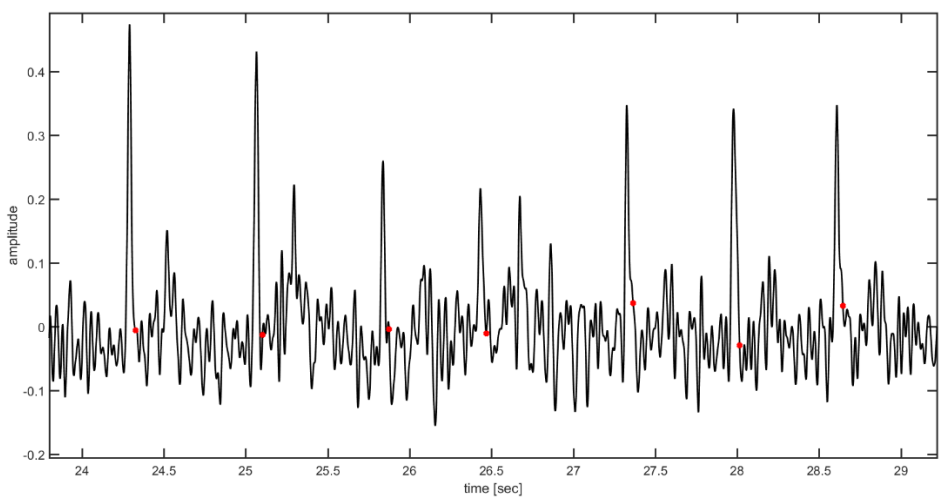

Figure 22 - Example of a beat with poor SNR at high frequencies.

The SNR is computed for each beat considering high frequency (HF) and low frequency (LF) noise, which are mainly due to muscle activity and remaining baseline wander respectively.

The SNR_{HF} is defined as the ratio of the peak-to-peak amplitude in an interval, that spans 100 samples before and 20 samples after the QRS mark, and the root-mean-square (RMS) value of the HF noise (using a Butterworth filter with cut-off frequency at 20 Hz) in a HR-dependent interval. The SNR_{LF} is defined as the ratio of the peak-to-peak amplitude of the exponentially update average beat of each class and the RMS value of the residual ECG after average beat subtraction and low-pass filtering (using a Butterworth filter with cut-off frequency at 20 Hz).

Beats whose SNR_{HF} or SNR_{LF} is lower than a threshold, set at 0.7 based on a study on a smaller dataset, are substituted by their corresponding averaged beats. The exponential updated average beat used for beat substitution is calculated as follows:

$$\mathbf{Y_R}(i+1) = \alpha \mathbf{Y_R}(i) + (1-\alpha)\mathbf{Y}(i+1)$$

where i denotes the beats index, $\mathbf{Y_R}(i)$ is the exponential average beat and $\mathbf{Y}$ is the next beat to be averaged. The average (red line in Figure 23) is carried out on the 5 normal previous beats, as in [1], in order to keep the respiratory information from the lead where the beat is not noisy. The coefficient α is the forgetting factor set to 0.1 as in [1] and the initialization of the exponential average beat is set to a zero vector.

The formula for the exponential update average beat applied on all the beats of each class is the same to the one used for beat substitution with the only difference that, in the first case, it is used to derive a beat model.

Note that Bailon et al. [1] applied the beat substitution on the 12-lead ECG used to derive the VCG, so as to keep in it the rotation information. Differently from the mentioned work, the beat substitution is here performed on the ECG leads directly given as an input to the EDR algorithms, since the dataset consists of two-leads ECG for each patient.

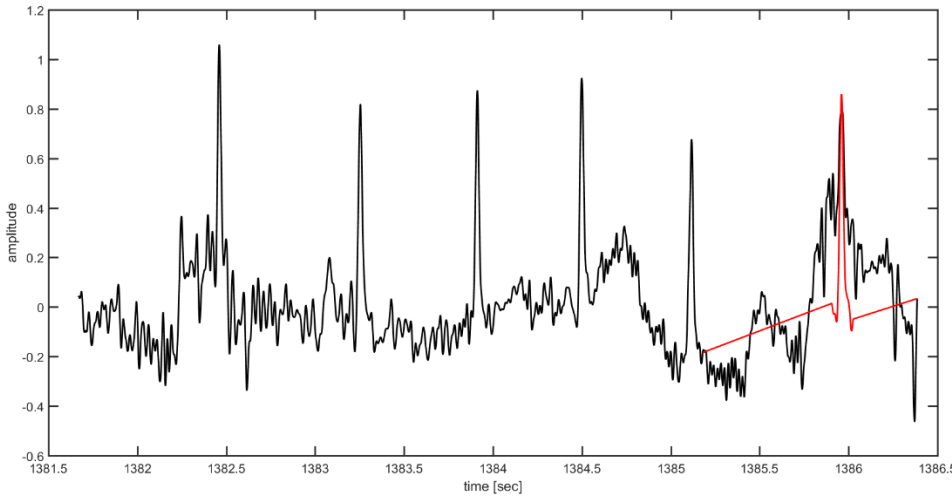

Figure 23 – Example of a noisy beat substitution.

5.4 F-WAVES REMOVAL FROM THE QRST SEGMENT

The surface ECG in atrial fibrillation is characterized by a fluctuating baseline, so-called f-waves, which occurs in place of the P waves. The presence of these f-waves could represent a source of noise for this study, given the possibility of introducing beat-to-beat modifications in the QRS complex unrelated with respiratory activity. In order to evaluate the influence of fibrillation activity on the EDR signal, a fibrillation signal is reconstructed from the previous TQ interval during the QRS segment and subtracted from each observed beat, adapting the method based on the extraction of a TQ-based fibrillation signal that is described in [29].

Prior to the reconstruction of the fibrillation signal, the detection of the TQ-interval, i.e. the segment between the end of the T-wave and the onset of the Q-wave, is required (Figure 24).

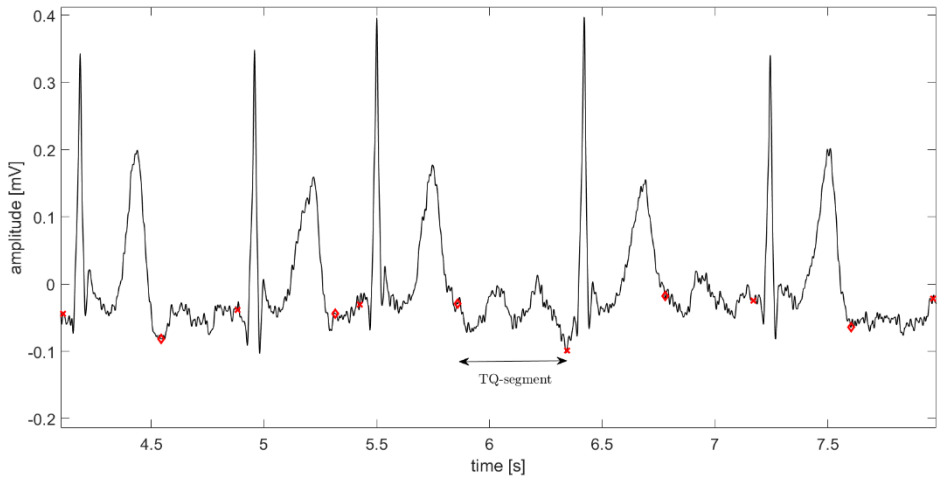

Figure 24 – Detection of consecutive TQ-intervals in an ECG segment.

Since in AF, the T wave is not always easily identifiable in presence of high amplitude f-waves, a fixed point for the end of the T wave is extracted from the average beat of each lead, excluding from the averaging those beats that have been rejected in the pre-processing phase. In case of TQ-segment shorter than 65 ms (minimum length for a fibrillation cycle), the TQ-based fibrillation signal is set to zero and no subtraction is carried out on the following QRS complex. The TQ-segments, that are long enough, are bandpass filtered in the frequency range [1 20] Hz with a 4th order Butterworth filter, to remove any residual baseline trend in the segment and bring out the fibrillation activity against the background noise.

Since the aim is to estimate the TQ-based fibrillation signal, which consists of consecutive fibrillation cycles, the information about the length, the morphology and the phase of a single fibrillation cycle within the TQ-segment need to be reliably extracted. The length of a fibrillation cycle, i.e. f-wave, is estimated from the autocorrelation function (ACF) of the filtered TQ interval by considering the time lag of the consecutive peak to the first negative peak in the function (Figure 25), as performed in [55]. Conversely, when the peak is

negative the overall TQ-segment is discarded since no clear periodic activity is found.

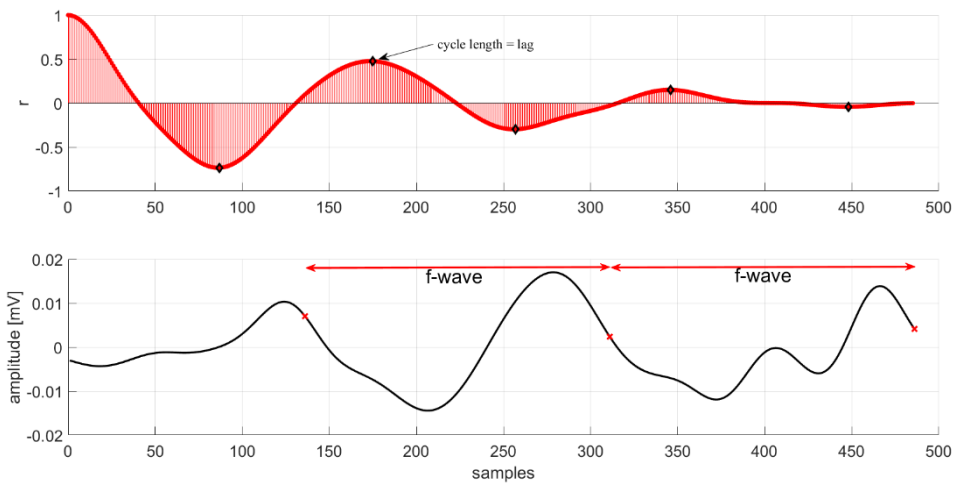

Figure 25 – Estimation of the fibrillation cycle length from the ACF of the relative TQ-segment.

The estimated fibrillation cycle length is verified to be neither shorter than 85 ms nor longer than 340 ms, given the oscillation frequency range of the f-waves in the range 3-12 Hz. It means that cycles lengths outside this range are considered unreliable and discarded.

The estimated length is used to extract the actual shape of the f-waves by averaging consecutive fibrillation cycles in the TQ-segment and to get rid of residual noise. The procedure starts from the fibrillation cycle closest to the Q-wave and goes backwards to the end of the T-wave, so keeping track of the information about the cycle phase.

The extracted fibrillation cycle prior to QRS complex is then replicated to cover the length of the following QRS interval. The outcome is low-pass filtered with a cut-off frequency of 40 Hz, to remove any high frequency component that may have been introduced in the replication phase due to amplitude mismatches between the starting and ending points of the fibrillation cycle.

The TQ-based fibrillation signal is then subtracted from the considered QRS complex as shown in Figure 26.

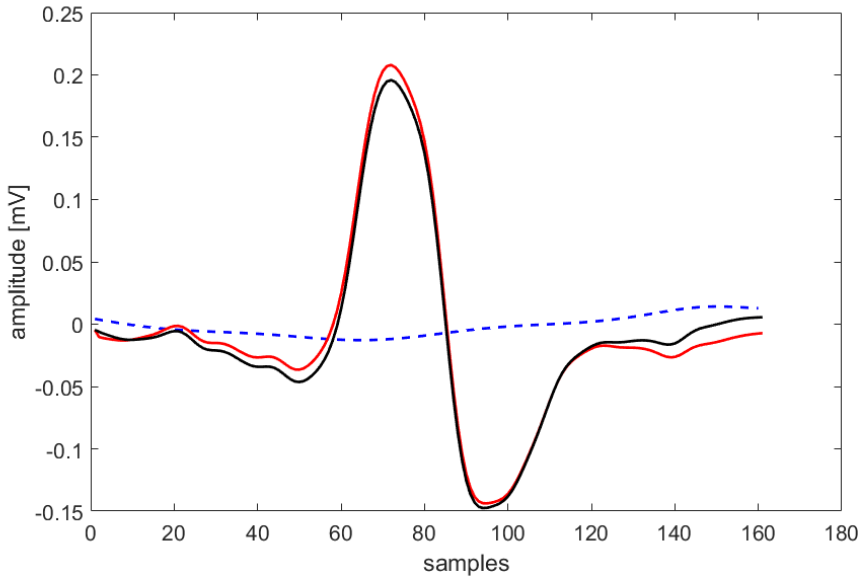

Figure 26 – QRS-complex before (black line) and after (red line) subtraction of the estimated TQ-based fibrillation signal (dashed blue line).

It is important to underline that the TQ-based fibrillation signal is constructed for each individual lead to allow for lead-independent AF properties, as in [29]. However, one relevant difference with the mentioned work is about the reconstruction of the fibrillation signal, which is carried out by taking advantage, where possible, of the information provided by adjacent TQ intervals. The fibrillation cycle prior to QRST complex is then replicated during the QRST interval but linearly weighing from one at the onset of the interval to zero at the end. An identical procedure is applied to the TQ segment following the QRST complex but in a time-reversed fashion. For the scope of this thesis, the use of TQ interval following the QRS complex has turned out to be unnecessary, since the interest is in the reconstruction of the fibrillation signal only during ventricles' depolarization, i.e. the QRS interval. Therefore, the extracted fibrillation cycle from the following TQ-interval would not be relevant and low weighted for the signal reconstruction. Moreover, when T-wave end is hard to accurately determine, especially in noisy signals, this

information may be even misleading and cause the introduction of artifacts in the QRS complex.

5.5 EDR ALGORITHMS

The main challenge of this thesis is to verify which EDR methods, listed in Chapter 4, can also be applied in case of atrial fibrillation. For this reason, the next step is to apply and test different EDR algorithms. As previously explained in Chapter 2, the focus inevitably is on the methods based on QRS complex morphology variations, since the characteristics of an ECG in AF do not allow exploiting HRV analysis for EDR extraction. Among them, the methods proposed more recently and with characteristics suitable to our study case are taken more in account.

5.5.1 QRS slopes and R-wave angles

In 2014 Lázaro et al. [17] proposed a new method for extracting the EDR signal based on QRS slopes and R-wave angle variations on two databases in tilt and stress test. More specifically, for each beat i and for each lead l, the upward and downward slopes of the R wave and the R wave angle, defined as the smallest angle formed by the straight lines that define these slopes, are measured.

To implement this method, the determination of the R-peak time instant $n_{\mathrm{R}\,l,i}$ in each beat is required, starting from the position of the given fiducial point. The R peak is found to be the maximum or the minimum peak in the interval from 100 ms before to 20 ms after the fiducial point, depending if the R-wave is upwards or downwards. The time instants corresponding to the Q-wave and the S-wave are defined respectively as the extreme points of the defined interval, $n_{\mathrm{Q}\,l,i}$ and $n_{\mathrm{S}\,l,i}$.

Subsequently time instants associated with the maximum variation points of the ECG signal between $n_{\mathrm{Q}\,l,i}$ and $n_{\mathrm{R}\,l,i}$ instants and between $n_{\mathrm{R}\,l,i}$ and $n_{\mathrm{S}\,l,i}$ instants are computed as follows:

$$n_{\mathrm{U}\,l,i} = \max_{n\in\left[n_{\mathrm{Q}\,l,i},\, n_{\mathrm{R}\,l,i}\right]}\{|l'_l(n)|\}$$

$$n_{\mathrm{D}\,l,i} = \max_{n\in\left[n_{\mathrm{R}\,l,i},\, n_{\mathrm{S}\,l,i}\right]}\{|l'_l(n)|\}$$

Where $l'_l(n)$ is the first derivative of the lead l:

$$l'_l(n) = l_l(n) - l_l(n-1)$$

Finally, a straight line is fitted to the ECG signal by least squares in a 8 ms-length interval centred at $n_{\mathrm{U}\,l,i}$ according to Lázaro et al. [17]; the same step is also carried out for the 8 ms-length interval centred at $n_{\mathrm{D}\,l,i}$. Since 8ms corresponds to 8 samples in a signal sampled at 1000Hz, it has been chosen to create a line, which spans 4 samples before and 4 samples after the considered central point. The extraction of the slope for the line that best fit (in a least-squares sense) the ECG is possible in MATLAB through the function polyfit, which returns the coefficients for a polynomial of a certain degree. The extracted slopes for a generic beat i are denoted $\mathfrak{T}_{US_{l,i}}$ and $\mathfrak{T}_{DS_{l,i}}$; each of them represents a sample in the relative EDR signal, which is then composed by series of all the upward or downward slope values of each QRS complex.

After the calculation of the slopes and assuming a two-dimensional Euclidean space coordinate system, the R wave angle can be defined by this general equation:

$$\phi = arctan\left(\left|\frac{\mathfrak{T}_1 - \mathfrak{T}_2}{1 + \mathfrak{T}_1\mathfrak{T}_2}\right|\right)$$

Where $\mathfrak{T}_1$ and $\mathfrak{T}_2$ denote the slopes of the straight lines forming the angle. The Figure 27 shows the relevant points on an example of QRS complex from the

database. The units of the horizontal axis (time) and vertical axis (voltage) were rescaled to match the particular case of conventional ECG tracings in clinical printouts, where a speed of 25mm/s and a fain of 10mm/mV are used as [17]:

$$\phi_{R_{l,i}} = arctan\left(\left|\frac{\mathfrak{T}_{US_{l,i}} - \mathfrak{T}_{DS_{l,i}}}{0.4\left(6.25 + \mathfrak{T}_{US_{l,i}}\,\mathfrak{T}_{DS_{l,i}}\right)}\right|\right).$$

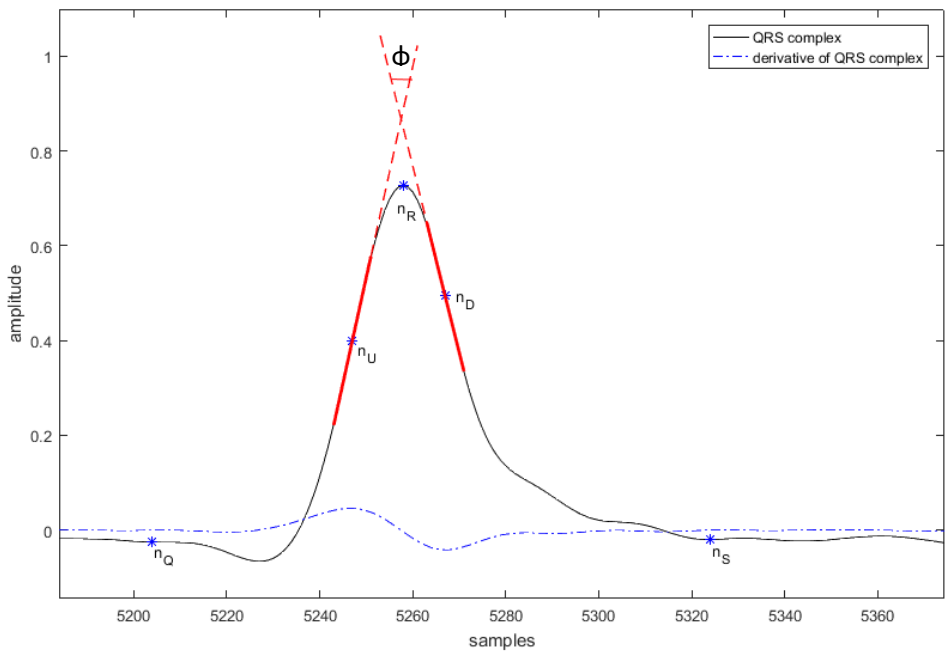

Figure 27 - Relevant points on an example of QRS complex. The thick red lines represent the two straight lines best suited to the QRS slopes by LS. The angle at the top of the R-peak represents the R-wave angle, given by the smallest angle formed by the two red lines.

Lázaro et al. [17] evaluated separately the QRS slopes and R-wave angle in estimating respiratory rate, but they found out that the combination of them reduces estimation error and increases measuring time with respect to considering them alone. Although the R-wave angles are computed from QRS slopes, their relation is non-linear, which may exploit complementary respiratory information to that obtained by the linear combination of QRS slopes [17].

Note that in [17] the method achieves the best results when it is applied on the three VCG leads, suggesting that inverse Dower transformation enhances beat morphological variations induced by respiration. Since the given database consists of two unspecified leads, it is not possible to derive the three orthogonal leads. However, the proposed technique was also tested on 12-leads ECG with good results, meaning that it is still reasonable to apply it onto the given database.

5.5.2 QRS area

Various EDR-methods based on QRS-area were proposed in past years and tested on healthy subjects. Some variants are implemented in this thesis with the purpose of testing their reliability for estimating rotations of the mean electrical axis related with respiration from a two non-orthogonal leads ECG corrupted by AF. Therefore, in all the presented methods, the projection of the mean electrical axis on the plane defined by these two leads is considered. The area of the i-th QRS complex is computed over a certain time interval in each lead, thus being proportional to the projection of the mean electrical axis on that lead [22].

The instantaneous projection of the mean electrical axis on the plane jk, defined by two generic leads j and k, at time instant t_i, can be defined as vector $\bar{\boldsymbol{m}}(t_i)$

$$\bar{\boldsymbol{m}}(t_i) = \begin{bmatrix} \frac{1}{\delta_1 + \delta_2} \int_{t_i+\delta_2}^{t_i-\delta_1} \|\boldsymbol{m}(t)\|_2 \cos(\theta_{jk}(t)) dt \\ \frac{1}{\delta_1 + \delta_2} \int_{t_i+\delta_2}^{t_i-\delta_1} \|\boldsymbol{m}(t)\|_2 \sin(\theta_{jk}(t)) dt \end{bmatrix} = \frac{1}{\delta_1 + \delta_2} \begin{bmatrix} A_j(t_i) \\ A_k(t_i) \end{bmatrix}$$

where $\theta_{jk}(t)$ is the angle between $m(t)$ and the reference lead j, $A_j(t_i)$ and $A_k(t_i)$ represents the area in lead j and k respectively. The integration interval over which the mean is computed is defined by δ_1 and δ_2. $\|.\|_2$ denotes the Euclidean distance. The term $\|\boldsymbol{m}(t)\|_2 \cos(\theta_{jk}(t))$ is representing the

projection of $m(t)$ on lead j and $\|\boldsymbol{m}(t)\|_2 \sin(\theta_{jk}(t))dt$ is the projection lead k.

The angle of projection of the mean electrical axis on the jk-plane with respect to lead j, as shown in Figure 28, can be estimated as:

$$\theta_{jk}(t_i) = \arctan(A_k(t_i)/A_j(t_i))$$

Finally, the fluctuations of this angle can be used as an EDR signal.

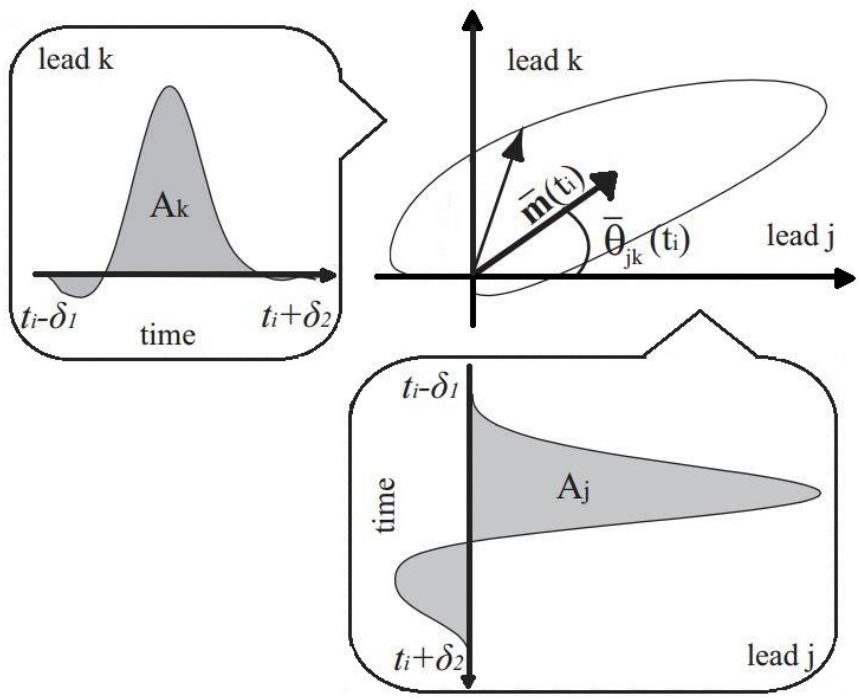

Figure 28 - Projection of the hearts mean electrical axis on the jk-plane. Modified figure from [29].

The reason for testing different methods based on QRS-area arises from the fact that the estimate is very sensitive to the window width, since the detection of the starting and ending interval's points becomes more challenging in AF with respect to a normal ECG due to the presence of f-waves. The values of δ_1 and δ_2 can be chosen to comprise the whole QRS complex, using a symmetric window around the R-peak, or an asymmetric window in order to reduce the QRS morphologic variations unrelated to respiration.

The variants to the QRS-area method tested in this thesis are inspired to the work of Moody et al. (1985) [2], Caggiano and Reisman (1996) [15], Mazzanti et al. (2003) [43] and Park et al. (2008) [44].

Moody et al. (1985)

The EDR signal is reconstructed by computing the area of each normal QRS complex in each of the two leads. In this case, the area is measured over a fixed window, which is determined on the average beat of each lead to match the interval from the PQ junction to the J-point of a normal QRS. Since the two leads are not orthogonal, a systematic but harmless error in axis direction estimation results [2].

Caggiano and Reisman (1996)

The three different methods proposed in this work for computing the QRS-area have been implemented. As a preliminary stage, each lead is shifted vertically by 110% of the absolute value of the minimum of the lead. This passage gives an ECG that contains all positive samples, as required before applying the following methods.

Fixed QRS Window, independent Leads Method

This method computes the area under the ECG during the QRS complex in a fixed window width, which is independent between the two leads. Thus, fixed window means that the width in each lead is the same for each QRS complex in that lead. More specifically, for each lead the R-wave and Q-wave are detected on the average beat to calculate the average Q-wave to R-wave length. The width of the fixed window is considered to be twice this average value. Known the relative time instants of the Q-wave with respect to the fiducial point and the average window width, the area under each QRS complex within the window is calculated in each lead. Then, the local baseline area is computed by

multiplying the minimum within the window per the length of the window. The local baseline area is subtracted from the previous calculated area and the resulting area is placed to correspond in time of the fiducial point. In this way, the obtained samples are unequally spaced and corresponding in time to the samples extracted with the other EDR methods.

Variable QRS Window, independent Leads Method

Differently from the previous method, the QRS complex is not assumed to be symmetrical, so the Q, R and S-waves are detected for each QRS complex. The detections for one lead are performed independently from the detections in the other lead.

Variable QRS Window, dependent Leads Method

In this case, the difference with the previous methods is that the two leads are not considered to be independent. The less noisy lead is selected to detect the Q, R and S-wave. The detection for the chosen lead are then referred as the Q, R and S-waves of the other lead. In this way, the same samples in time are considered for the calculation of the area under the QRS complex in each lead.

Mazzanti et al. (2003)

The area of each QRS complex is computed by using an approximation through the trapezoidal method, instead of summing up the amplitudes in a certain interval of interest as in the previous methods.

The calculation is carried out by fitting trapezoids to the ECG in an interval from 60 ms before to 20 ms after the R-peak, as in [1], and taking the total covered area. The selected time interval is considered to respond properly to the need of reducing the influence of f-waves in the considered QRS interval.

Park et al. (2008)

At last, the implementation of this method has required to take a fixed window of length 60 ms centred at the R-wave for the computation of the QRS area.

5.5.3 R amplitude

The modulation of R wave amplitude due to respiration was extensively studied, as explained in the Chapter 4. In this thesis, the algorithm proposed in 2001 by Mason et al. [16] is implemented, since it exploits two methods for deriving an EDR signal from a single ECG channel. The amplitude of the R-peak is measured both with respect to the baseline and to the amplitude of the S wave. The EDR signal based on the measure of the R-wave amplitude with respect to the S wave amplitude demonstrated to obtain higher sensitivity and positive predictivity compared to the EDR signal based on the R-wave with respect to baseline [16].

Note that the location of each QRS complex and the R wave peak in the ECG are determined using the given fiducial point as done before. The S-wave is found by searching for the minimum value (or the maximum value in case of downward R wave) of the ECG in a time window of 0.1 second after the R-peak. The difference in amplitude between the R-peak and the baseline, or the S wave, represents a sample of the EDR signal, then generated by linking successive points.

The following pictures (Figure 29 and Figure 30) show an example of the considered points by the R amplitude method.

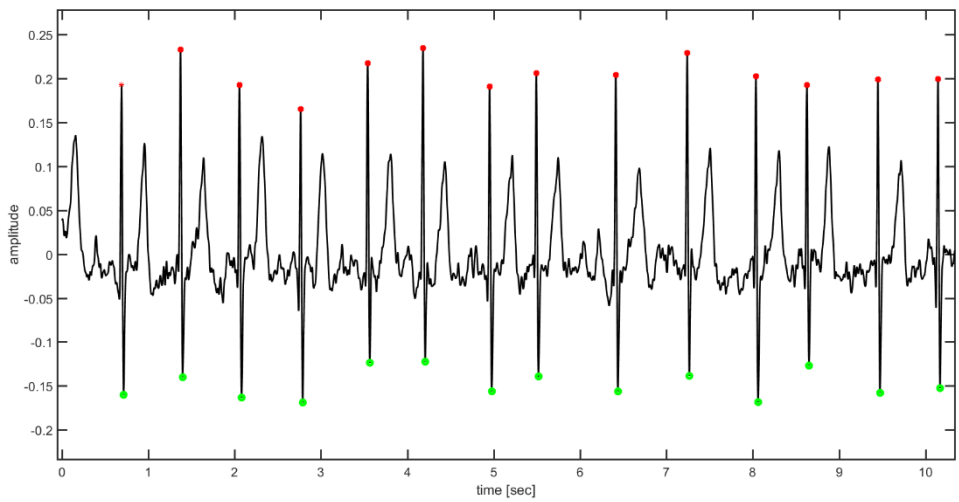

Figure 29 - The red dots point the position of the R peak and the green ones the position of the S wave for the calculus of the R amplitude EDR method.

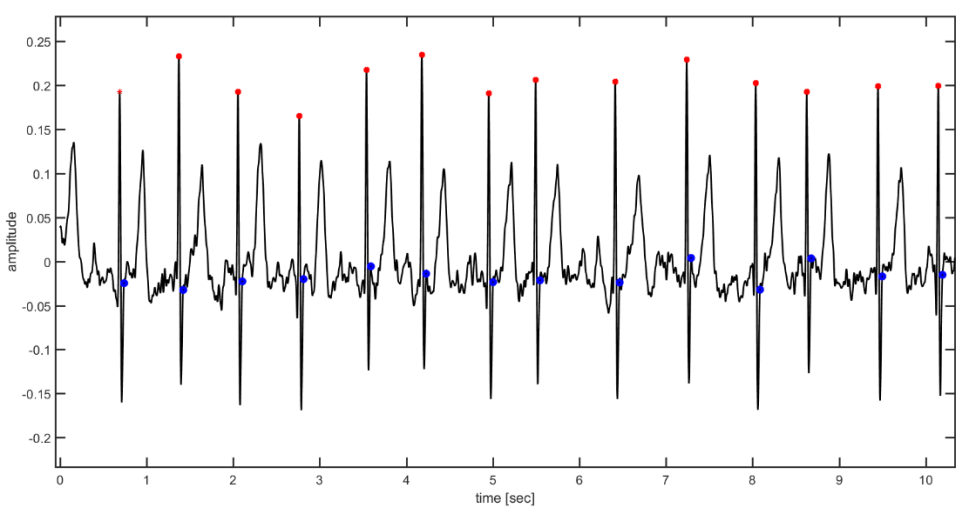

Figure 30 - The red dots point the position of the R peak and the blue ones the position of the fiducial point for the calculus of the R amplitude EDR method.

5.5.4 VCG loop alignment

The LS estimation of the rotation angles of the heart electrical axis based on successive QRS-VCG loop was proposed initially by Leanderson et al. [40] in 2003 and it was then successively improved by Bailon et al. in 2006 [1]. The latter version of the algorithm is applied in this thesis and it is here explained in detail.

The technique exploits the fact that successive QRS-VCG loops have similar morphology with a slightly different direction in space relative to a reference QRS-VCG during a respiratory cycle. Hence, it is possible to estimate a series of least-square (LS) rotation angle, which defines the EDR signal.

The method performs minimization of a normalized distance ε between a reference loop ($N\times3$ matrix $\mathbf{Y_R}$, where the columns contain the X,Y,Z leads) and each observed loop ($(N+2\Delta)\times3$ matrix $\mathbf{Y}$), with respect to rotation (3×3 matrix $\mathbf{Q}$), amplitude scaling (scalar γ), and time synchronization ($N\times(N+2\Delta)$ matrix $\mathbf{J}_\tau$), where N is the number of samples of the QRS complex analysis window, defined as:

$$\epsilon_{min} = \min_{\gamma,\tau,\mathbf{Q}}(\epsilon) = \min_{\gamma,\tau,\mathbf{Q}} \frac{\|\mathbf{Y_R} - \boldsymbol{\gamma}\,\mathbf{J}_\tau\mathbf{Y}\mathbf{Q}\|_F^2}{\|\boldsymbol{\gamma}\,\mathbf{J}_\tau\mathbf{Y}\mathbf{Q}\|_F^2}$$

The matrix $\mathbf{J}_\tau$ is equal to $[\mathbf{0}_{\Delta-\tau} \quad \mathbf{I} \quad \mathbf{0}_{\Delta+\tau}]$, where the parameter Δ denotes the number of symmetrically augmented samples which allow for time synchronization with τ = -Δ, …, Δ. The dimensions of the $\mathbf{0}_{\Delta-\tau}$, $\mathbf{0}_{\Delta+\tau}$ and $\mathbf{I}$ matrices are $N\times(N-\Delta)$, $N\times(N+\Delta)$ and $N\times N$, respectively. The operator $\|\cdot\|_F^2$ denotes the Frobenius norm.

The rotation matrix $\mathbf{Q}$ can be viewed as three successive rotations around each axis (lead), defined by the rotation angles ϕ_X, ϕ_Y and ϕ_Z:

$$\mathbf{Q} = \begin{bmatrix} 1 & 0 & 0 \\ 0 & \cos(\phi_X) & \sin(\phi_X) \\ 0 & -\sin(\phi_X) & \cos(\phi_X) \end{bmatrix} \begin{bmatrix} \cos(\phi_Y) & 0 & \sin(\phi_Y) \\ 0 & 1 & 0 \\ -\sin(\phi_Y) & 0 & \cos(\phi_Y) \end{bmatrix} \times \begin{bmatrix} \cos(\phi_Z) & \sin(\phi_Z) & 0 \\ -\sin(\phi_Z) & \cos(\phi_Z) & 0 \\ 0 & 0 & 1 \end{bmatrix}.$$

The normalized distance ε is minimized by first finding the estimates of γ and $\mathbf{Q}$ for every value of τ and then selecting that τ for which ε is minimum. For a fixed τ, the optimal estimator of $\mathbf{Q}$ is given by $\widehat{\mathbf{Q}}_\tau = \mathbf{V}_\tau \mathbf{U}_\tau^T$ where the matrices $\mathbf{U}_\tau$ and $\mathbf{V}_\tau$ contain the left and right singular vectors from the singular value decomposition (SVD) of $\mathbf{Z}_\tau = \mathbf{Y}_R^T \mathbf{J}_\tau \mathbf{Y}$. The estimate of γ is obtained by

$$\hat{\gamma}_\tau = \frac{tr(\mathbf{Y}_R^T \mathbf{Y}_\mathbf{R})}{tr\left(\mathbf{Y}_R^T \mathbf{J}_\tau^T \mathbf{Y} \widehat{\mathbf{Q}}_\tau\right)}$$

The parameters $\widehat{\mathbf{Q}}_\tau$ and $\hat{\gamma}_\tau$ are calculated for all values of τ, with $\widehat{\mathbf{Q}}$ resulting from that τ which yields the minimal error ε. Finally, the rotation angles ϕ_X, ϕ_Y and ϕ_Z are derived from $\widehat{\mathbf{Q}}$.

For reducing the influence of exercise-induced ST changes on the estimates, the work of Bailon et al. [1] follows up the idea of Leanderson et al. [40] introducing an exponentially update reference loop defined as:

$$\mathbf{Y}_\mathbf{R}(i+1) = \alpha \mathbf{Y}_\mathbf{R}(i) + (1-\alpha)\, \mathbf{Y}(i+1)$$

Where i denotes the beat index at time instant t_i. The parameter α is chosen such that morphologic variation is tracked while adaptation to noise is avoided. The initial reference loop $\mathbf{Y}_\mathbf{R}(1)$ is defined as the average of the first ten loops, on condition that every loop has a cross-correlation coefficient with the first loop that exceed 0.9 in all leads. In our work, the QRS complex analysis window has been adapted to the given fiducial points, so it comprises 120 ms (100ms before and 20ms after the fiducial point) and it symmetrically augmented by 30

ms to allow time synchronization in steps of 1 ms. A forgetting factor of α = 0.8 is used in the present study.

Note that the method requires three orthogonal leads in order to generate the VCG loop and it needs all these channels to create the matrices for extraction of the angles in contrast to the Lázaro et al. [17] methods, which are single-channel. Therefore, the method described above is modified to adapt to the case of two unspecified leads ECG.

In this case the QRS complex is projected on a plane, so the minimization of a normalized distance ε between a reference loop ($N\times2$ matrix $\mathbf{Y_R}$) and each observed loop ($(N+2\Delta)\times2$ matrix $\mathbf{Y}$) with respect to rotation (2×2 matrix $\mathbf{Q}$), amplitude scaling (scalar γ), and time synchronization ($N\times(N+2\Delta)$ matrix $\mathbf{J}_\tau$) is defined as above and it is applied for each beat, see Figure 31 and Figure 32.

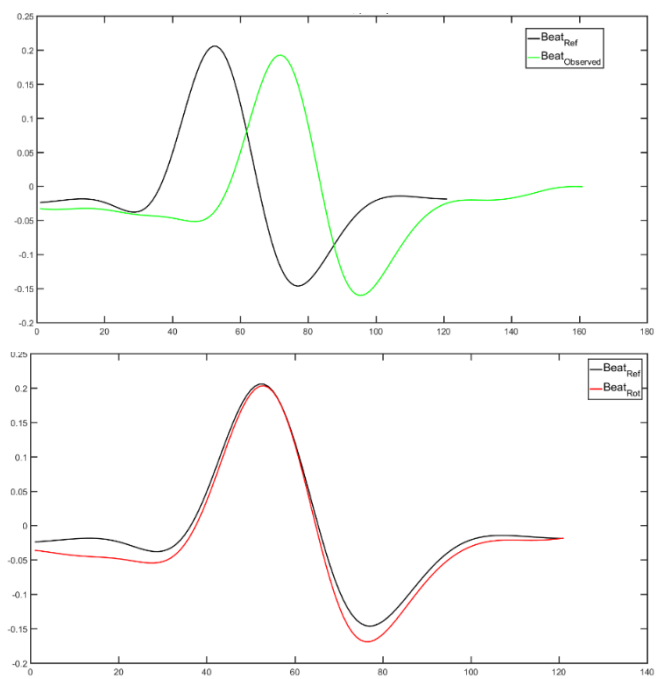

Figure 31 - Example of a reference beat (black) and an observed beat (green) on a single lead before minimization (top image) and after minimization (bottom image) of the normalized distance between them with respect to rotation, amplitude scaling and time synchronization.

This gives as result the matrix $\widehat{\mathbf{Q}}$, which minimizes the normalized distance ε and is the optimal estimator of **Q** for fixed τ, as explained above. The EDR sample is extracted as an angle of this matrix, which is strictly dependent on the used leads. For this reason, the new EDR signal cannot contain the whole respiratory information that could be extract by the heart, because the VCG is not used and thus a systematic error in the axis direction estimate results from this computationally convenient assumption [2].

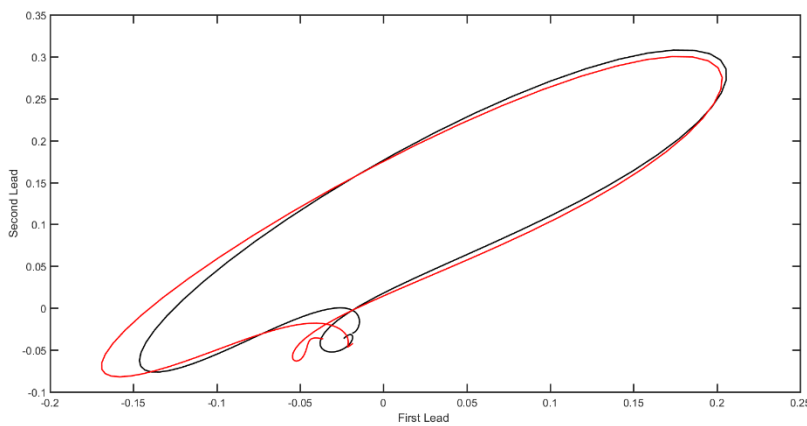

Figure 32 - Example of the reference loop (black) and the observed loop (red) on the plane defined by the two leads.

5.6 POST-PROCESSING OF EDR

The raw EDR signal coming out from the EDR algorithm already exhibits the oscillatory waveform characteristic of a respiratory signal (

Figure 33).

Depending on the method, one or more EDR signals can be extracted and each of them is a beat-to-beat series, whose samples account for a specific QRS morphologic feature. Moreover, at this stage the samples of the EDR signal are unequally spaced, since the sampling rate is determined by the beats time occurrences in the ECG. Consequently, the signal is still strongly dependent on

the beat quality of the original ECG, so it may contain outliers due to minor artifacts in the QRS complex and missing estimates caused by the abnormal/noisy beats, which have been previously rejected. Therefore, the output of the EDR algorithm needs to pass through some basic processing steps before trying to estimate the dominant frequency in the signal. Inspiring to the work of Lázaro et al. [17], the post-processing stage consists of:

- Outlier rejection;
- Linear interpolation;
- Resampling at 4Hz;
- Band-pass filtering;
- Unreliable estimates removal in EDR.

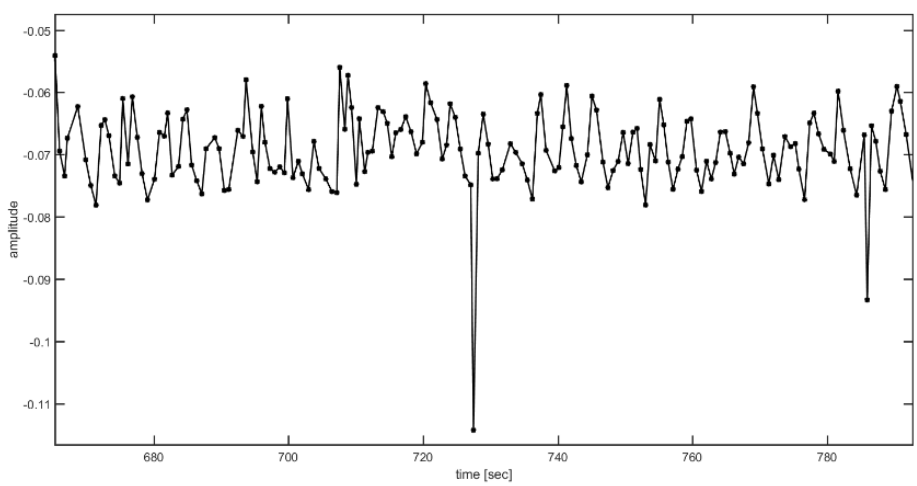

Figure 33 - EDR signal: series of samples from a QRS feature of each beat.

The presence of outliers in the EDR signal may result in a disturbance for the estimation of the dominant frequency. For this reason, the estimates that are suspected to be unreliable must be discarded. The adopted outlier correction algorithm removes every sample outside the interval $[med_y - \eta_y,\ \ med_y + \eta_y\ ]$, where med_y is the median of previous N_sample_{EDR}, and η_y is the standard deviation (STD) of those N-samples times a constant C [1].

The constant C is set to 5 and the N_sample_{EDR} is chosen by considering an interval of 30 sec, which has demonstrated to work properly on the examined database. In particular, N_sample_{EDR} is made dependent on the mean HR of each patient, in order to handle the sample density of the EDR signal, which becomes even more unstable in atrial fibrillation. Therefore, N_sample_{EDR} spans from 17 to 41 samples according to the minimum and maximum heart rate (52 beats/min – 123 beats/min) in the considered database.

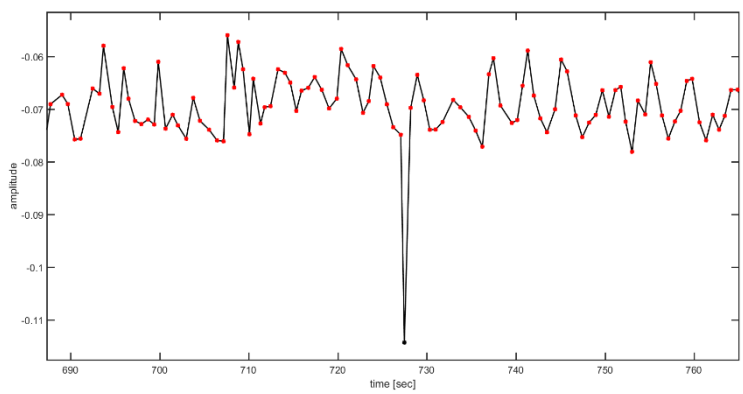

Figure 34 - Comparison between the original EDR (black) and the EDR samples after the outlier correction (red).

The EDR signal coming out from outlier rejection, see Figure 34, presents missing values in correspondence of the discarded beats and detected outliers. Since in the next stages the signal will be resampled and filtered, there is a serious risk of introducing distortions in correspondence of those gaps. This problem has been solved by replacing the missing samples through linear interpolation on the existing ones, that has required to use the function `interp1` in MATLAB. The interpolation is a polynomial fitting of given samples and depends on the order of the polynomial. The linear interpolation is performed by using a straight line to interpolate the samples as show in the Figure 35.

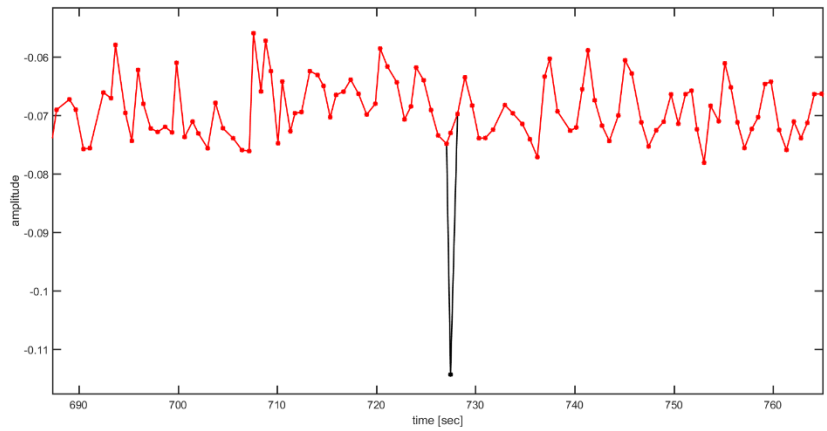

Figure 35 - Section of the EDR signal after the linear interpolation (red line). The black line shows the original EDR signal before the outlier correction, in that way it could be observed as the outlier is replaced by a sample obtained from a linear interpolation.

The EDR signal is then resampled at 4 Hz and interpolated using a cubic spline so as to derive an evenly sampled signal. The interpolation is carried out by applying the MATLAB function `interp1` setting this time the third-order polynomial fitting. As described in [20], the interpolated EDR y(t) is computed for the interval $[t_i\ t_{i+1}]$ by incorporating the three samples $x(t_i)$, $x(t_{i+1})$ and $x(t_{i+2})$ into the Taylor series expanded around t_i, where $x(t_i)$ are the samples of successive beats located at the times t_i with i=0, 1, ….

$$y(t) = y(t_i) + (t - t_i)y^{(1)}(t_i) + \frac{(t - t_i)^2}{2}y^{(2)}(t_i) + \frac{(t - t_i)^3}{3}y^{(3)}(t_i)$$

Where:

$$y^{(1)}(t_i) \approx \frac{x(t_{i+1}) - x(t_i)}{t_{i+1} - t_i};$$

$$y^{(2)}(t_i) \approx \frac{6\left(y(t_{i+1}) - y(t_i)\right)}{\Delta t_{i_1}^2} - \frac{2\left(2y^{(1)}(t_i) + \left(y(t_{i+2}) - y(t_i)\right)/\Delta t_{i_2}\right)}{\Delta t_{i_1}};$$

$$y^{(3)}(t_i) \approx -\frac{12\left(y(t_{i+1}) - y(t_i)\right)}{\Delta t_{i_1}^3} + \frac{6\left(y^{(1)}(t_i) + \left(y(t_{i+2}) - y(t_i)\right)/\Delta t_{i_2}\right)}{\Delta t_{i_1}^2}.$$

The performances of the cubic spline technique are critically dependent on the accuracy and the distribution in time of the samples. In other words, the cubic spline approach has the advantage that it results in linear filtering with a time-variable cut-off frequency, in the sense that it better tracks fast changing, due to more samples become available at faster heart rates. On the other hand, polynomial fitting performs poorly when the available samples are too far apart [20]. Therefore, the EDR signal, which is unevenly sampled due to the irregular HR in case of AF, may betray a poor quality in those segments, where the samples are sparser than in other areas.

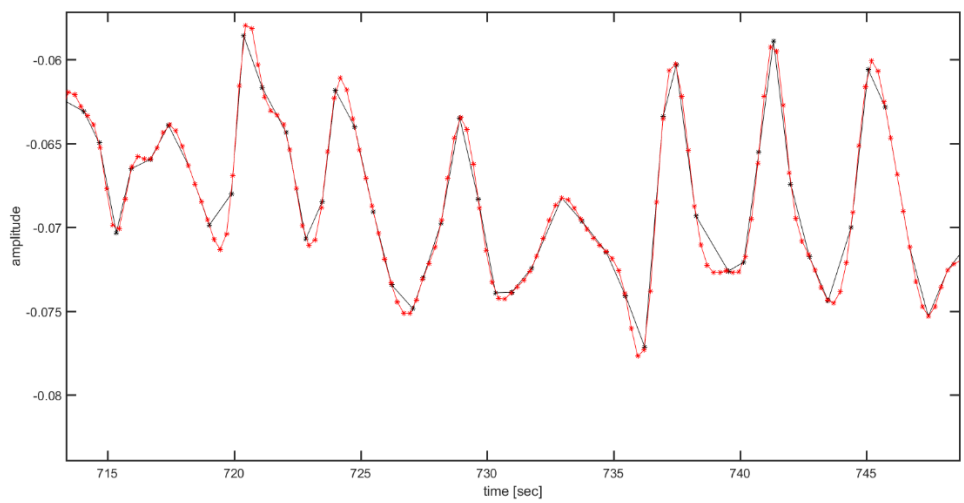

Figure 36 - Segment of EDR signal where the red dots are new samples after the resampling. The black dots and line is the EDR after the linear interpolation.

The interpolated EDR signal, see Figure 36, is filtered with a fourth-order Butterworth bandpass filter in the frequency interval from 0.075 to 1 Hz, as done in the work of Lázaro et al. [17]. The MATLAB function filtfilt is used for forward and backward filtering as in the pre-processing phase. This step is important to clean the signal from noise components that may mask the respiratory trend.

At this stage, the EDR signal presents values for the entire recording. However, some samples could be unreliable since they are obtained through interpolation in previous steps of the post-processing phase. The presence of long intervals with inconsistent samples may have negative effects on the estimation of the respiratory rate, due to spurious breathing cycles that may be counted. For this reason, the length of time intervals with unreliable samples due to outliers and beats classified as abnormal is determined. When the length of these time intervals exceeds 5 secs, the enclosed samples of the filtered EDR are discarded, as shown in Figure 37, since they are likely to lead to a spurious spectrum in the respiratory frequency estimation.

It has been verified that consecutive EDR samples, suspected to be unreliable, have potentially no negative effect in the estimation of the respiratory rate if they cover a time interval shorter than 5 seconds. The assumption is that no sudden changes in respiratory frequency can be observed is such a short interval. On the other hand, the advantage of keeping these intervals lies in the possibility of extracting the respiratory rate by basing the estimate on the previous samples.

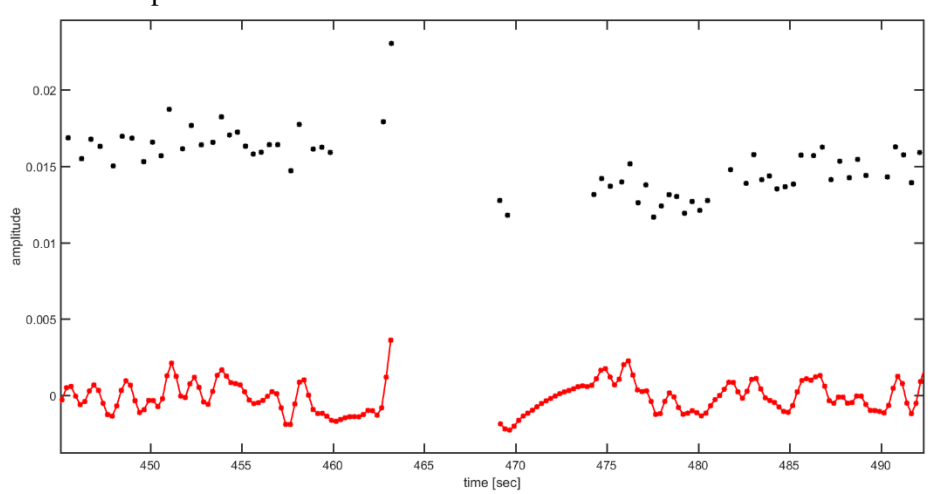

Figure 37 - The black dots are the original samples of the EDR; in which holes (missing samples classified as abnormal beats or noisy beats for both leads) are clearly visible. Due to the time of the missing samples lasting more than 5 sec., the correspondent samples of this time are removed from the post-processed EDR obtaining the final EDR (red line).

5.7 PRE-PROCESSING OF THE BELT SIGNAL

The belt respiratory signal works in this thesis as ground truth to verify the consistency of the EDR signal. However, the raw signal cannot be directly employed but a pre-processing phase is required to remove potential artifacts. An example of such pre-processing stage is shown in Figure 38. This stage mostly follows the post-processing phase applied on the EDR signal and setting differently some parameters. It is necessary, for example, to consider a different number of samples for the outlier rejection algorithm, so as to calculate the median and the standard deviation over the same time interval used for the EDR signal, i.e. 30 seconds. Since the respiratory signal is evenly sampled at 50Hz, the N_sample_{resp} parameter is set to 1500 samples. Considering a time interval of 30 seconds, the outlier detection is carried out considering not less than the previous 4 breathing cycles, since the slowest respiratory frequency for the exanimated database is 9 breaths/minute. The factor C which multiplies the standard deviation is set to 7, in order to include parts of the signal with a larger variance and reliably exclude potential artifacts in the signal.

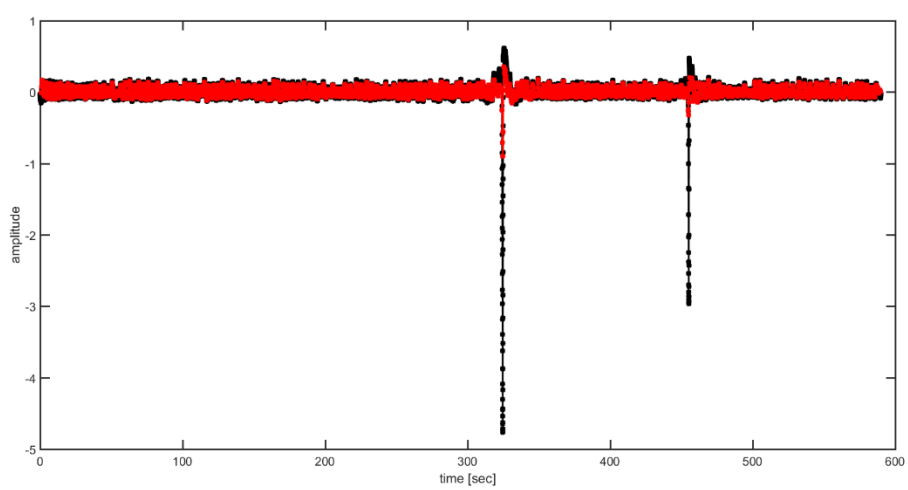

Figure 38 – The black line is the original respiration signal, while the red line shows the signal without the samples considered as outliers.

The next step is the linear interpolation to handle missing values in the respiratory signal after rejection of the outliers. The resampling at 4Hz is performed by considering the same time instants previously used for the resampling of the EDR signal, so achieving the time synchronisation of the two signals. In that way, the first samples of the respiratory signal are rejected to carry out the comparison by starting at the time instant of the first heartbeat, where the first EDR sample is extracted. For both steps, the interp1 MATLAB function is used.

A fourth-order Butterworth bandpass filter is also applied to the respiratory signal in order to keep the frequencies in the range between the 0.075Hz and 1 Hz, as performed on the EDR signal. As done previously, the MATLAB function filtfilt is applied to perform forward-backward filtering.

As last stage, the cancellation of the unreliable sample intervals longer than 5 secs is equally applied to the respiratory signal, as done in the post-processing for the EDR signal.

5.8 RESPIRATORY RATE ESTIMATION ALGORITHM

In order to assess the extracted EDR signal in the frequency domain, a respiratory rate estimation algorithm is implemented in the thesis. Given that the heart rate (HR) is usually greater than twice the respiration rate in normal cases, the frequency of respiratory effort can be measured well from this limited set of samples through the EDR signal without any risk of aliasing [2]. In case of atrial fibrillation, the estimation is more challenging because of the irregular heart rate, but the frequency ratio between HR and respiration frequency rate is still valid on average for the patients in the analysed database. In Figure 39, it is possible to see this relationship between the HR (orange columns) and RR (blue dots) for all the signals in the database. For more details, refer to the Table 8 in the appendix A.

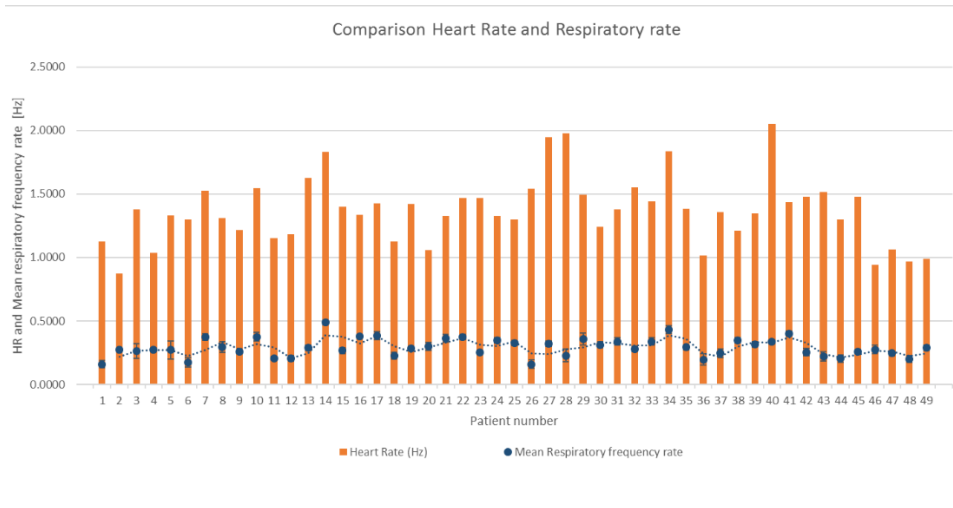

Figure 39 - Comparison Heart Rate and Respiratory rate.

The estimation of the respiratory rate can be performed using either non-parametric or parametric methods. In the non-parametric approach, the respiratory frequency is estimated from the location of the largest peak in the respiratory frequency band of the power spectrum of the multichannel EDR signal, by using the Fourier transform if the signal is evenly sampled or the Lomb's method if the signal is unevenly sampled. Parametric methods, such as AR modelling, automatically decompose the spectral components and, consequently, estimate the respiratory frequency. Yet another technique is based on signal modelling for identifying and quantifying the spectral component related to respiration [22].

The method to estimate the respiratory rate used in this thesis is the one proposed by Lázaro et al. [17], since it demonstrated to be reliable and robust in different conditions and because it is designed to combine the information coming from different EDR.

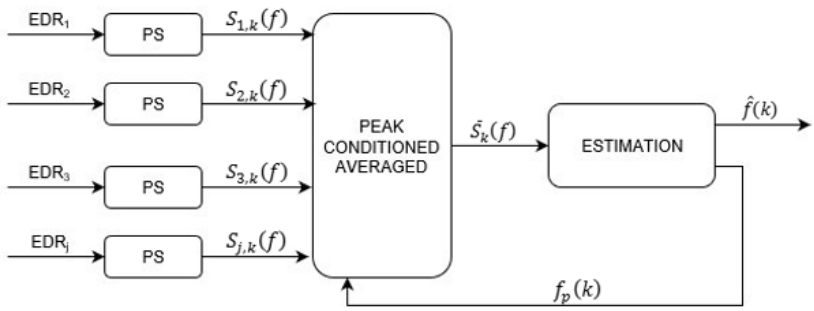

Figure 40 – Block diagram of respiratory rate estimation algorithm.

The algorithm can be divided into 3 phases (see Figure 40):

- The power spectrum (PS) estimation

The PS estimation is performed by using the Welch periodogram. For the *j*-th signal and the *k*-th running interval of T_s-s length, the power spectrum $S_{j,k}(f)$ is generated by an average of PS obtained performing the Welch periodogram on subintervals of T_m-s length ($T_m < T_s$) with an overlap of $T_m/2$ s, after a power normalization in [0,1] Hz. A spectrum is generated every t_s secs. The parameter values in this work are: $T_s = 40\ s$, $T_m = 12\ s$ and $t_s = 5\ s$.

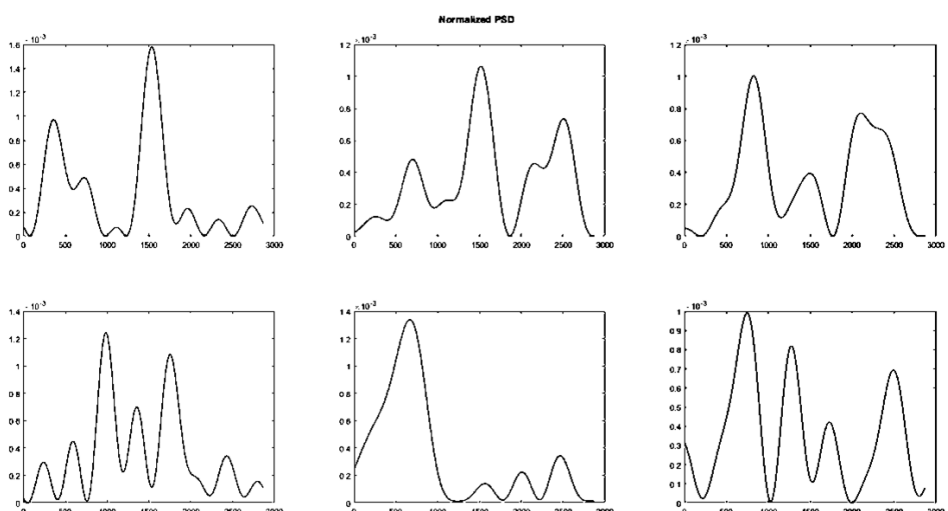

Figure 41 - The six plots are the normalized power spectral density of the subintervals Tm in the first interval Ts.

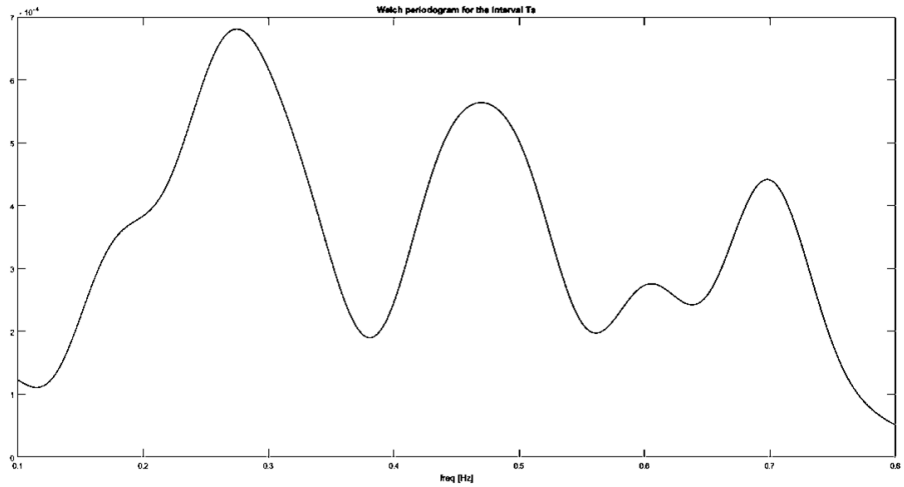

Figure 42 - Average power spectrum of the spectra presented in the Figure 41, which is considered the spectrum for the interval Ts.

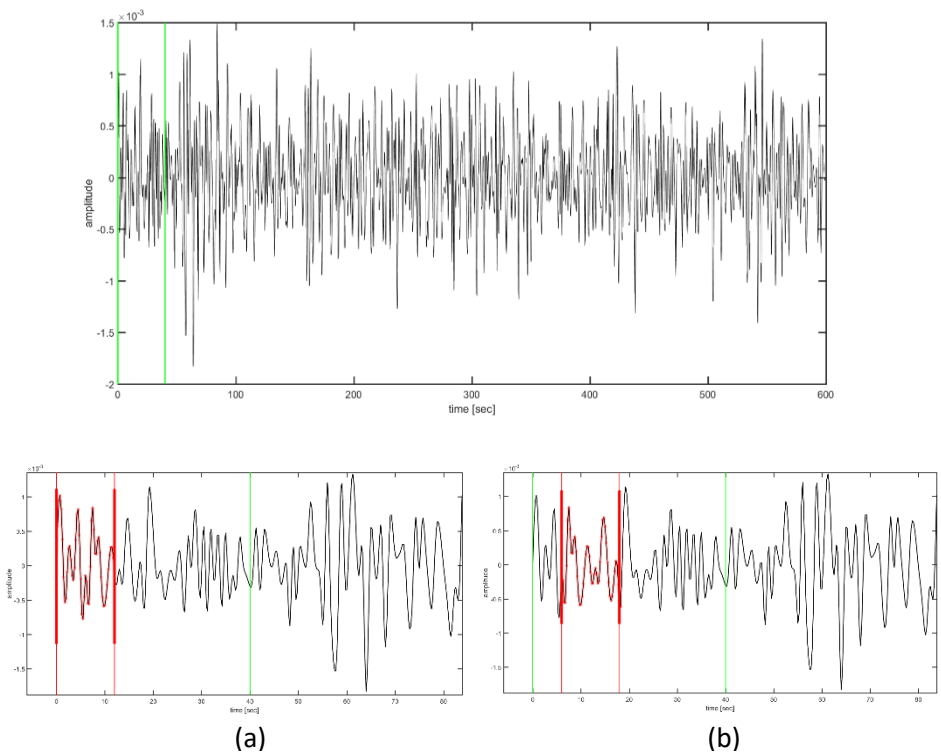

Figure 43 - The top picture plots the EDR signal, where the first Ts time interval (between the green lines) is enhanced. Along this interval the Welch periodogram is performed on subinterval of length Tm with overlap of Tm/2. The pictures (a) and (b) show the first and the second Tm intervals (between the red lines).

Figure 41, Figure 42 and Figure 43 show an example for a PS estimation over a TS interval.

- The peak-conditioned average

First, the location of the largest peak $f_P^I(j,k)$ is detected for each power spectra $S_{j,k}(f)$. Then a reference interval $\Omega_R(k)$, where respiratory rate is estimated to be, is defined as:

$$\Omega_R(k) = [f_R(k-1) - \delta, \quad f_R(k-1) + \delta\,]$$

Where $f_R(k-1)$ is a respiratory frequency reference obtained from previous $(k-1)$ steps. Parameter δ was set to 0.08 in order to allow moderate changes in respiratory rate. Note in Figure 44 as $f_P^{II}(j,k)$ is chosen as the nearest peak to $f_R(k-1)$, among all peaks larger than 85% of $f_P^I(j,k)$ inside $\Omega_R(k)$.

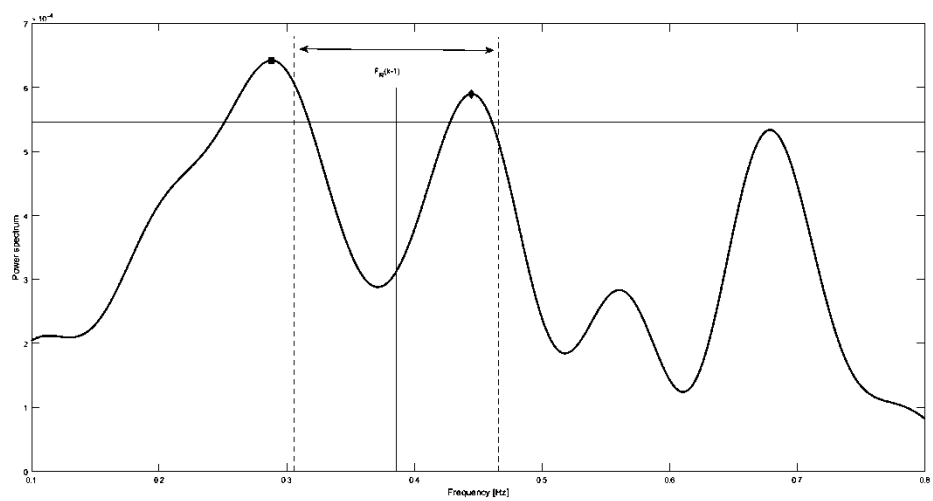

Figure 44 - The plot shows the selection of $f_P^I(j,k)$ and $f_P^{II}(j,k)$ for an example of power spectra density $S_{j,k}(f)$ and for a given $f_R(k-1)$. The highest peak $f_P^I(j,k)$ (black square) is discarded because it is outside the $\Omega_R(k)$, thus another peak (black diamond) higher than 85% of the highest peak and in the interval is selected as $f_P^{II}(j,k)$.

Subsequently, L_s spectra $S_{j,k}(f)$ are "peak-conditioned" averaged according to:

$$\bar{S}_k(f) = \sum_{l=0}^{L_S-1} \sum_j \chi_{j,k-l}^A \chi_{j,k-l}^B S_{j,k-l}(f)$$

where L_s is set to 5 as in Lázaro et al. [17].

χ^A and χ^B are the two criteria used to average only peaked spectra. In other word, χ^A lets those spectra whose peakness is greater than a fixed value take part in the average according to:

$$\chi^A_{j,k-l} = \begin{cases} 1, & P_{j,k} \geq \xi \\ 0, & otherwise \end{cases}$$

Parameter ξ was set to 0.60 after an optimization phase on the studied dataset. In the estimation of the respiratory frequency from the reference signal the parameter ξ has been raised to 0.75, since the respiratory spectra are peakier than the EDR spectra [1].

On the other hand, χ^B lets those spectra whose peakness is greater than the others of different EDR signals for the same time instant take part in the average according to:

$$\chi^B_{j,k-l} = \begin{cases} 1, & P_{j,k} \geq \max_j\{P_{j,k}\} - \lambda \\ 0, & otherwise \end{cases}$$

Parameter λ was set to 0.07 because that value was observed to achieve a good compromise for peak spectrum acceptance/rejection. $P_{j,k}$ is defined by the percentage of power around $f_P^{II}(j,k)$ with respect to the total power in $\Omega_R(k)$:

$$P_{j,k} = \frac{\int_{min\{f_P^{II}(j,k)+0.4\delta,\ f_R(k-1)+\delta\}}^{min\{f_P^{II}(j,k)-0.4\delta,\ f_R(k-1)-\delta\}} S_{j,k}(f)df}{\int_{f_R(k-1)-\delta}^{f_R(k-1)+\delta} S_{j,k}(f)df}.$$

Given the average spectra $\bar{S}_k(f)$, the algorithm searches the largest peak $f_P^{Ia}(k)$ into it and subsequently $f_P^{IIa}(k)$ is defined as before. Finally, the reference frequency $f_R(k)$ is updated as:

$$f_R(k) = \beta f_R(k-1) + (1-\beta) f_p(k)$$

β denotes the forgetting factor which is set to 0.9 since in rest-phase no fast changes in the respiratory frequency are expected. $f_p(k)$ is instead defined as

$$f_p(k) = \begin{cases} f_P^{IIa}(k), & \exists f_P^{IIa}(k) \\ f_P^{Ia}(k), & otherwise \end{cases}.$$

- The respiratory rate estimation

The estimated respiration rate $\hat{f}(k)$ is defined as:

$$\hat{f}(k) = \alpha \hat{f}(k-1) + (1-\alpha) f_p(k)$$

$$\alpha = \begin{cases} \alpha_{2,} & \exists f_P^{IIa}(k) \\ \alpha_{1,} & otherwise \end{cases}$$

Where $\alpha_2 \leq \alpha_1$ providing more memory when $f_P^{IIa}(k)$ cannot be set. Parameters α_1 and α_2 are set to 0.7 and 0.3 respectively fixing the maximum allowed changes in respiratory frequency inside (α_2) and outside (α_1).

Note that if no spectrum takes part in the average to determine $\bar{S}_k(f)$, the algorithm increases the reference interval by doubling the δ value and repeat the process from the search of $f_P^{II}(j,k)$ in the individual power spectra. In the case that no spectrum is peaked enough after this second iteration, respiratory rate is not estimated at that time instant.

At initialization time, in order to reduce the risk of spurious frequency selection, δ is set to 0.2 Hz and $f_R(0)$ is set to 0.275 Hz, allowing the algorithm to pick peaks inside the normal range of spontaneous respiratory rate ([0.075 0.475] Hz). Occasionally, respiratory rate can be outside this band so the algorithm may not be initialized as proposed.

Chapter 6. EDR ALGORITHMS ASSESSMENT

This chapter explains how the assessment of the EDR signals is carried out to measure the performances of the different tested methods.

6.1 ASSESSMENT PARAMETERS

In [2] and [24] the ECG-derived respiratory waveforms are assessed visually by comparing them with a reference respiratory signal. However, this visual validation is subjective and not easily reproducible [16]. The work of Mason et al. [16] proposed a quantitative and objective evaluation method based on an approach to detection of heartbeats in the ECG. The times of the derived breaths are compared with the times of the corresponding reference breaths and from them they calculated the sensitivity and the positive predictivity of the methods.

Later in 2006, Bailon et al. [1] proposed to evaluate the EDR algorithms defining an absolute and a relative error trend for each subject q at those indeces k that indicate the averaged spectrum $\overline{S_k}(f)$ from which $\hat{f}(k)$ is estimated. The evaluation parameters proposed by Bailon et al. [1], later adopted also by Lázaro et al. in [17], [56] and [57], are used in the present work as follows.

The absolute error is defined as:

$$\Delta f_q(k) = \left|\widehat{f_q}(k) - \widehat{f_{r,q}}(k)\right| \tag{1}$$

The relative error is defined as:

$$\Delta f_{q\%}(k) = \frac{\left|\widehat{f_q}(k) - \widehat{f_{r,q}}(k)\right|}{\widehat{f_{r,q}}(k)} \times 100\% \tag{2}$$

Where $\widehat{f_q}(k)$ is the estimate frequency from EDR and $\widehat{f_{r,q}}(k)$ is the estimate frequency from the reference respiratory signal. For each subject, the mean and SD of the error trends characterizes the intrasubject error as follows:

$$\mu_q = \frac{1}{N_q}\sum_{k=1}^{N_q}\Delta f_q(k) \tag{3}$$

$$\sigma_q{}^2 = \frac{1}{N_q - 1}\sum_{k=1}^{N_q}\left(\Delta f_q(k) - \frac{1}{N_q}\sum_{k=1}^{N_q}\Delta f_q(k)\right)^2 \tag{4}$$

From the previous values, the intersubject mean of the intrasubject errors is defined by the pair (μ, σ):

$$\mu = \frac{1}{S}\sum_{q=1}^{S}\frac{1}{N_q}\sum_{k=1}^{N_q}\Delta f_q(k) \tag{5}$$

$$\sigma^2 = \frac{1}{S}\sum_{q=1}^{S}\frac{1}{N_q - 1}\sum_{k=1}^{N_q}\left(\Delta f_q(k) - \frac{1}{N_q}\sum_{k=1}^{N_q}\Delta f_q(k)\right)^2 \tag{6}$$

where N_q is the number of the averaged spectra in which respiratory frequency could be estimated from both the ECG and the respiratory signal and S is the number of subjects. The intersubject error defines quantitively how much closer is the frequency estimate from the EDR signal to the one from the reference signal by considering all the estimates of the S-subjects.

The mean and the standard deviation for the relative error is also calculated as for the absolute error both over each subject and over all the dataset.
In addition to the mentioned works, the Root Mean Square error (RMS) is also computed for each subject, as follows:

$$RMS = \sqrt{\frac{1}{N_q}\sum_{k=1}^{N_q}\left(\Delta f_q(k)\right)^2} \tag{7}$$

Note that the RMS quantifies the difference between the estimated values and the actual values.

The parameter $T_{\%}$ is computed as the average of the percentage of the total duration of the recording when respiratory frequency could be estimated from both the ECG and the respiratory signal for each subject:

$$T_{\%} = \frac{N_q}{Ntot_q} \times 100 \tag{8}$$

where $Ntot_q$ indicates the total number of the averaged spectra

The last two parameters RMS and $T_{\%}$ are also averaged over all the S-subjects in order to obtain a general value of accuracy and robustness on the given dataset.

Other extracted parameters are the mean and the standard deviation of the estimate frequency from the EDR signal and the respiration for each patient:

$$\mu_{EDR} = \frac{1}{N_q}\sum_{k=1}^{N_q} \widehat{f_q}(k) \qquad {\sigma_{EDR}}^2 = \frac{1}{N_q - 1}\sum_{k=1}^{N_q}\left(\widehat{f_q}(k) - \frac{1}{N_q}\sum_{k=1}^{N_q}\widehat{f_q}(k)\right)^2 \tag{9}$$

$$\mu_r = \frac{1}{N_q}\sum_{k=1}^{N_q} \widehat{f_{r,q}}(k) \qquad {\sigma_r}^2 = \frac{1}{N_q - 1}\sum_{k=1}^{N_q}\left(\widehat{f_{r,q}}(k) - \frac{1}{N_q}\sum_{k=1}^{N_q}\widehat{f_{r,q}}(k)\right)^2 \tag{10}$$

These values provide information about the ranges of the respiratory frequency estimates from both signal for each subject, allowing a more general evaluation of the level of similarity.

Note that the presented assessment parameters are computed two times for each method on the same subjects, in order to assess the performances with and without performing f-wave cancellation. To distinguish between the two categories of results, the superscripts " f " and "$no\ f$" are introduced, which indicate respectively if the parameter is computed by keeping f-waves or by removing them from the ECG.

6.2 STATISTICAL TESTS

Statistical tests are carried out to understand if the respiratory frequencies estimate from EDR and respiration is significantly different on a statistical point of view. In particular, the Lilliefors test, two-sided goodness-of-fit test, is performed to check, if a data population comes from a distribution in the normal family (null hypothesis), against the alternative that it does not come from such a distribution. The Lilliefors test statistic is suitable when the parameters of the null distribution are unknown, so they must be estimated, and it is defined as:

$$D^* = \max_x \left| \hat{F}(x) - G(x) \right| \tag{11}$$

where $\hat{F}(x)$ is the empirical cumulative distribution function of the sample data and $G(x)$ is the cumulative distribution function of the hypothesized distribution with estimated parameters equal to the sample parameters. This test is implemented in MATLAB with the function lillietest, which returns by default 1 if the test rejects the null hypothesis at the 5% significance level, and 0 otherwise. The test is separately applied on $\Delta f_q^f(k)$ and on $\Delta f_q^{no\,f}(k)$ of each subject and overall of all subjects, considering the difference with sign instead of the absolute value. It is also applied on the difference $\mu_{EDR}^f - \mu_{EDR}^{no\,f}$ on the entire dataset.

Whenever the population has normal distribution, a paired t-test may be applied to verify if the test statistic follows a Student's t-distribution under the null hypothesis. The “paired” or “repeated measures” t-test is applied to control if the difference between two datasets comes from a normal distribution with mean equal to zero and unknown variance.

Moreover, the two-sample Kolmogorov-Smirnov test is applied to verify the provenance of the samples from the same distribution (null hypothesis). These are considered continuous but are otherwise unrestricted. The two-sample K–S test is one of the most useful and general nonparametric methods that evaluates

the difference between the cumulative distribution functions of the distributions of the two sample data vectors over the range of x in each data set. The test statistic is applied through the MATLAB function `kstest2`, in which the statistic is defined as:

$$D^* = \max_x \left| \hat{F}_1(x) - \hat{F}_2(x) \right| \tag{12}$$

where $\hat{F}_1(x)$ is the proportion of x_1 values less than or equal to x and $\hat{F}_2(x)$ is the proportion of x_2 values less than or equal to x. The result is positive if the test rejects the null hypothesis at the 5% significance level, and 0 otherwise.

All the mentioned statistical tests return also a p-value, which quantifies the idea of statistical significance of evidence, in other words the probability of observing the result or a more extreme one assuming that the null hypothesis is true.

Chapter 7. RESULTS

In this chapter, the results of the different EDR methods are reported in tables and illustrated with plots. These are obtained after an optimization phase, where all parameters of the algorithms involved in the workflow have been set by studying the performances on a randomly selected subgroup of subjects. The methods are evaluated on a dataset containing 2-leads ECGs and a respiratory signal simultaneously recorded from 49 subjects during an event of AF in rest-phase. The evaluation is generally carried out by measuring the similarity of the post-processed EDR signal to the pre-processed respiratory signal on an intrasubject and intersubject level.

For each subject, the outcome of designed workflow allows a visual comparison of the EDR signal with the reference respiratory signal in the time domain and in the frequency domain. Examples extracted by applying the QRS slope and R-wave angle method on one of the subjects are shown in Figure 45 and Figure 46.

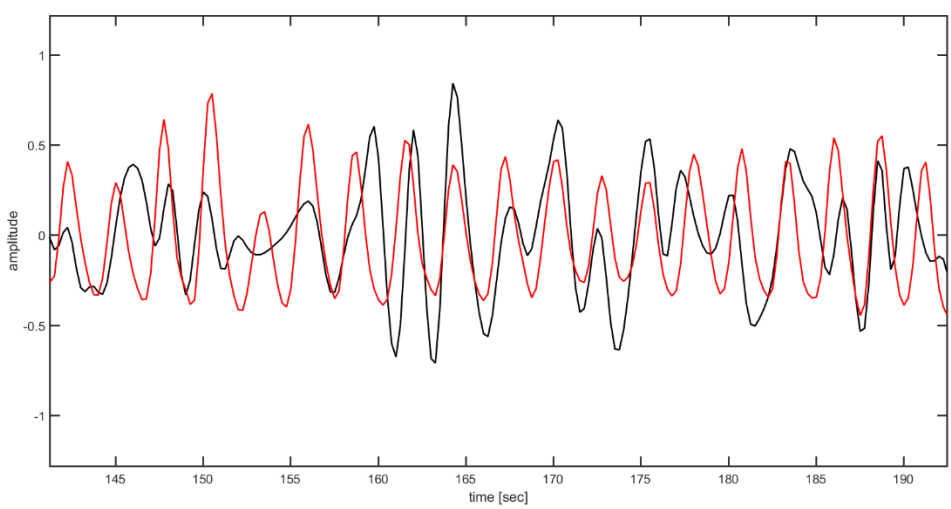

Figure 45 - Comparison of one EDR signal (black line) with the reference respiratory signal (red line). The EDR signal is derived from the $\mathfrak{T}_{DS}$ series of one lead by using the QRS-slopes method.

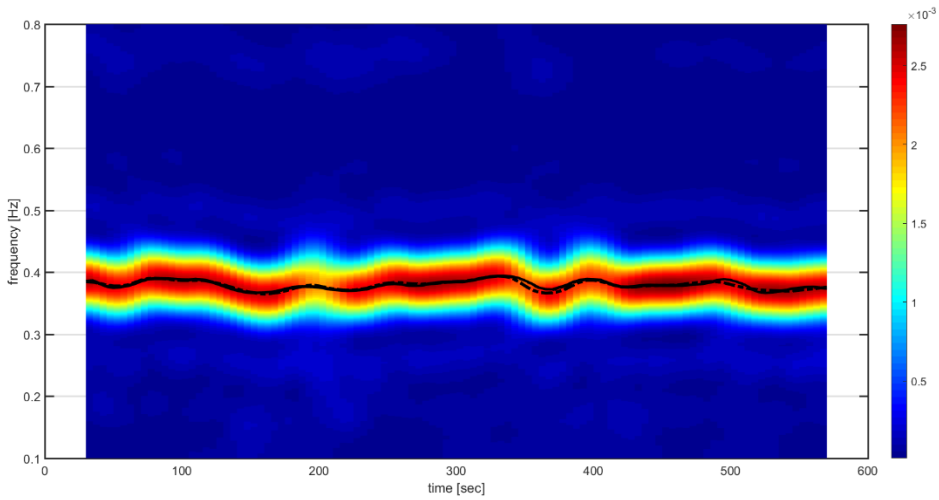

Figure 46. Time frequency map of the respiratory signal, where the different colours in the map indicates the PSD at any frequency (y-axis) and time instant (x-axis). The dashed and the solid black lines represent the extracted dominant frequency rate respectively from the respiratory signal and from the EDR signals (QRS slopes and R-wave angle method) over time.

The mean and the standard deviation (STD) of the estimated dominant frequency rate $\mu_{EDR}^{f} \pm \sigma_{EDR}^{f}$, $\mu_{EDR}^{no\,f} \pm \sigma_{EDR}^{no\,f}$ and $\mu_r \pm \sigma_r$ are computed for each patient as well the percentage of the total duration of the recording when respiratory frequency could be estimated from both the ECG and the respiratory signal ($T_{\%}^{f}$ and $T_{\%}^{no\,f}$).

In order to numerically evaluate the EDR signal, the RMS error, the mean and the standard deviation (STD) of $\Delta f_q^{f}(k)$, $\Delta f_{q\%}^{f}(k)$, $\Delta f_q^{no\,f}(k)$ and $\Delta f_{q\%}^{no\,f}(k)$ are computed, so providing the absolute and the relative intrasubject error for each subject.

The implemented EDR methods are tested on the entire dataset and the results are shown through Bland-Altman plots, which is a method of data plotting used in evaluating the agreement among a method with a gold standard, as it is intended in this work. Each of the n subjects is represented on the graph by

assigning the average of the two mean estimated respiratory frequency from the EDR (μ_{EDR}) method and from the reference respiratory signal (μ_r) as the abscissa (x-axis) value, while the difference between these two values as the ordinate (y-axis) value. This plot allows identification of any systematic difference between the results or possible outliers. The mean difference is the estimated bias, whereas the SD of the differences measures the random fluctuations around this mean. In particular, the 95% limits of agreement for each comparison (average difference ± 1.96 standard deviation of the difference) is used instead of the SD, which is called LoA and accounts for how far apart measurements by 2 methods were more likely to be for most individuals. If the differences within mean ± 1.96 SD are not clinically important, the two methods may be used interchangeably [58].

The performances of each method are also displayed by using Box and Whisker plots depicting the mean RMS values for each subject in groups according to the method through their quartiles. They also include lines extending vertically from the boxes (whiskers) indicating variability outside the upper and lower quartiles and individual points as outliers. Boxplots are non-parametric; i.e. they display variation in samples of a statistical population without making any assumptions of the underlying statistical distribution. However, they are very useful for comparing distributions between several groups or sets of data.

The method evaluation is also carried out by computing the intersubject mean of the means and the standard deviations of $\Delta f_q^f(k)$, $\Delta f_{q\%}^f(k)$, $\Delta f_q^{no\,f}(k)$ and $\Delta f_{q\%}^{no\,f}(k)$ for all the subjects. The mean percentage of the record durations of the dataset where an estimate is given from both signals is also calculated. At last, the Kolmogorov-Smirnov test is applied to evaluate if a significant statistical difference subsists between results with and without cancellation of f-waves, basing on the similarity of μ_{EDR}^f and $\mu_{EDR}^{no\,f}$ for all the subjects.

The results of all the tested EDR methods are reported in the following sections, so that each section (from Section 7.1 to Section 7.4) refers to one method tested on all the subjects of the dataset. For each method, a comparison of the performances with and without the removal of the f-waves from the ECG is carried out by reporting the relative Bland-Altman plots. The inter-subject mean on all means and SDs of the absolute and relative errors computed on each subject and the percentage of frequency estimates on the total length of the signal are shown in a table. Section 7.5 shows in parallel the results from all the tested EDR methods on the entire dataset, with and without removal of the f-waves.

7.1 QRS SLOPES AND R-WAVE ANGLES

The following figures show the results for the QRS slopes and R-wave angles method, explained in the Section 5.5.1, with and without applying the f-waves removal algorithm. The Bland-Altman plots (Figure 47 and Figure 48), which consider the mean estimated respiratory frequency, display that the LoAs and the mean difference between $\mu_{EDR}^{no\ f}$ and μ_r is almost equal to the mean difference between μ_{EDR}^{f} and μ_r.

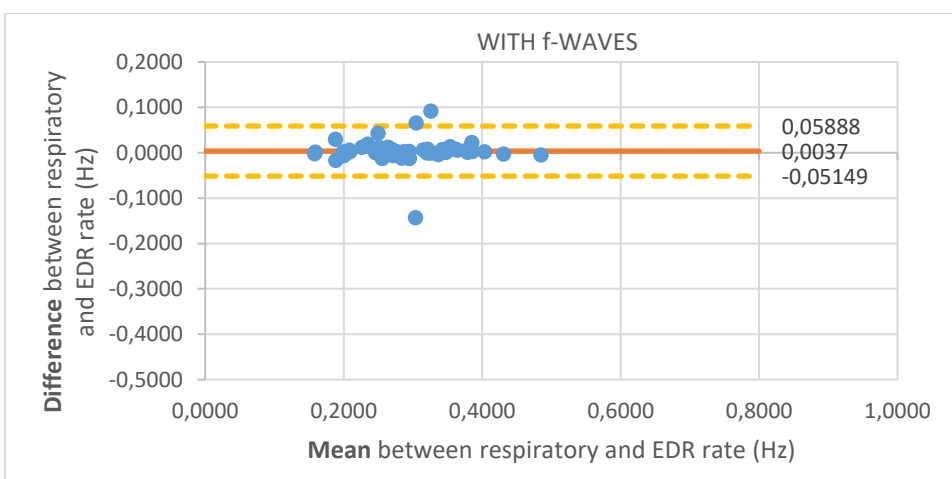

Figure 47 - Bland-Altman plot of QRS slopes and R-wave angles without applying the f-wave removal algorithm.

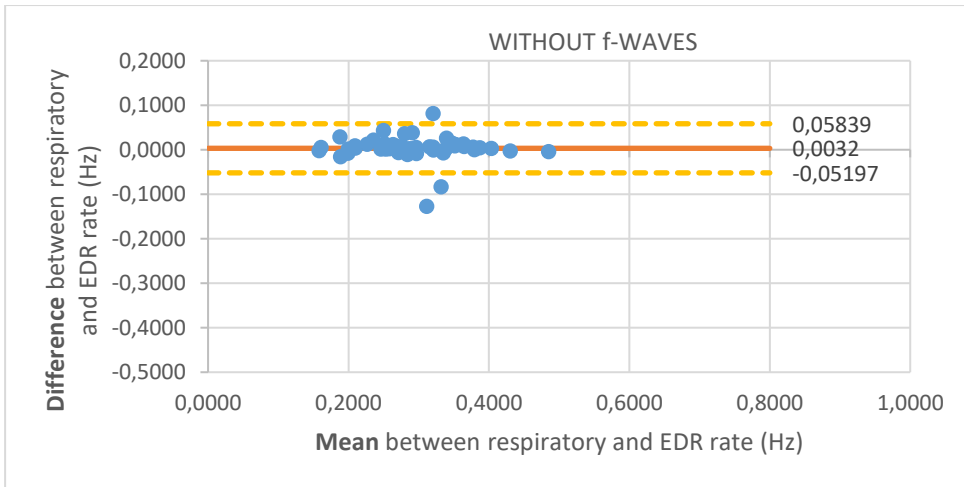

Figure 48 - Bland-Altman plot of QRS slopes and R-wave angles applying the f-wave removal algorithm.

However, the observations without removing the f-waves seem to be clustered around the horizontal line closer than adding this step, meaning that the results are more accurate in the first case. This is proved by the Box and Whisker plot in Figure 55, where the RMS errors, as calculated in (7), are 0.0320 ± 0.0271 Hz (mean and SD) when keeping the f-waves in the QRS interval and 0.0345 ± 0.0287 Hz (mean and SD) when removing them.

The statistical analysis proves that the difference between the EDR respiratory rates and the reference respiratory rates for each patient do not come from a distribution in the normal family for the majority of the patients.

The two-sample Kolmogorov-Smirnov test is then applied on μ_{EDR}^{f} and $\mu_{EDR}^{no\ f}$ extracted from the entire dataset. It returns that there is no statistical evidence against the hypothesis that these two populations of data originate from the same distribution.

	$\Delta f_q(k)$ (Mean and SD) [Hz]	$\Delta f_{q\%}(k)$ (Mean and SD) [%]	Time measuring mean [%]
with f-waves	0.0227 +/- 0.0217	8.4489 +/- 8.8259	91.23%
without f-waves	0.0241 +/- 0.0240	9.0013 +/- 9.8603	91.21%

Table 1.

The Table 1 compares the mean absolute and the relative intersubject errors, as calculated in (5) and (6), and shows the time measuring mean (%) on the recordings, as calculated in (8).

7.2 QRS AREA

The second typology of EDR algorithms that have been implemented in this work refer the methods based on QRS area as explained in the Section 5.5.2.
The Table 2 shows that the method based on a fixed QRS window considering the two leads independently outperforms the others. Thus, the technique is selected for the comparison with other EDR methods and the results are also extracted by applying the f-waves removal stage.

	$\Delta f_q(k)$ (Mean and SD) [Hz]	$\Delta f_{q\%}(k)$ (Mean and SD) [%]	Time measuring mean [%]
Moody et al. [2]	0.0557 +/- 0.0425	21.2751 +/- 17.5902	85.44
Fixed QRS window, independent Leads method [15]	0.0385 +/- 0.0311	14.3286 +/- 12.4901	88.01
Variable QRS window, independent Leads method [15]	0.0497 +/- 0.0384	18.5201 +/- 15.6750	86.72
Variable QRS window, dependent Leads method [15]	0.0412 +/- 0.0334	15.8648 +/- 13.8838	87.12
Mazzanti et al. [43]	0.0621 +/- 0.0442	23.7768 +/- 18.3057	85.41
Park et al. [44]	0.0537 +/- 0.0414	20.6166 +/- 17.2553	85.62

Table 2.

The Bland-Altman plots (Figure 49 and Figure 50) for the selected QRS area method shows a better alignment of the data along the mean with less outliers after the removal of the f-waves. Moreover, the LoAs and the mean the

difference are lower between $\mu_{EDR}^{no\ f}$ and μ_r, with respect to μ_{EDR}^{f} and μ_r . These results are confirmed by the Box and Whisker plot in Figure 55, since the RMS errors, as calculated in (7), are 0.0504 ± 0.0352 Hz (mean and STD) and 0.0481 ± 0.0294 Hz (mean and SD) before and after F-waves removal respectively.

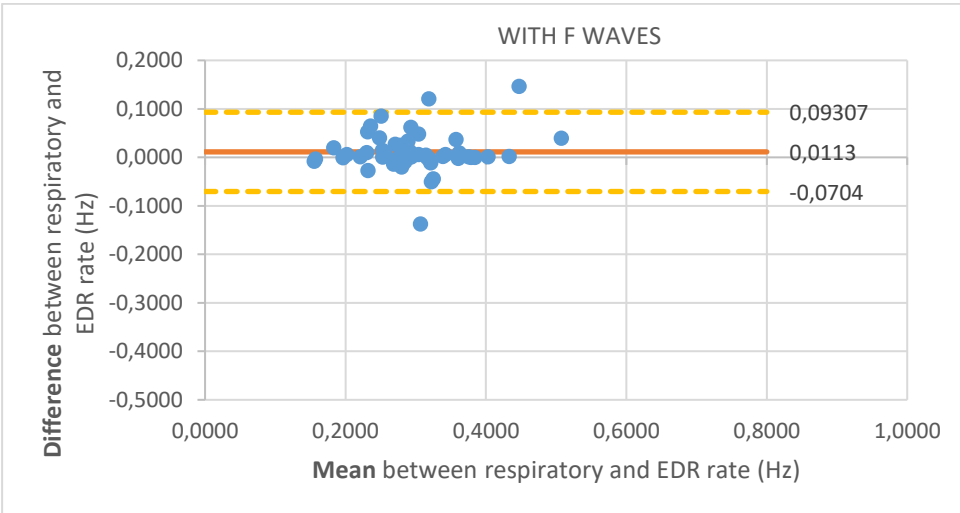

Figure 49 - Bland-Altman plot of QRS area without applying the f-wave removal algorithm.

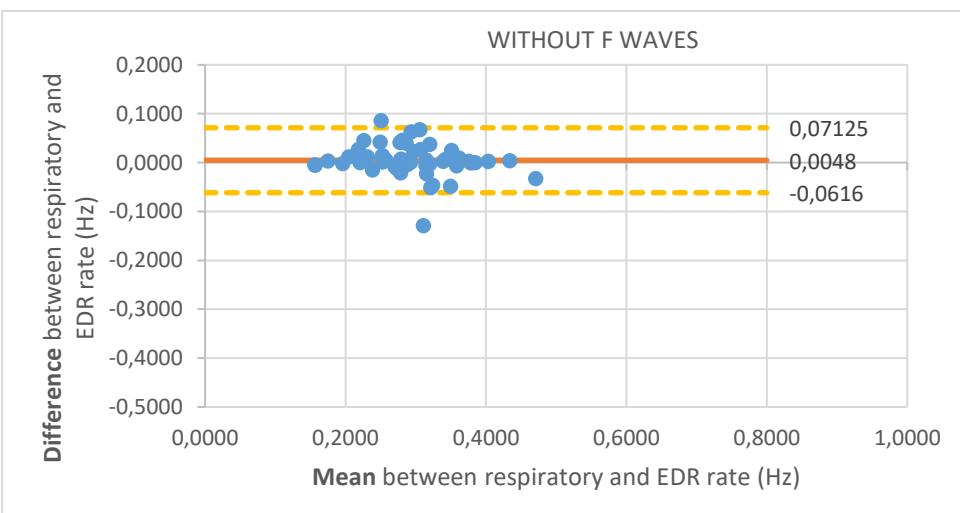

Figure 50 - Bland-Altman plot of QRS area applying the f-wave removal algorithm.

The statistical analysis proves that the difference between the EDR respiratory rates and the reference respiratory rates for each patient do not come from a distribution in the normal family for the majority of the patients.

The two-sample Kolmogorov-Smirnov test is then applied on μ_{EDR}^{f} and $\mu_{EDR}^{no\ f}$ extracted from the entire dataset. It returns that there is no statistical evidence against the hypothesis that these two populations of data originate from the same distribution.

	$\Delta \boldsymbol{f}_{\boldsymbol{q}}(\boldsymbol{k})$ **(Mean and SD) [Hz]**	$\Delta \boldsymbol{f}_{\boldsymbol{q}\%}(\boldsymbol{k})$ **(Mean and SD) [%]**	**Time measuring mean [%]**
with f-waves	0.0385 +/- 0.0311	14.3286 +/- 12.4901	88.01%
without f-waves	0.0359 +/- 0.0313	13.4456 +/- 12.5386	88.83%

Table 3.

The Table 3 compares the mean absolute and the relative intersubject error, as calculated in (5) and (6), and shows the time measuring mean (%) on the recordings, as calculated in (8). It can be observed that the error slightly decreases and the percentage of estimation increases applying the f-waves removal algorithm.

7.3 R AMPLITUDE

Analogously as before, the following plots show the results of R amplitude technique, explained in the Section 5.5.3, comparing between before and after removal of f-waves. In the former (Figure 51), the points, which represent the patients, are less clustered around the horizontal line than in Figure 52, meaning that the removal of the f-waves from the QRS complex makes improvements to the base method. This is confirmed also by the decreasing of the bias in the Bland-Altman plot. However, the LoA limits are affected by the presence of an outlier, which turns out to be a critical case for all the methods.

The Box and Whisker plot in Figure 55 displays the distribution of the RMS error in both cases, as calculated in (7), where it is visible a difference between

them. In particular, the mean and the SD before and after performing f-waves removal are 0.0351 ± 0.0245 Hz and 0.0334 ± 0.0262 Hz respectively.

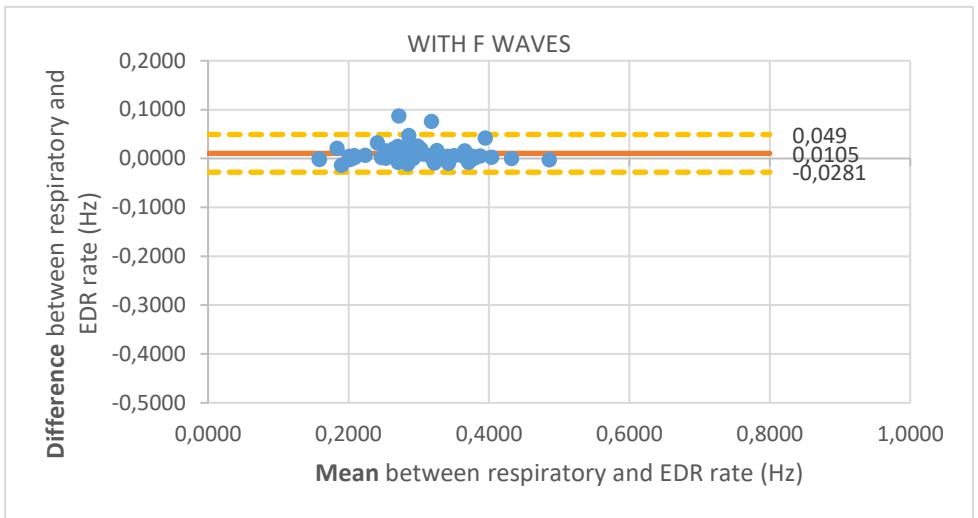

Figure 51 – Bland-Altman plot of R amplitude without applying the f- wave removal algorithm.

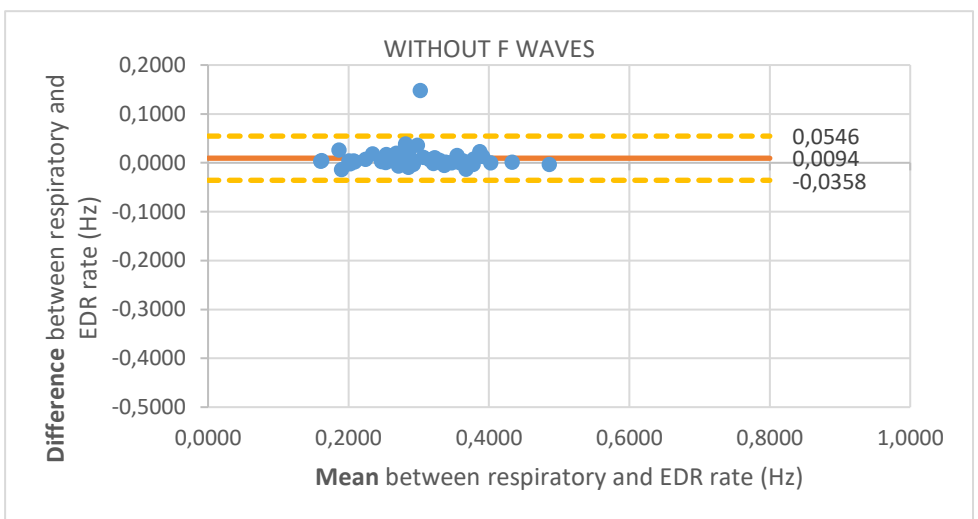

Figure 52 – Bland-Altman plot of R amplitude applying the f-wave removal algorithm.

The statistical analysis proves that even in this case the difference between the EDR respiratory rates and the reference respiratory rates for each patient do not come from a distribution in the normal family for the majority of the patients.

The two-sample Kolmogorov-Smirnov test applied on μ_{EDR}^{f} and $\mu_{EDR}^{no\,f}$,from the entire dataset, returns that there is no statistical evidence against the hypothesis that these two populations of data originate from the same distribution.

	$\Delta \boldsymbol{f}_{\boldsymbol{q}}(\boldsymbol{k})$ (Mean and SD) [Hz]	$\Delta \boldsymbol{f}_{\boldsymbol{q}\%}(\boldsymbol{k})$ (Mean and SD) [%]	Time measuring mean [%]
with f-waves	0.0244 +/- 0.0248	9.4073 +/- 10.2806	91.21%
without f-waves	0.0236 +/- 0.0231	9.2207 +/- 9.5416	91.15%

Table 4.

The Table 4 compares the mean absolute and the relative intersubject error, as calculated in (5) and (6), and shows the time measuring mean (%) on the recordings, as calculated in (8). It is possible to notice that a decreasing in the errors does not lead to an improvement of the percentage of the measured time.

7.4 VCG LOOP ALIGNMENT

In this section, the results for the VCG-loop alignment method as proposed by Bailon et al. [1] and explained in the Section 5.5.4, are shown through the following plots (Figure 53 and Figure 54). Due to the variability of the signal quality in the dataset, it was not possible to run the EDR algorithm with the same parameters over the entire dataset, since for some subjects it was required to set a lower threshold as minimum correlation value between the transformed and reference loop during the definition of the reference loop. Therefore, the threshold is reduced from 0.9 to 0.55 only for these subjects, so as to avoid deteriorations of the performances over the entire database. It has been considered more reasonable to adopt an optimized threshold for most of the subjects in the dataset and to handle differently the characteristics of this subgroup of signals. The ECG signals of these subjects exhibit residual noise in one of the leads, that is likely to lower the maximum achievable correlation value among consecutive beats. Adding the f-waves removal stage to the

workflow, a decay of the performances is observed. Indeed, the differences between respiratory and EDR rates are more spread out between higher LoAs than not removing the f-waves from the QRS complex.

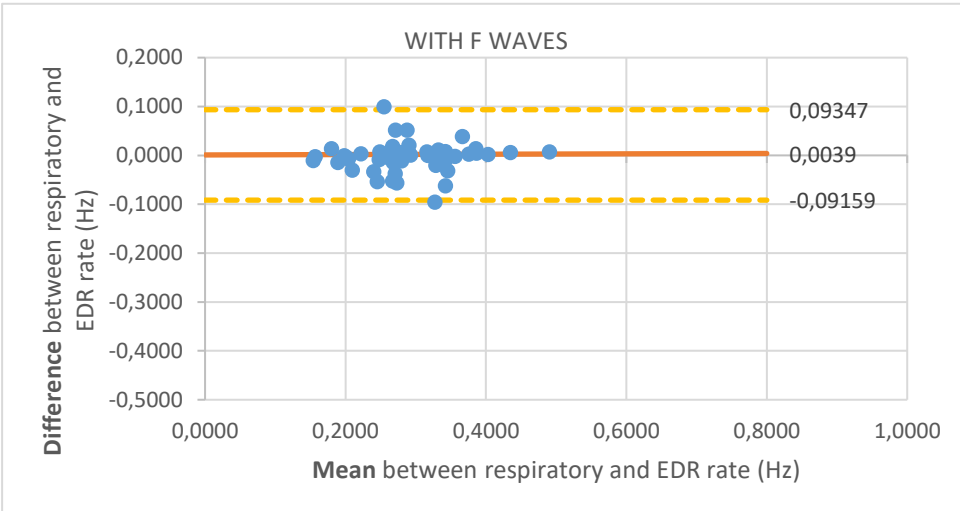

Figure 53 - Bland-Altman plot of VCG alignment the f-wave removal algorithm.

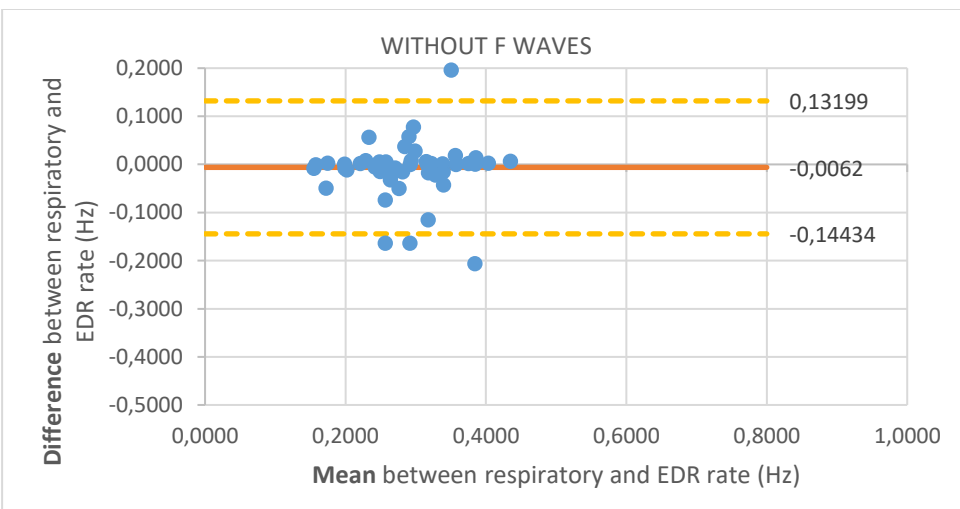

Figure 54 - Bland-Altman plot of VCG alignment applying the f-wave removal algorithm.

The decay of performances is also shown by the Box and Whisker plot Figure 55, where the mean and the SD before and after removing the f-waves from the

ECG, calculated in (7), are 0.0524 ± 0.0437 Hz and 0.0669 ± 0.0574 Hz respectively.

However, the two-sample Kolmogorov-Smirnov test applied on μ_{EDR}^{f} and $\mu_{EDR}^{no\ f}$ from all the subjects returns that there is no statistical evidence against the hypothesis that these two populations of data originate from the same distribution even in this case.

	$\Delta \boldsymbol{f}_{\boldsymbol{q}}(\boldsymbol{k})$ **(Mean and SD) [Hz]**	$\Delta \boldsymbol{f}_{\boldsymbol{q}\%}(\boldsymbol{k})$ **(Mean and SD) [%]**	**Time measuring mean [%]**
with f-waves	0.0401 +/- 0.0328	15.0385 +/- 12.6971	87.42%
without f-waves	0.0540 +/- 0.0370	19.3036 +/- 13.7946	86.32%

Table 5.

The Table 5 compares the mean absolute and the relative intersubject errors, as calculated in (5) and (6), and shows the time measuring mean (%) on the recordings, as calculated in (8). By performing the removal of the f-waves, it can be observed that the errors become larger and the mean measuring time decreases.

7.5 COMPARISON AMONG EDR METHODS

The comparison among the tested EDR methods is shown in the Table 6, which present the mean intersubject absolute error (Hz) and the mean intersubject relative error (%) with the percentage of the frequency estimating time over the entire length of the signal, as calculated in (5), (6) and (8). These results are extracted from all the 49 subjects in the dataset.

Methods over 49 patients		Intrasubject ABOSOLUTE ERROR (Hz)		Intrasubject RELATIVE ERROR (%)		Time measuring (%) Mean
		Mean	SD	Mean	SD	
QRSarea	with F	0.0385	0.0311	14.33	12.49	88.01%
	without F	0.0359	0.0313	13.45	12.54	88.83%
Ramplitude	with F	0.0244	0.0248	9.41	10.28	91.21%
	without F	0.0236	0.0231	9.22	9.54	91.15%
VCGalign	with F	0.0401	0.0328	15.04	12.70	87.42%
	without F	0.0540	0.0370	19.30	0.04	86.32%
QRSslopes-angle	with F	0.0227	0.0217	8.45	8.83	91.23%
	without F	0.0241	0.0240	9.00	9.86	91.21%

Table 6 - Comparison of the methods in terms of mean intrasubject error and time measuring mean on the entire dataset.

The Box and Whisker plot in Figure 55 displays the distribution of the RMS errors for each method. The plot allows also a comparison between estimation errors with and without removing the f-waves from the QRS interval for each method. In particular, the mean and the SD of these results are shown in the Table 7.

Methods		RMS	
		Mean	SD
QRSarea	with F	0.0504	0.0352
	without F	0.0481	0.0294
Ramplitude	with F	0.0351	0.0245
	without F	0.0334	0.0262
VCGalign	with F	0.0524	0.0437
	without F	0.0669	0.0574
QRSslopes R angle	with F	0.032	0.0271
	without F	0.0345	0.0287

Table 7. Comparison of the methods in term of mean and SD of the RMS error on the entire dataset

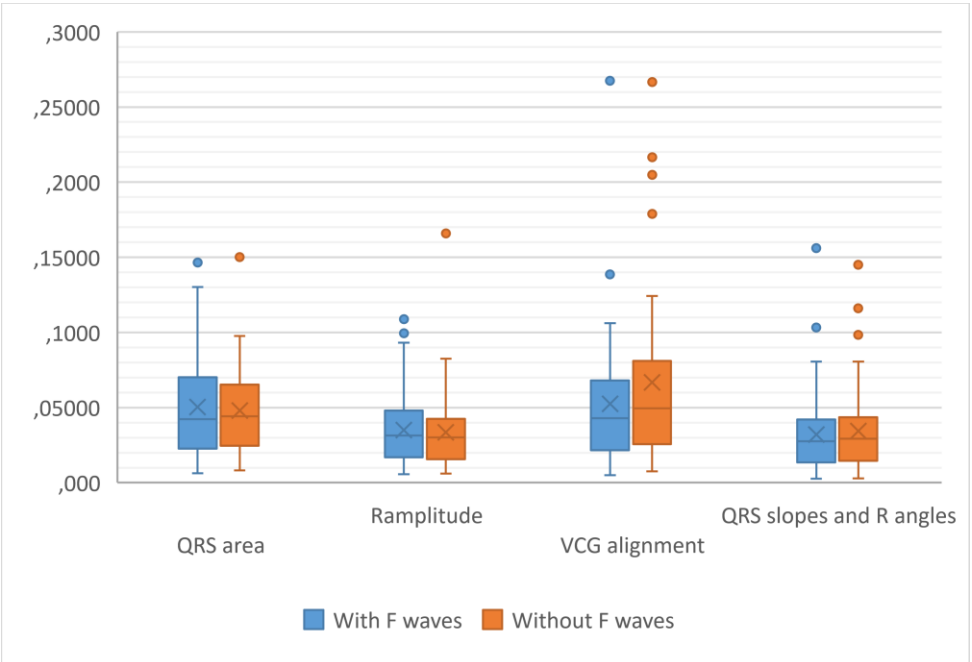

Figure 55 – Comparison of the estimation errors among the different methods with and without applying the f-waves removal algorithm.

Figure 56 shows an example of a subject where the tested methods have achieved different performances. The analysis of the performance variability of each method on different subjects and among the methods on the entire dataset represents an important part of this work. Indeed, a further study has been conducted with the aim to investigate deeper this issue on the analysed dataset. As will be explained in Discussion section, the residual noise affecting the QRS complex could be a crucial factor for EDR methods performances. Figure 57 shows an example where the QRS slopes and R angles method fails because of background noise for the first lead. In this case, the time instants associated with the maximum variation points of the ECG signal are not reliable for the extraction of respiratory information due to an alteration of the QRS complex.

Another loss of accuracy in the results could be ascribed to the leads configuration. For instance, Figure 58 presents an example of ECG on which all the tested methods perform poorly, even though the noise level does not seem to be critical for this case. For these subjects, the results improve when the EDR method is applied on only one of the two leads and independently from applying the removal of f-waves, as it is shown in Figure 59.

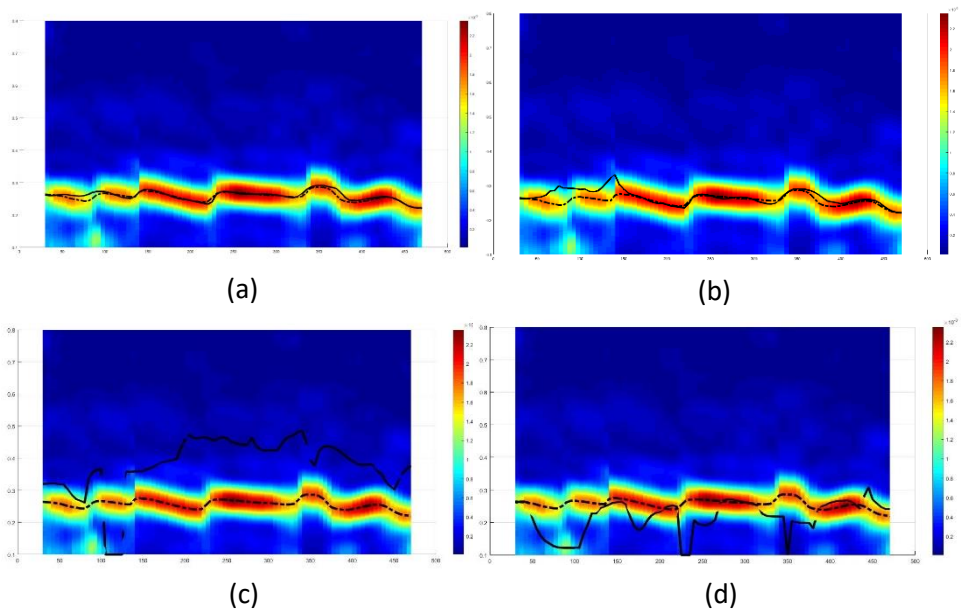

Figure 56. Frequency maps of the respiratory signal and estimated respiratory rates reference signal and EDR signals obtained from the different methods on one patient: (a) QRS slopes and R wave angles, (b) R amplitude, (c) QRS area and (d) VCG alignment. The dashed and the solid black lines represent the extracted dominant frequency rate respectively from the respiratory signal and from the EDR signals over time.

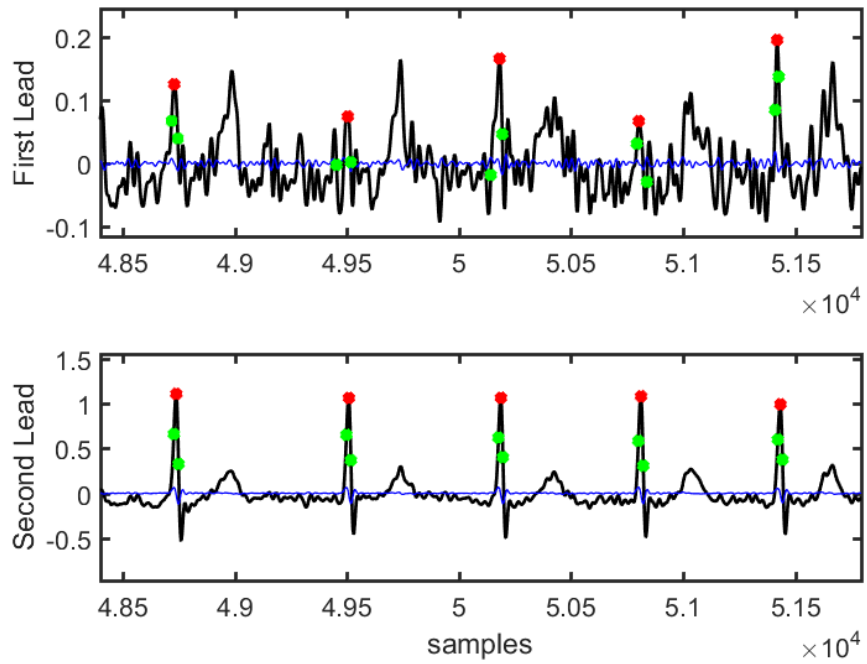

Figure 57. Noisy ECG where the QRS-slopes and R-wave angles method fails for a problem in the extraction of the features, which is visible in the first lead in comparison with the second one.

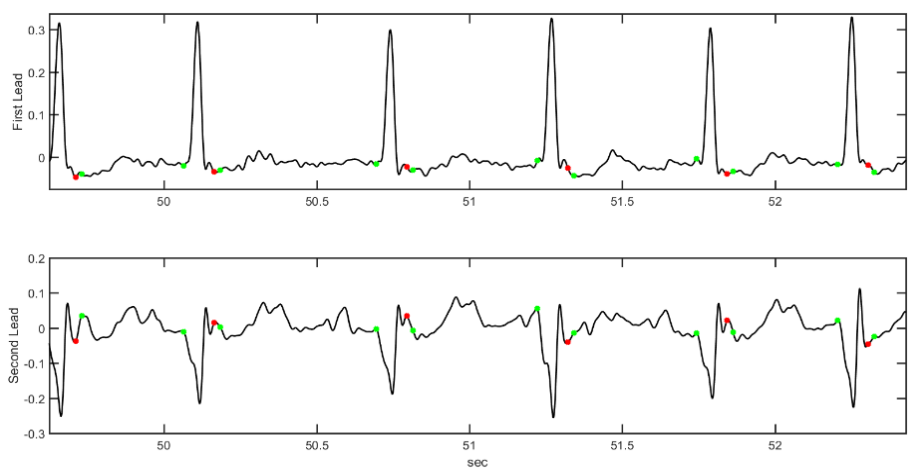

Figure 58. ECG of a patient where all the tested methods performed poorly. The relative respiratory frequency map and estimated respiratory rates from EDR signals and reference signals are shown in Figure 59 .

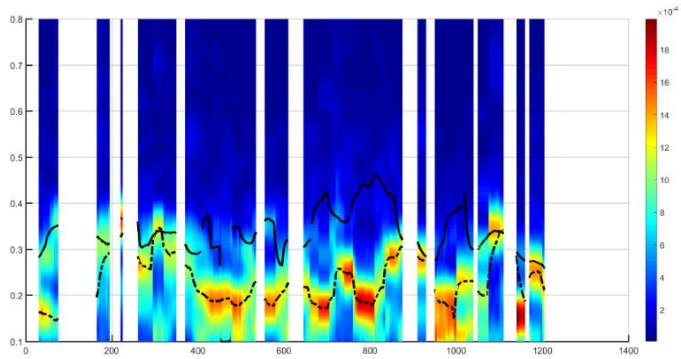

(a)

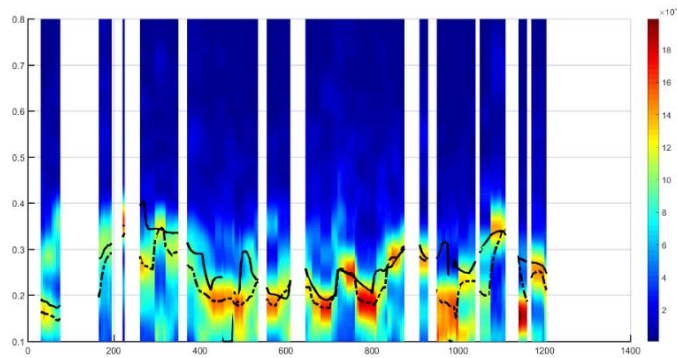

(b)

Figure 59 – Comparison of the results by applying the QRS slopes and R angles on both leads (a) and only the first lead (b). The plots are frequency maps, where the different colours indicate the PSD at any frequency and time instant. The dashed line and the solid line represent respectively the respiratory rate extracted from the reference signal and the respiratory rate extracted from the EDR signals over time.

Chapter 8. DISCUSSION

The aim of this thesis is to verify the feasibility of extracting respiration in case of AF exploiting beat-to-beat morphologic variations in the ECG. Different EDR methods have been tested on a dataset of 49 patients in AF and their performances are evaluated through comparison with the simultaneously recorded respiratory signals. The study of these performances with respect to previous works on patients with AF cannot be completely pursued, because either they are based on a small subgroup of patients or they do not provide a comparable assessment of the performances.

The results show that the method based on QRS slopes and R waves angles estimated the respiratory frequency of the subjects in the dataset more accurately than did the other tested methods, achieving a mean intrasubject error $\mu = 0.0227 \pm 0.0217$ $(8.45\% \pm 8.83\ \%)$. The same method reported an estimation error in [17], $\mu = 0.0046 \pm 0.0304$ $(0.52\% \pm 8.99\ \%)$, of an order of magnitude lower compared to the one obtained in this work, whereas the estimation error reported in [1] by applying QRS-VCG loop alignment method , $\mu = 0.022 \pm 0.016$ $(5.9\% \pm 4\ \%)$, was lower but in the same order of magnitude.

The main reason is that the recordings of the database used in [1] and [17] were from healthy subjects, although in a highly noise environment like stress testing, while from patients with AF in this work. In general, all the tested methods performed poorer with respect to previous studies on healthy subjects due to the different characteristics of **AF recordings**, which make the methods' performances to deteriorate and motivated this work.

An aspect to consider in the decay of the method's accuracy is the **actual respiratory frequency**, whose pattern is much more unpredictable for a patient during an atrial fibrillation event with respect to a healthy subject. The respiratory frequency is expected to be higher in patients with atrial fibrillation,

but the unimodal pattern, typical of healthy subjects in resting conditions, can be lost in subjects with a cardiac dysfunction in the same conditions, mainly due to the subjective state of anxiety. The intrinsic variability in the characteristics of the pathology among different subjects and the subjective unpredictable influence on respiration may also explain the variance in the performances of the EDR methods on a large dataset.

The uncontrolled firing rate of the atrial cells makes unfeasible to exploit HRV to extract respiration, so the QRS-morphologic variations in consecutive beats represents the alternative way to pursue the scope. However, there is no evidence against the fact that the QRS-complex may also suffer of atrial fibrillation-induced morphologic variations, mainly due to the presence of underlying f-waves in the signal. The fibrillatory activity is generally evident in the isoelectric segment, but much less during the QRST interval, so the influence of the chaotic atrial activity on the signal recorded remains unknown during ventricular contractions. This issue motivates the evaluation of the methods' performances in parallel with and without considering a method for the cancellation of f-waves from the QRS complex. Moreover, the fibrillation activity generally determines the appearance of a fluctuating baseline in the ECG, which has a spectral content wider than normal, so it is more difficult to remove completely without distorting the desired information.

However, the **subtraction of f-waves** from the QRS complex did not produce any clear improvement of the performances, but rather led to a slight deterioration of results in terms of mean intrasubject error $\mu = 0.0241 \pm 0.0240$ $(9.00\% \pm 9.86\,\%)$ for the method based on QRS slopes and R waves angles. The same consideration applies also to QRS area and R amplitude methods, even though in these cases a slight decrease is observed in the mean intrasubject errors, which pass from $\mu = 0.0385 \pm 0.0311$ $(14.33\% \pm 12.49\,\%)$ to $\mu = 0.0359 \pm 0.0313$ $(13.45\% \pm 12.54\,\%)$ for QRS area method and from $\mu = 0.0244 \pm 0.0248$ $(9.41\% \pm 10.28\,\%)$ to $\mu =$

0.0236 ± 0.0231 ($9.22\% \pm 9.54\%$) for R amplitude method respectively. As regarding the QRS loop alignment method, f-wave cancellation is instead associated to a decay of performances with a mean intrasubject error $\mu = 0.0540 \pm 0.0370$ ($19.30\% \pm 13.79\%$), which raises from $\mu = 0.0401 \pm 0.0328$ ($15.04\% \pm 12.70\%$) obtained without cancellation of f-waves. This suggests that this method is the most sensitive to morphologic variations introduced in the QRS complex by the f-wave subtraction technique applied in this thesis. Looking at the results on single patients, it has been observed that the worsening of the performances is mainly due to noisy conditions, when a reliable estimation of f-waves in the signal becomes more challenging. Nevertheless, the Kolmogorov-Smirnov test applied on the estimated mean frequency rates μ_{EDR}^{f} and $\mu_{EDR}^{no\,f}$, separately for all the tested methods, confirmed that there is also no statistical evidence of a change in the performances by performing the f-wave subtraction from the QRS complex.

The reason for that is difficult to determine because of the underlying mechanisms of the pathology, which are known to unpredictably affect the normal functioning of the heart conduction system. How AF affects the beat-to-beat morphologic variations in the ECG may be more difficult to ascertain than just considering the fibrillation trend immediately prior to each single ventricular contraction. However, by applying the f-waves subtraction method as in this work, it has been observed that the disturbing effect of the fibrillation activity depends on the length of the fibrillation cycle, which is generally longer or comparable with the QRS interval length. This means that, in practice, the impact of the fibrillation activity on the single QRS-morphology is mostly limited to just one f-wave (two at maximum for very rapid f-waves) rather than to a series of them. Consequently, the reliability of estimation of the fibrillation cycle with its morphology and phase, represents a crucial factor, due to the risk of distorting the desired information in the ECG signal. In this context, it must

be reported that the adopted TQ-based fibrillation signal method presented in some cases sensitivity to the noise in the isoelectric interval, which could be the cause of worsening of the results for some patients. Therefore, it may be also advisable to test the neutrality of the EDR methods performances to the f-wave removal from the QRS complex by applying another technique or making the technique used here more robust to noise.

The comparison of the results reported in Section 7.5 of all the four tested methods provide other points to discuss. Table 6 clearly shows that the EDR methods which extract EDR signals independently for the two leads, i.e. those based on QRS slopes and R-wave angle and based on R-wave amplitude, outperformed the other two methods which combine information from both leads, i.e. methods based on QRS area and QRS-loop alignment, in terms of RMS error on the dataset.

This means that combining information from **two different leads** to extract a single EDR signal does not necessarily provides better results, but at the contrary poorer performances, like in this case, can also be observed. The reason for that is very likely to be related with the configuration of the leads used to extract the ECG signal, on which the EDR method is applied. In this work, two unspecified leads are used to extract respiration, which can be even diversified between different subjects included in the dataset. This implies that the respiratory effects clearly noticeable in one lead may happen to be masked by combining this information with those from a lead, where the respiratory induced variations are either covered by noise or are much less evident (an example is shown in Figure 58 and Figure 59 Results section). It is known, after all, that the ECG respiratory-induced modulations cannot be equally observed in all the leads, since each of them singularly offer just a partial view of the heart. In general, using more leads is advantageous, since, by considering a more complete picture of the heart, it increases the probability of observing

respiration-induced ECG variations. However, the selection of a subgroup of optimal leads depending on the EDR method is a common procedure when testing EDR algorithms. The work of Lázaro et al. [17] states, for example, that there are preferential leads to use for EDR algorithms and, in particular, that the area covered by the posterior leads is the one less suited for EDR, since respiration induced changes at those ECG leads results in lower performance for the QRS area slopes and R wave angle method. Other examples of optimal leads selection referring to EDR methods based on QRS area can also be found in [2], [15] and [43]. In [2] it is also argued that the use of the leads that are not orthogonal is plausible, but it could result in a systematic error in heart axis direction estimation, so affecting the results by a loss of information, which need to be considered in a comparison to other EDR methods.

As regarding VCG-loop alignment, instead, the validity of this method has been only tested in literature on the three orthogonal leads, by extracting three angle series, which are then used to estimate the respiratory rate. Consequently, the method used in this work has been adapted to the case with two unspecified leads, so extracting a single angle series. Moreover, in [17] it is remarked that VCG-loop alignment method with the inverse Dower transformation outperforms the same techniques with 12-ECG, suggesting that three orthogonal leads enhance beat morphological variation induced by respiration. This can explain the fact that the VCG-loop alignment method does not give good results as well as the QRS slope and R-wave angle method, which is not strictly related with the use of three orthogonal leads. This may explain the higher estimation error compared to other methods.

Another aspect which arises from the analysis of the results is the sensitivity to **noise**, which influence the EDR estimation differently for the different methods. QRS slopes and R wave angles and R amplitude series seem to be more robust to noise and artefacts, that may still be present in the QRS complex, compared

to the other methods. The reason for that may refer to the QRS-morphology characteristics that these methods exploit to derive the respiratory information. These are extracted from time instants with a sufficiently high SNR, like those associated with the maximum variation points in QRS complex or with the R wave peak. This may suggest that, in presence of noisy conditions and during cardiac dysfunctions, the entire morphology of the beat is not reliable to provide respiratory information from the whole QRS interval, but rather a shorter interval around the R-peak needs to be selected. If true, this would penalize the methods that consider the whole QRS interval and extract one angle series by joining the information of both leads. It follows that, if one of the two leads present an insufficient SNR, as shown in one example in Figure 57 in Results section, the outcoming EDR signal will be affected. This observation is in agreement with the results of Lázaro et al. [17], which affirms that QRS slopes and R wave angles are more robust than VCG method in those situations when there is so much noise in one of the leads. After all, each one of EDR signals obtained by QRS slopes and R-wave angle are based on one lead, so only those EDR signals based on that noisy lead are affected and their contribution to the respiratory rate estimate can be attenuated by the peaked–conditioned PS average. In this context, the substitution of noisy beats may also play a role in the accuracy of EDR estimation. In this work, the beats with a low SNR in one of the leads are substituted directly in the leads, on which the EDR method is then applied, instead of doing it in the 12 leads-ECG used to derive the VCG, as performed in [1]. That is thought to keep the respiratory information from the lead in which the beat morphology is not noisy, but at the same time may cause a distortion of the desired information that is arduous to quantify when dealing with two-unspecified leads. After all, the derivation of the minimum SNR level for an ECG lead, which guarantees the possibility of reliably extract the EDR signal from it would help for a better understanding of the results. However, the derivation of such a level is all but an easy task, since it involves

the ECG signal quality assessment during an arrhythmia, an area that has attracted a lot of research interest and where there is still much to be searched out.

Chapter 9. CONCLUSION

9.1 OVERVIEW AND CONCLUSIONS

Among the biological signals, the ECG signal is one of the most widely recorded and it contains useful information regarding cardiovascular activity and other adjacent systems. One of these is the respiratory system, which, due to its bidirectional interaction with the cardiac system, affects the ECG signal in different ways. Exploiting this relation, many algorithms have been implemented to obtain a surrogate respiratory signal from the ECG, with the main scope of replacing the common used cumbersome devices in those clinical applications where their use is unmanageable.

This work investigates the possibility of reliably extracting an EDR signal even from patients with atrial fibrillation, since the validity of EDR algorithms has been proved on healthy subjects and no studies have focused systematically on this specific matter so far. The aim is pursued by selecting for the scope the EDR algorithms based beat-to-beat morphological variations, by starting from the assumption that the heart rate modulation induced by respiration is lost in AF, because of the rapid and irregular beating which characterizes the pathology.

Four EDR methods are selected for implementation and adapted to be applied on a dataset containing two unspecified leads ECG and a simultaneously recorded belt respiratory signal for each patient affected by permanent atrial fibrillation. The recordings were of about ten minutes long, acquired in rest phase and the subjects were supposed to breathe spontaneously.

From an initial database of 57 patients, eight of them were excluded because of insufficient quality of the respiratory signal, high number of ectopic beats and the heart rate too low to assure aliasing-free estimation of the respiratory frequency.

All the EDR methods have required a pre-processing of the ECG. The pre-processing consists of a filtering stage and beats analysis. The filtering stage is applied to remove baseline wander, powerline interference and high frequency noise, so as to enhance the respiratory information. The beats analysis is applied, instead, for the rejection of beats with an abnormal morphology in both leads and the rejection or substitutions of noisy beats, depending on respectively if the occur in both leads or in just one of them. Then, an algorithm for subtraction of f-waves from the QRS interval selectively applied and the results of the methods are evaluated with and without performing this stage in order to determine any difference in terms of estimation accuracy.

Afterwards, the outcome EDR signal passes through a post-processing phase, which mostly resembles the pre-processing of the respiratory signal and consists of an outlier correction stage, resampling at 4 Hz and band-pass filtering, in order to make the characteristics of the signals suitable for the respiratory rate estimation algorithm.

The performances of the EDR methods are then evaluated by comparing the respiratory rate extracted from the surrogate respiratory signal with the respiratory rate computed on the reference signal. The assessment is carried out looking at the mean absolute and relative intrasubject error and RMS error on the entire dataset. The eventual benefit of performing f-waves removal in QRS complex is studied by comparing the estimation errors and verifying significant statistical differences between estimated mean respiratory rates by applying the same EDR method, when activating or deactivating the execution of this stage. The mean intrasubject errors and the Kolmogorov-Smirnov test suggest that there is no clear improvement in estimation accuracy for all the tested EDR by subtracting the fibrillation activity from the morphology of the beats, by applying the technique as in this thesis.

The VCG loop alignment method shows, at contrary, a significant decay of the performances in terms of mean intrasubject error passing from $\mu = 0.0401 \pm$

$0.0328\ (15.04\% \pm 12.70\ \%)$, without f-waves removal, to $0.0540 \pm 0.0370\ (19.30\% \pm 13.79\%)$, after f-waves removal. It reveals the sensitivity of this method to changes in QRS morphology due to f-wave subtraction, which may be not completely reliable when the technique is applied in noisy conditions.

The QRS slopes and R wave angle method achieved the lowest estimation error on the dataset $\mu = 0.0227 \pm 0.0217\ (8.45\% \pm 8.83\ \%)$, which, although higher, is still comparable as order of magnitude with previous studies on healthy subjects.

In general, the methods that extract respiratory information independently from the two leads outperformed the others combining this information in a unique rotation angle series. This confirms that sensitivity of the methods to lead configuration and to noisy conditions are important issues that need to be addressed in research studies in this area.

In conclusion, this study indicates that it is reasonable pursuing the extraction of an EDR signal in patients with atrial fibrillation. By focusing the efforts in this field, higher estimation accuracy of the EDR methods can be attained. The method of Lázaro has demonstrated to be the most promising one for this application, while the f-waves subtraction from QRS interval performed in this work has not produced a clear advantage to the EDR methods performances.

9.2 FUTURE WORK

This study presents an initial attempt to test the reliability of EDR methods in order to extract respiration in patients with atrial fibrillation. The results suggest that further studies are justified in order to improve the robustness and the accuracy of the techniques in such conditions. Suggestions about possible future developments of this work follow.

The designed code workflow could be still improved in some stages. The pre-processing and the beat analysis are fundamental steps whose modification could lead to an effective increment of the accuracy in the results. Every change has to be though to suit the specific characteristics of the ECG in atrial fibrillation. Particular attention must be paid to the exclusion of abnormal beats and the substitution of the noisy ones. The technique applied in this work to perform f-waves subtraction from the QRS complex has not proved to clearly enhance the respiratory information against the fibrillation activity. However, the method has demonstrated to work well only in presence of distinct f-waves and to suffer the presence of overlapping noise in the TQ segment. Thus, other techniques with a greater robustness to noise should be tested for better understanding the extent of the influence of f-waves in masking the respiratory modulation in the QRS morphology.

Moreover, it would be also interesting to test the EDR methods on a different database with three orthogonal leads or the 12-leads ECG. The availability of a complete description of the heart would make possible a detailed analysis of the results in relation to the leads configuration. The tested methods have demonstrated in previous studies to work better especially on the VCG, since it enhances the ECG respiratory modulation induced by respiration. In this way, even the comparison of the performances of the different methods during AF would be more meaningful and may lead to new findings. The sensitivity to noise is another aspect that should be investigated deeper, since it has been observed that the quality of the signals is affecting the performance accuracy.

Moreover, the reliability of the EDR signal could be investigated also in the context of clinical studies. It may be interesting to compare, for example, the performances during rest phase and tilt test in order to understand if the activation of the autonomic nervous system, in the second case, influences the respiratory rate estimations.

The evidence of these problems could be a starting point for future studies that have as their ultimate goal the development of an accurate and robust EDR algorithm.

APPENDIX

A. DATASET

Table 8 - Mean of the Heart Rate and mean ± standard deviation of the respiratory frequency rate for each subject in the database. The last column presents the percentage of estimate for the respiratory frequency rate, which is obtained by applying the algorithm proposed in the section 5.8 in order to compare reliably the respiratory and the EDR respiratory rates.

Patient	Heart Rate (beat/min)	Heart Rate (Hz)	Mean Respiratory frequency rate	SD Respiratory frequency rate	% Estimation of Respiratory frequency rate
1	67.6271	1.1271	0.1594	0.0282	89.78%
2	52.4407	0.8740	0.2746	0.0094	98.64%
3	82.7926	1.3799	0.2620	0.0574	65.89%
4	62.2562	1.0376	0.2753	0.0166	86.60%
5	79.7184	1.3286	0.2722	0.0715	68.81%
6	77.9895	1.2998	0.1734	0.0378	86.29%
7	91.3979	1.5233	0.3739	0.0281	65.45%
8	78.4925	1.3082	0.2936	0.0428	94.55%
9	72.9353	1.2156	0.2570	0.0139	100.00%
10	92.6997	1.5450	0.3753	0.0331	94.93%
11	69.2329	1.1539	0.2080	0.0144	100.00%
12	71.1013	1.1850	0.2034	0.0207	97.09%
13	97.3747	1.6229	0.2897	0.0197	78.95%
14	109.8799	1.8313	0.4875	0.0186	100.00%
15	84.0755	1.4013	0.2663	0.0224	100.00%
16	80.2201	1.3370	0.3790	0.0070	100.00%
17	85.4697	1.4245	0.3846	0.0316	88.28%
18	67.4408	1.1240	0.2252	0.0259	97.27%
19	85.2640	1.4211	0.2855	0.0129	100.00%
20	63.3829	1.0564	0.3014	0.0314	89.57%
21	79.5887	1.3265	0.3614	0.0311	84.25%
22	88.0387	1.4673	0.3743	0.0209	89.68%
23	88.0515	1.4675	0.2526	0.0144	100.00%
24	79.5393	1.3257	0.3474	0.0188	99.32%
25	77.9600	1.2993	0.3269	0.0221	98.28%
26	92.5943	1.5432	0.1586	0.0345	96.28%
27	116.7071	1.9451	0.3215	0.0227	94.07%
28	118.7084	1.9785	0.2283	0.0498	77.12%
29	89.6762	1.4946	0.3574	0.0465	78.62%
30	74.5295	1.2422	0.3124	0.0239	85.34%
31	82.5521	1.3759	0.3387	0.0299	82.01%
32	93.2235	1.5537	0.2800	0.0200	98.00%
33	86.2888	1.4381	0.3393	0.0313	87.43%
34	110.1384	1.8356	0.4322	0.0325	95.70%
35	83.0049	1.3834	0.2925	0.0192	100.00%
36	60.8465	1.0141	0.1968	0.0436	83.19%
37	81.5520	1.3592	0.2453	0.0325	89.11%
38	72.4573	1.2076	0.3470	0.0209	94.20%
39	80.6165	1.3436	0.3175	0.0209	92.14%
40	123.1744	2.0529	0.3378	0.0148	100.00%
41	86.2448	1.4374	0.4024	0.0200	99.49%
42	88.6083	1.4768	0.2549	0.0287	69.37%
43	90.8650	1.5144	0.2205	0.0361	97.86%
44	78.0766	1.3013	0.2052	0.0289	98.36%
45	88.4998	1.4750	0.2581	0.0176	95.05%
46	56.4088	0.9401	0.2761	0.0338	88.97%
47	63.5894	1.0598	0.2458	0.0181	98.21%
48	57.9336	0.9656	0.1988	0.0258	96.04%
49	59.2919	0.9882	0.2891	0.0211	100.00%

REFERENCES

[1] R. Bailon, L. Sörnmo and P. Laguna, "A robust method for ECG-based estimation of the respiratory frequency during stress testing," *IEEE TRANSACTION ON BIOMEDICAL ENGINEERING,* vol. 53, pp. 1273-1285, July 2006.

[2] G. B. Moody, R. G. Mark, A. Zoccola and S. Mantero, "Derivation of Respiratory Signals from Multi-lead ECGs," *in Computers in Cardiology, IEEE Computer Society Press,* vol. 12, pp. 113-116, 1985.

[3] J. Felblinger and C. Boesch, "Amplitude demodulation of the electrocardiogram signal (ECG) for respiration monitoring and compensation during MR examinations," *Magn Reson-Med,* vol. 38, no. 1, pp. 129-136, 1997.

[4] L. G. Lindberg, H. Ugnell and P. A. Oberg, "Monitoring of respiratory and heart rates using a fibre-optic sensor," *Medical Biological Engineering Computing,* vol. 30, pp. 533-537, 1992.

[5] R. Atri and M. Mohebbi, "Obstructive sleep apnea detection using spectrum and bispectrum analysis of single-lead ECG signal," *Physiological Measurement Institute of Physics and Engineering in Medicine,* vol. 36, p. 1963–1980, 2015.

[6] D. Dobrev and I. Daskalov, "Two-electrode telemetric instrument for infant heart rate and apnea monitoring," *Medical Engineering and Physics,* vol. 20, pp. 729-734, 1998.

[7] T. Gravelyn and J. Weg, "Respiratory rate as an indicator of acute respiratory dysfunction," *J. Am. Med. Assoc.,* vol. 244, no. 10, pp. 1123-1125, 1980.

[8] C. Seymour, K. J. C. Cooke, T. Watkins, S. Heckbert and T. Rea, "Prediction of critical illness during out-of-hospital emergency care," *JAMA,* vol. 304, no. 7, pp. 747-54, 2010 Aug 18.

[9] N. James, G. Adams and A. Wilson, “Determination of anaerobic threshold by ventilation frequency,” *Int. J. Sports Med.,* vol. 10, no. 3, pp. 192-196, 1989.

[10] P. Langley, E. Bowers and A. Murray, “Principal Component Analysis as a Tool for Analyzing Beat-to-Beat Changes in ECG Features: Application to ECG-Derived Respiration,” *IEEE TRANSACTIONS ON BIOMEDICAL ENGINEERING,* vol. 57, no. 4, pp. 821-829, APRIL 2010.

[11] S. Chugh, R. Havmoeller, K. Narayanan, D. Singh, M. Rienstra, E. Benjamin, R. Gillum, Y. Kim, J. J. McAnulty, Z. Zheng, M. Forouzanfar, M. Naghavi, G. Mensah, M. Ezzati and C. Murray, “Worldwide epidemiology of atrial fibrillation: a Global Burden of Disease 2010 Study,” *Circulation,* vol. 129, no. 8, pp. 837-47, 2014 Feb.

[12] M. Zoni-Berisso, F. Lercari, T. Carazza and S. Domenicucci, “Epidemiology of atrial fibrillation: European perspective,” *Clin Epidemiol.,* vol. 6, p. 213–220, 2014.

[13] V. Pichot, F. Chouchou, J. Pepin, R. Tamisier, P. Lévy, I. Court-Fortune, E. Sforza, J. Barthélémy and F. Roche, “ECG-derived respiration: A promising tool for sleep-disordered breathing diagnosis in chronic heart failure patients,” *International Journal Cardiology,* vol. 186, pp. 7-9, 2015.

[14] W. Hau-Tieng, C. Yi-Hsin, L. Yu-Ting and Y. Yung-Hsin, “Using synchrosqueezing transform to discover breathing dynamics from ECG signals,” *Applied and Computational Harmonic Analysis,* vol. 36, pp. 354-359, 2014.

[15] D. Caggiano e S. Reisman, «Respiration derived from the electrocardiogram: a quantitative comparison of three different methods,» in *Proceedings of IEEE 22nd Annual NE Bioengineering Conference*, 1996.

[16] C. Mason and L. Tarassenko, “Quantitative assessment of respiratory derivation algorithms,” in *23rd Annual EMBS International Conference*, Instanbul, Turkey, 2001.

[17] J. Lázaro, A. Alcaine, D. Romero, E. Gil, P. Laguna, E. Pueyo and R. Bailòn, “Electrocardiogram Derived Respiratory Rate from QRS Slopes and R-

Wave Angle," *Annals of Biomedical Engineering,* vol. 40, no. 10, pp. 2072-2083, 2014.

[18] J. Betts, P. Desaix, E. Johnson, J. Johnson, O. Korol, D. Kruse, B. Poe, J. Wise, M. Womble and K. Young, Anatomy and Physiology, OpenStax College, 2013.

[19] Guyton and Hall, Textbook of Medical Physiology, Saunders, 2010.

[20] L. Sörnmo and P. Laguna, Bioelectrical signal processing in cardiac and neurological applications, Elsevier Inc., 2005.

[21] L. P.D. and e. al., "Respiratory sinus arrhytmia in consious humans during spontaneous respiration," *Respiratory Physiology and Neurobiology,* vol. 174, pp. 111-118, April 2010.

[22] G. Clifford, F. Azuaje and P. McSharry, Advanced methods and tools for ecg data analysis, Norwood, MA, USA: Artech House, Inc., 2006.

[23] R. Neff, J. Wang, S. Baxi, C. Evans and D. Mendelowitz, "Respiratory Sinus Arrhythmia Endogenous Activation of Nicotinic Receptors Mediates Respiratory Modulation of Brainstem Cardioinhibitory Parasympathetic Neurons," *Circulation Research,* vol. 93, pp. 565-572, 2003.

[24] A. Travaglini, C. Lamberti, J. DeBie and M. Ferri, "Respiratory Signal Derived from Eight-lead ECG," vol. Computers in Cardiology Proceedings, pp. 65-68, 1998.

[25] D. Cysarz, R. Zerm, H. Bettermann and M. Kröz, "Comparison of respiratory rates derived from heart rate variability," *Annals of Biomedical Engineering,* vol. 36, no. 12, pp. 2085-2094, 2008.

[26] M. Stridh, *Signal Characterization of Atrial Arrhythmias using the Surface ECG,* Department of Electroscience of Lund University, 2003.

[27] W. Einthoven, G. Fahr and A. De Waart, "On the direction and manifest size of the variations of potential in the human heart and on the influence of the position of the heart on the form of the electrocardiogram," *Pfluger's Arch. f. d. ges. Physiol.,* vol. 50, pp. 275-315, 1913.

[28] F. Martini, Fundamentals of Anatomy and Physiology, Pearson, 2006.

[29] S. Martin and S. Leif, “Spatiotemporal QRST Cancellation Techniques for Analysis of Atrial Fibrillation,” *IEEE TRANSACTIONS ON BIOMEDICAL ENGINEERING,* vol. 48, p. 1, JANUARY 2001.

[30] G. Mazeika and R. Swanson, “RRespiratory Inductance Plethysmography: An Introduction,” Pro-Tech Services, Inc., 2007.

[31] TMSI and J. Peuscher, “Measuring respiration,” January 2013. [Online]. Available: https://www.tmsi.com/products/accessories?task=callelement&format=raw&item_id=42&element=fe0c95f3-af08-4719-bc51-36917715660d&method=download.

[32] t. f. e. Wikipedia, “Respiratory Inductance Pletismography,” Wikimedia Foundation, Inc, 23 01 2017. [Online]. Available: https://en.wikipedia.org/wiki/Respiratory_inductance_plethysmograp.

[33] M. Malik and A. J. Camm, Heart Rate Variability, Futura Publishing Company, 1995.

[34] J. Hayano, F. Yasuma, A. Okada, S. Mukai and T. Fujinami, “Respiratory Sinus Arrhythmia - A Phenomenon Improving Pulmonary Gas Exchange and Circulatory Efficiency,” *Circulation,* vol. 94, no. 4, pp. 842-847, 1996.

[35] R. Pallas-Areny, J. Colominas-Balague and F. J. Rosell, “The Effect of Respiration-Induced Heart Movements on the ECG,” *IEEE Transactions on Biomedical Engineering,* vol. 36, no. 6, pp. 585-590, 1989.

[36] G. Friesen, T. Jannett, M. Jadallah, S. Yates, S. Quint and H. Nagle, “A Comparison of the Noise Sensitivity of Nine QRS Detection Algorithms,” *IEEE TRANSACTIONS ON BIOMEDICAL ENGINEERING,* vol. 30, no. 1, pp. 85-98, 1990.

[37] B. Pilgram and M. Renzo, “Estimating respiratory rate from instantaneous frequencies of long term heart rate tracings,” *Proc. Computers in Cardiology,* p. 859–862, 1993.

[38] F. Pinciroli, G. Pozzi, P. Rossi, M. Piovosi, A. Capo, R. Olivieri and M. Della Torre, “A respiration-related EKG database,” *Proc. Computers in Cardiology,* p. 477–80, 1988.

[39] M. Vararini, M. Edmin, F. Allegri, M. Raciti, F. Conforti, A. Magerata, A. Taddei, R. Francesconi, G. Kraft, A. Abbate and C. Marchesi, “Adaptive filtering of ECG signal for deriving respiratory activity,” in *Proceedings of the Computers in Cardiology, IEEE Computer Society Press*, 1990.

[40] S. Leanderson, P. Laguna and L. Sörnmo, “Estimation of the respiratory frequency using spatial information in the VCG,” *Med. Eng. Phys.,* vol. 25, p. 501–507, 2003.

[41] L. Zhao, S. Reisman and T. Findley, “Derivation of Respiration from Electrocardiogram during Heart Rate Variability Studies,” *Computers in Cardiology Proceedings,* pp. 53 - 56, 1994.

[42] P. De Chazal, C. Heneghan, E. Sheridan, R. Reilly, P. Nolan and M. O'Malley, “Automated processing of the single-lead electrocardiogram for the detection of obstructive sleep apnoea,” *IEEE Transactions on Biomedical Engineering,* vol. 50, no. 6, pp. 686-696, June 2003.

[43] B. Mazzanti, C. Lamberti and J. de Bie, “Validation of an ECG-Derived Respiration Monitoring Method,” *Computers in Cardiology, IEEE,* vol. 30, p. 613−616, 2003.

[44] S. Park, Y. Noh, S. Park and H. Yoon, “An improved algorithm for respiration singal extraction from electrocardiogram measured by conductive textile electrodes using instantaneous frequency estimation,” *Medical and Biological Engineering and Computing,* vol. 46, pp. 147-158, 2008.

[45] Z. Khaled and G. Farges, “First Approach for Respiratory Monitoring by Amplitude Demodulation of the Electrocardiogram,” in *Engineering in Medicine and Biology Society, 1992 14th Annual International Conference of the IEEE*, 1992.

[46] C. O'Brien and C. Heneghan, “A comparison of algorithms for estimation of a respiratory signal from the surface electrocardiogram.,” *Computers in Biology and Medicine,* vol. 37, pp. 305-314, 2007.

[47] F. Pinciroli, R. Rossi and L. Vergani, “Detection of electrical axis variation for the extraction of respiratory information,” *Proc. Computers in Cardiology,* p. 499–502, 1986.

[48] W. Yi and K. S. Park, Derivation of Respiration from ECG Measured Without Subject's Awareness Using Wavelet Transform, vol. Proceedings of the Second Joint EMBS/EIMES Conference, Houston, TX, USA: IEEE, 2002.

[49] J. Boyle, N. Bidargaddi, A. Sarela and M. Karunanithi, "Automatic detection of respiratory rate from ambulatory single-lead ECG," *IEEE Transactions on Information Technology in Biomedicine,* vol. 13, no. 6, pp. 890-896, 2009.

[50] A. Bianchi, G. Pinna, M. Croce, M. Rovere, R. Maestri, E. Locati and S. Cerutti, "Estimation of the respiratory activity from orthogonal ECG leads," *Proc. Computers in Cardiology,* vol. 30, pp. 85-88, 2003.

[51] J. Flaherty, S. Blumenschein, A. Alexander, R. Gentzler, T. Gallie, J. Boineau and M. Spach, "Influence of respiration on recording cardiac potentials. Isopotential surface-mapping and vectorcardiographic studies," *The American Journal of Cardiology,* vol. 20, no. 1, pp. 21-28, 1967.

[52] R. Wang and T. Calvert, "A model to estimate respiration from vectocardiogram measurements," *Ann. Biomed. Eng.,* vol. 2, pp. 47-57, 1974.

[53] "Matlab - the language of technical computing.," [Online]. Available: http://www.mathworks.se/products/matlab/.

[54] A. Martínez, R. Alcaraz and J. Rieta, "Detection and Removal of Ventricular Ectopic Beats in Atrial Fibrillation Recordings Via Principal Component Analysis," in *33rd Annual International Conference of the IEEE EMBS*, Boston, Massachusetts USA,, August 30 - September 3, 2011.

[55] A. Shimizu, T. Ueyama, M. Yoshiga, A. Sawa, S. Suzuki, N. Sugi and M. Matsuzaki, "Spectral Analysis of Atrial Fibrillation Cycle Lengths Comparison Between Fast Fourier Transform Analysis and Autocorrelation Function Analysis Using Multipurpose Physio-Informatic Analysis Software," *Circulation Journal,* vol. 71, p. 242–251, February 2007.

[56] J. Lázaro, A. Alcaine, D. Romero, E. Gil, P. Laguna, L. Sörnmo and R. Bailon, "Electrocardiogram Derived Respiration from QRS slopes: Evaluation with

Stress Testing Recordings," *Computing in Cardiology,* vol. 40, pp. 655-658, 2013.

[57] J. Lázaro, A. Alcaine, E. Gil, P. Laguna and R. Bailon, "Electrocardiogram Derived Respiration from QRS slopes," in *35th Annual International Conference of the IEEE EMBS*, Osaka, Japan, 3-7 July, 2013.

[58] J. Bland and D. Altman, "Statistical methods for assessing agreement between two methods of clinical measurement," *Lancet,* vol. 327, no. 8476, p. 307–310, 1986.